Investigation on Digitized RF Transport over Fiber

Yizhuo (Veronica) Yang

A Thesis Submitted in Fulfillment of the
Requirements for the Degree of Doctor of Philosophy

March, 2011

Department of Electrical and Electronic Engineering,
The University of Melbourne,
Australia, 2011

Abstract

Wireless network based on radio-over-fiber (RoF) technologies is a promising solution to meet the ever increasing demand for larger transmission bandwidth. Such architecture moves most of the processing, routing and switching functionalities to a centralized location with optical fiber backhaul providing high speed interconnection to a large number of antenna base stations. This thesis is focused on the investigation and development of novel technologies for the implementation of radio-over-fiber networks in order to realize ultra-high-speed, high-quality, and multi-service links that connect large numbers of radio base stations with the central office, simplify the architecture of remote base stations, and achieve both cost and energy efficiency.

A digitized RF-over-fiber transmission scheme based on bandpass sampling theory and commercial-available analog-to-digital/digital-to-analog converters (ADC/DAC) is introduced in this thesis. It takes advantage of the higher performance of digital optical links, the benefits of direct RF distribution to realize simpler base stations, and the use of existing optical access and metro network infrastructures. Theoretical analysis of the digitized RF-over-fiber link is carried out by examining noise sources; a comparison between digitized and analog RF-over-fiber links is made in terms of signal-to-noise ratio (SNR) and dynamic range. A low-cost digitized RF-over-fiber uplink transmission is demonstrated using commercially available Field-programmable Gate Array (FPGA) boards. This technique is further expanded to subcarrier multiplexed (SCM) RoF networks.

An efficient bidirectional transmission scheme for Hybrid Fiber-Radio (HFR) access using digitized RF-over-fiber technique is proposed, and it can support multiple wireless signals distribution for both uplink and downlink. Experimental demonstration of a proof-of-concept DRoF-HFR link for the simultaneous transmission of GSM, UMTS and WiMAX wireless services is presented. Error-free transmission is achieved for all three wireless signals in both

the downstream and upstream directions. The thesis also investigated on the downlink power amplification requirement for wireless services at different wireless carrier frequencies.

A digitized radio-over-fiber link for 18 GHz RF signal transmission has been successfully demonstrated with error-free detection. The investigations on the impacts of carrier frequency, bit rate, ADC resolution and sampling rate on the system performance are presented. Two enhanced digitized RF-over-fiber techniques are proposed to reduce the optical data rate and moderate the hardware requirement.

Finally, the thesis investigates the power consumptions and energy-saving potentials of the fiber-wireless integration techniques. A mathematical model for estimating the base station power consumption is developed by evaluating power consumption of each component within the base station and applied to various base station architectures in accordance with different transport schemes of the wireless signals.

Acknowledgements

I would like to express my deepest gratitude to my supervisors, Professor Ampalavanapillai Nirmalathas and Associate Professor Christina Lim. I am very grateful for their supervision, consistent guidance, support and patience. I would not have such achievement without their help and support.

Also, I have to thank Dr. Alan Lee. It was his encouragement that helped me to overcome some hard times during my PhD especially when I first started. I also appreciate his help with the experiments. I must also thank my seniors Prasanna Gamage, Qi Yang and Yuan Zhou for their assistant and useful discussions.

I would like to thank all my friends Yuanyuan He, Lele Zhang, Feng Li, Michael Feng, Jack Wang, James Li, Ji Li, Chi Li, Liang Chen, Gangxiang Shen and Dongxia Xu for their friendship and help in general.

I am forever indebt to my parents, Yuchun Yang and Jiali Lin, for their unconditional love and endless support.

Declaration

This thesis comprises my own work and, except where acknowledged, includes no material previously published by any other person. I declare that none of the work presented in this thesis has been submitted for any other degree or diploma at any university and that this thesis is less than 100,000 words in length, including figures, tables, bibliographies, appendices and footnotes.

Table of Contents

Chapter 1

Introduction

1.1 Broadband Access Networks

Our new age society is becoming more informationally and visually oriented. The increasing demand on multimedia communications, such as text, audio, data, video, and image services, requires reliable broadband data transmission systems [1.1], and it is the driving force that propel the broadband network and its backbone become the necessary and critical infrastructure to underpin the economic activities globally [1.2]. Presently the “last mile” remains an unsolved dilemma for the world's telecommunications carriers, despite the many attempts to undertake this problem [1.3] [1.6].

1.1.1 Digital Subscriber Line (DSL)

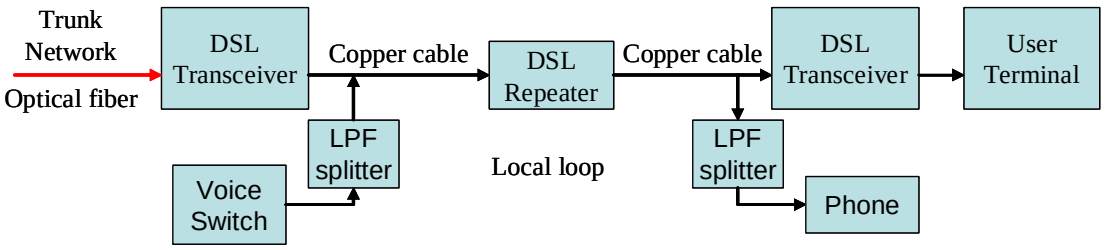

Fig.1.1 DSL architecture

Digital Subscriber Line and Cable modems are the most popular last mile solutions at the current stage (Fig. 1.1). DSL technology paved way to use existing twisted-pair phone lines

for broadband connection. Higher speed DSL connections like asymmetric digital subscriber line (ADSL), high data rate digital subscriber line (HDSL) and symmetric digital subscriber line (SDSL) are developed to extend the range of DSL (from the cable company to a node near the home user) services on copper lines [1.5]. This technology requires multiplexing equipment, such as a DSL Access Multiplexer (DSLAM) to be located at the central office (CO) to aggregate traffic for the backbone transport. At the subscriber, a splitter must be installed at the demarcation point (within the premise) to separate the voice and data traffic.

However, it cannot provide true broadband services in a deterministic way. DSL technology is plagued by the actual topology of copper to which it is attached, and is limited in capacity (several Mbps) and distance (from the central office). Cable modems have higher capacity, yet the channel is shared and the amount of bandwidth at any given time is not guaranteed [1.3]. Typical distance limitations for the lowest bit rates are about 18,000 feet (5.49 km). To extend DSL's reach, most high end DSL links have fiber running up to the DSL Access Multiplexer (DSLAM) and copper from there to the users [1.6].

1.1.2 Hybrid Fiber Coax (HFC)

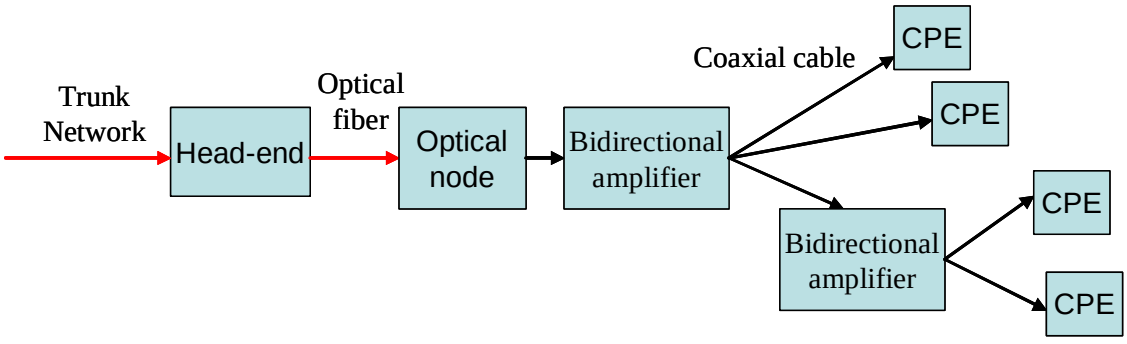

Fig.1.2 HFC architecture

Hybrid Fiber Coax systems (Fig. 1.2) are being deployed in local loops in several countries. The supporters of this approach believe that the conventional twisted pair does not provide enough bandwidth relative to it costs [1.6]. The HFC technology exploits the bandwidth

capacity of fiber and cable television coaxial cable. The HFC network employs an optical fiber facility running from the central office (head-end) to a neighborhood node (optical node). At this node, users are connected by coaxial cable. The coaxial cable is shared with frequency division multiplexing (FDM).

The HFC networks are inherently analog and the FDM RF signal sees the fiber-copper channels (or copper-fiber in the reverse link) arranged in tandem. Therefore the noise, distortion and attenuation are cumulative [1.7]. HFC also has its own technical and operational issues. On the technical side, the upstream bandwidth is small and noisy. Due to the shared bandwidth, security can be an issue. On the operational side, the RF amplifiers bring a higher operational cost and a lower reliability [1.4].

1.1.3 Fiber-to-the-Home (FTTH)

The driving force for Fiber-to-the-Home network is the increasing bandwidth demand. Passive optical network (PON) provides simplicity and low network costs, and is believed to be the best architecture to deploy FTTH (Fig. 1.3). The TDM-PON is a typical point to multipoint optical access network, connecting the optical line terminal (OLT) in the local exchange with many residential and business customers by means of passive splitters located in the field [1.4, 1.8, and 1.9].

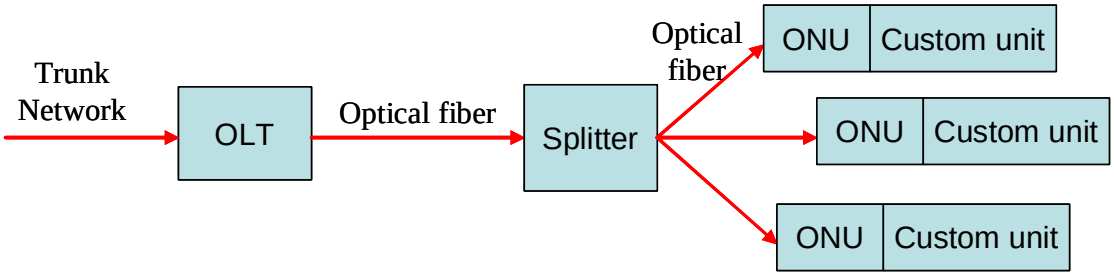

Fig.1.3 FTTH architecture

With optical-to-electronic and signal conversions necessary at every home, the initial cost of the network is higher than the rest. When an existing copper network already exists additional costs are incurred by laying a new optical fiber network, so it may make sense for the incumbents to utilize their existing network before considering a FTTH solution. The demand for huge bandwidth that fiber can offer is still not clear, as major applications requiring fiber capacity are not yet in existence. Providing network power to subscriber equipment especially telephones is still a problem. Current regulations concerning the broadband markets are not clear. All these factors contribute to the uncertain future of FTTH [1.10].

1.1.4 Fiber-Wireless (Fi-Wi) Integration

The future generation broadband access does not only require large operating bandwidth but also needs high flexibility and mobility. This leads to the integration of fiber and wireless broadband infrastructures via a common backhaul networks supporting both wired and wireless connectivity. The most widely used technology behind Fi-Wi is the radio-over-fiber (RoF) technology, which refers to the transmission of radio frequency signal from the central office to the base station (BS) over optical fiber and using wireless communication for the transmission between the base station and the custom user (Fig. 1.4). It combines the capacity of optical networks with the flexibility and mobility of wireless networks to provide broadband multimedia access [1.5, 1.11, and 1.12].

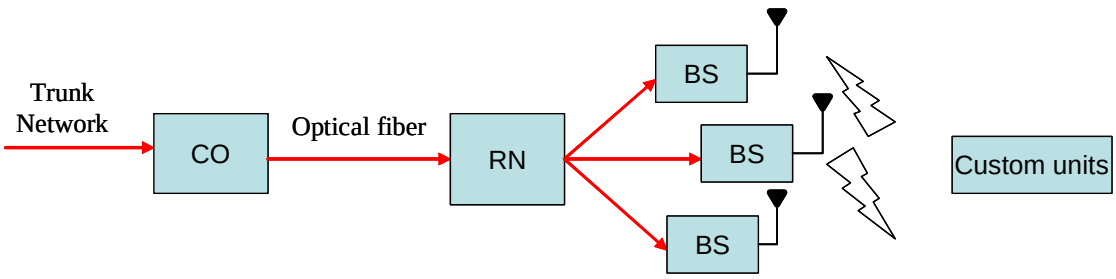

Fig.1.4 Fi-Wi architecture

One of the major issues of RoF is the nonlinear distortions of the optical link, which are from both the optical fiber and the components of the optical link [1.13]. Frequency up-conversion/down-conversion has attracted much attention, as it can not only avoid signal deterioration due to the fiber dispersion but also circumvent using high frequency photonic and RF devices. However, it will increase the complexity of the BSs [1.14, 1.15]. The typical radio-over-fiber system also suffers from severely limited Spurious Free Dynamic Range (SFDR), since the RoF link is accomplished by analogue modulation of an optical or microwave carrier [1.16].

1.2 Fiber-Wireless Networks

1.2.1 Radio-over-Fiber Technology

The increasing demand for larger capacity and higher transmission speeds to accommodate for data-intensive multimedia and real-time applications is unanimous across both mobile and fixed wireless access environments. The current available wireless services, such as GSM, WiMAX, LTE, and WiFi, are operating at lower microwave region (<5 GHz). It has a limited ability to allocate the large spectrum bandwidths required for broadband radio applications. Current trends in cellular networks are to reduce cell size to satisfy the demands of larger bandwidth from users, and to exploit the unused bandwidths at millimeter wave (mm-wave) frequencies to avoid spectral congestion in lower frequency bands. However, reducing the radio cell size or raising the carrier frequency lead to expensive radio systems, because of the high installation and maintenance costs. It will demand a large number of base stations to cover a service area, and the development of cost-effective base stations becomes a key to success in the market [1.17, 1.18]. In the meantime, the traditional microwave backbone with its limited capacity and large propagation loss places a heavy burden on the growth of truly broadband wireless access networks. Governments around the world have recognized the necessity and long-term benefits of the deployment of the optical access

networks [1.19]. Such accelerated deployment of optical access networks will in turn drive more development of the metropolitan and long-haul optical backbone.

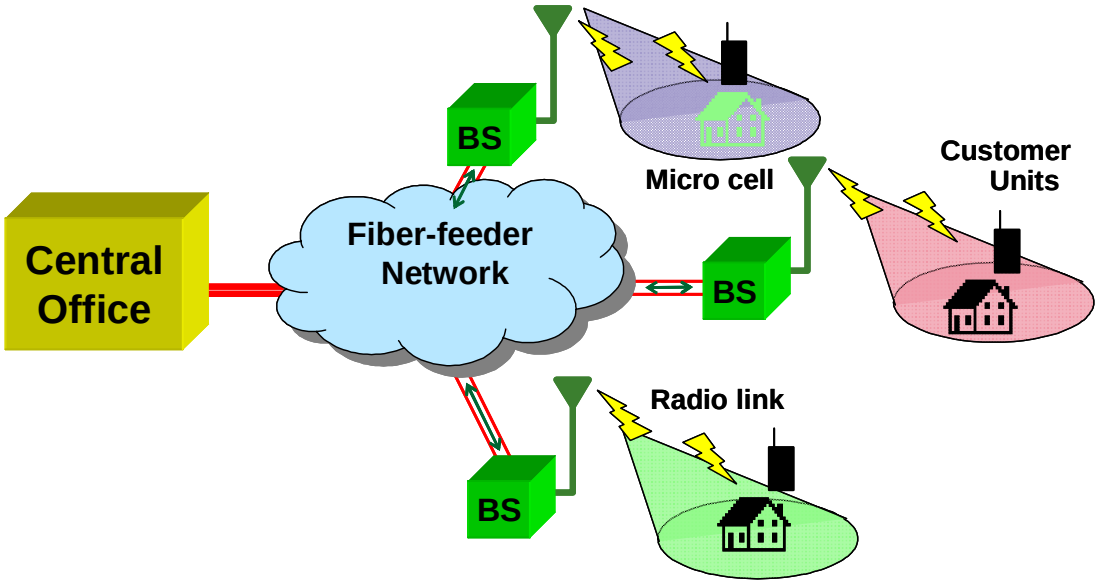

Fig.1.5 Schematic diagram of a fiber-radio network

The fiber-wireless networks, so called radio-over-fiber technology, were first demonstrated for cordless or mobile telephone service in 1990 [1.20]. This technique takes advantage of the fiber optical backhaul to provide high-speed interconnection between the central office and large number of base stations as shown in Fig. 1.5. Such architecture moves most of the processing, routing and switching functionalities to a centralized location, reduces the radio system costs by simplifying the remote base stations, and enhances the sharing of expensive radio equipment located at the central office.

1.2.2 Converged optical access networks

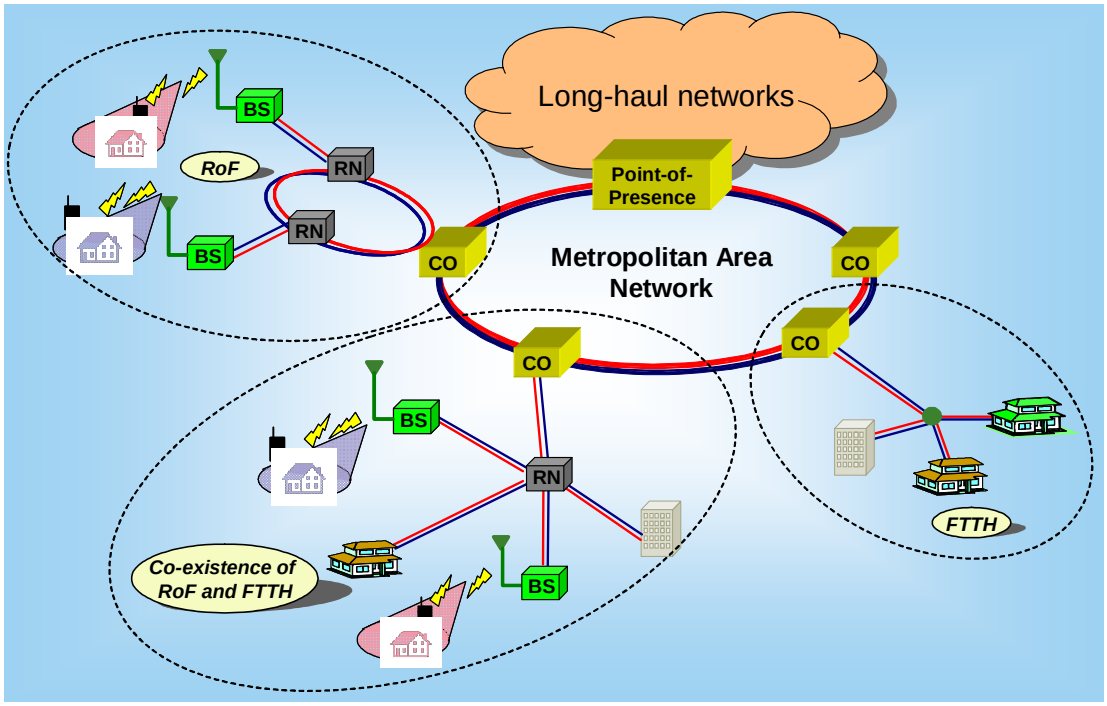

Fig.1.6 PON based hybrid optical access networks supporting RoF and FTTH

With the trend of deploying optical fiber network closer and closer to the subscriber premises, EPON, GPON and WDM-PON are the popular standards within the wireline access environment. On the other hand, broadband wireless access technologies such as WiFi/WiMAX/3G are becoming popular as they are more scalable and flexible with added mobility feature. To make full use of the huge capacity of optical fiber and the mobility function in wireless scheme, the integration of wireless and optical networks is a promising research direction [1.23]. Hence, the high cost of separated wireless and wired-line access networks necessitates the integration of the two distributed networks into a single shared backbone infrastructure [1.2, 1.21].

Radio-over-fiber and fiber-to-the-home systems are promising candidates in wireless and wired-line access networks, respectively. As the PON system is believed to be promising for FTTH, PON based RoF becomes a natural solution. Fig. 1.6 depicts the architecture of a

PON that seamlessly integrates RoF and FTTH via a common unified optical backbone. To meet the demand of such architecture, optical access platform enabling both analog and digital modulation is a must, which allows both analog RoF and digital FTTH to co-exist. The primary concern is to transmit both radio frequency (RF) signal and baseband (BB) signal over a signal fiber in a cost-efficient way with acceptable performance [1.22].

1.3 Thesis Outline

The main objective of this thesis is to investigate and develop a variety of technologies for radio-over-fiber systems that can support high-performance and high-speed wireless services and to realize both cost and energy efficiencies with a simplified structure of the remote wireless base station. Apart from that we have to also ensure that these proposed technologies are able to co-exist with the current optical access networks to maximize the infrastructure sharing. A novel digitized RF-over-fiber technique is proposed, and investigations on the link performance are carried out using both mathematical modeling and experimental demonstration. This technique is further investigated to enable subcarrier multiplexed hybrid fiber-radio networks. Disadvantages of this technique are also identified and discussed. To overcome these issues, approaches using oversampling-and-decimation and multi-level optical transmission are proposed and demonstrated to enhance the digitized RF-over-fiber link. Finally, the power consumptions of fiber-wireless integration networks are studied using a power estimating model and detailed investigations of power consumption in digitized RF-over-fiber technique are carried out by examining the special class of ADCs for bandpass sampling.

This thesis is organized as follows:

Chapter 2: Radio-Over-Fiber Techniques

This chapter presents a comprehensive literature review of radio-over-fiber techniques. A variety of fiber-radio system configurations is included. The implementation issues, such as

radio signal generation, dynamic range limitation, chromatic dispersion and base station simplification, and the previously proposed solutions are discussed in details. Multiplexing techniques incorporating radio-over-fiber systems are presented. Finally, the power consumption and energy-efficient solutions in both wired and wireless access networks are presented.

Chapter 3: Digitized Radio-Over-Fiber Technique

In this chapter, we propose a digitized radio-over-fiber technique based on the bandpass sampling theory and the digital optical link. We present a comprehensive analysis on the digitized RF link using a theoretical model based on different noise sources, and compare the SNR and dynamic range between digitized and analog links. An uplink experimental demonstration is realized using a commercially available A/D converter and FPGA board, and the results have confirmed that digitized RF-over-fiber links can support extended reach well in excess of 60 km and can be easily integrated with any digital optical transmission technologies. We also experimentally investigate the link characteristics by varying the ADC resolution, the carrier frequency, the symbol rate and the sampling rate.

Chapter 4: Multi-Channel Digitized RF-over-fiber Transmission

In this chapter, we extend our study and propose a multi-channel digitized radio-over-fiber transmission scheme based on multi-band bandpass sampling and realize frequency down conversion of multiple channels using a single ADC and a single DAC. We thoroughly analyze multi-channel DRoF link, and compare the results with conventional analog links in terms of SNR, dynamic range and the performance degradation with increasing channel number. The experimental demonstration of a DRoF uplink for multi-channel simultaneously transmission is realized using commercially available FPGA and ADC. By the appropriate selection of sampling rates determined by bandpass sampling, we successfully down-convert all signal bands to the first Nyquist zone and recover the data with satisfactory EVM

performances. Both theoretical and experimental results show that the DRoF technique is sufficient to construct a high-performance cost-effective RF-over-fiber link.

Chapter 5: Bidirectional Hybrid-Fiber Radio using Digitized RF-over-Fiber

In this chapter, we, for the first time, propose a downlink transmission scheme using digitized RF-over-fiber technique without physical mixers and local oscillators. We experimentally demonstrate an efficient Hybrid Fiber-Radio transmission for both the downlink and the uplink paths based on the digitized RF-over-fiber technique for multiple wireless service transmission. By using a single ADC and a single DAC, multiple wireless signals of different standards can be simultaneously transported resulting in a simple base station structure without the needs for analog devices for frequency up- and down-conversion. Error-free detection of the HFR-DRoF link is achieved for the simultaneous transmission of three different wireless standards: GSM, UMTS, and WiMAX. We also experimentally investigate the power requirement for the downlink transmission of multiple wireless services using digitized RF-over-fiber scheme to quantify the frequency up-conversion efficiency.

Chapter 6: High-frequency RF transport over Enhanced Digitized RF-over-fiber link

In this chapter, we first realize the transmission of high frequency RF signal up to 18 GHz via a digitized RF-over-fiber link, which takes advantage of the high performance and the straightforward implementation of digital optical links. Experimental results show that there is a tradeoff between the system performance and the hardware requirements caused by the optical data rates and the ADC resolutions, and investigations are carried out by varying the ADC bit resolutions and the sampling rates. Secondly, we propose a modified DRoF link utilizing oversampling and decimation to enhance the ADC bit resolution and reduce the overall bit rate and moderate the hardware requirements in the link. In the meantime, the energy consumption of the ADC and DAC can be greatly improved as power dissipation is

exponentially related to the bit resolution; and the noise performance can also be improved for higher frequency operation using oversampling and decimation scheme. Additional signal processing functions are necessary in this approach. Thirdly, we introduce a multi-level optical link to the digitized RF-over-fiber technique, which can reduce the overall optical data rate, moderate the requirements of O-E and E-O devices, and also maintain a simple base station configuration.

Chapter 7: Energy consumption of Integrated Optical-Wireless Access

In this chapter, we investigate the power consumptions and energy-saving potentials of radio-over-fiber techniques. In Section 7.2, we study the power consumptions of the fiber optical backhaul and the conventional microwave backhaul, and the fiber optical backhaul shows its energy-saving advantage in terms of the link propagation loss and the hardware power consumption. In Section 7.3, we demonstrate an estimating model of the base station power consumption and apply to various base station architectures. The digitized RF/IF-over-fiber techniques consume the least power, whilst the currently used baseband-over-fiber technique consumes the most. In section 7.4, we focus on the digitized RF-over-fiber link and investigate the power consumption of the special ADCs for bandpass sampling. The sampling rate and the bit resolution are found to be the deciding parameters of the ADC power consumption. The power consumption of the ADC employed in the proposed digitized RoF link is found to be much less than in the direct-digitized RF link.

Chapter 8: Conclusion

In this chapter, we present the important conclusions derived from this research project and also suggestions for the future investigations based on the findings in this thesis.

1.4 Original contributions of this thesis

The major contributions of this thesis are related to the theoretical analysis and experimental demonstration of fiber-wireless integration networks incorporating the digitized RF distribution technique, the experimental implementation of bi-directional multi-service hybrid fiber-radio networks based on digitized RF-over-fiber technique, the enhancement techniques for the digitized RF-over-fiber links, and the investigation of the power consumption in radio-over-fiber networks. The following is a brief description of the original contributions from the research undertaken in this thesis. Publications arising from this work are listed in Section 1.5.

Chapter 3:

- Proposed a novel digitized radio-over-fiber transmission scheme based on ADCs and bandpass sampling theory
- Mathematically modelled the digitized RF-over-fiber link, and estimated the SNR and dynamic range of this link
- Experimentally demonstrated a digitized RF-over-fiber uplink transmission using commercial-available FPGA and ADC
- Experimentally investigated the link performance in terms of ADC resolution, carrier frequency, symbol rate and sampling rate

Chapter 4:

- Proposed a multi-channel digitized radio-over-fiber transmission scheme based on multi-band bandpass sampling and realize frequency conversion of multiple channels using a single ADC and a single DAC

- Thoroughly analyzed the SCM-DRoF link, and compare with the conventional analog links in terms of the SNR, dynamic range, and the performance degradation with channel number increasing

- Demonstrated a SCM-DRoF uplink for multi-channel simultaneously transmission by using commercially available FPGA and ADC

Chapter 5:

- Proposed for the first time a downlink transmission scheme using digitized RF-over-fiber technique without the use of physical mixers and local oscillators

- Demonstrated an efficient Hybrid Fiber-Radio transmission for both the downlink and the uplink paths based on the digitized RF-over-fiber technique for multiple wireless signals transmission

- Experimentally investigated the power requirement for the downlink transmission of multiple wireless services using digitized RF-over-fiber scheme to quantify the frequency up-conversion efficiency

Chapter 6:

- Realized the transmission of high frequency RF signal up to 18 GHz via a digitized RF-over-fiber link by taking advantage of the high performance and the straightforward implementation of the digital optical links

- Proposed a modified DRoF link utilizing oversampling and decimation to enhance the ADC bit resolution and reduce the overall bit rate in the optical link

- Introduced a multi-level optical link to the digitized RF-over-fiber technique in order to reduce the overall optical data rate, moderate the requirements of O-E and E-O devices, and maintain a simple base station configuration

Chapter 7:

- Investigated the power consumptions and energy-saving potentials of the radio-over-fiber techniques
- Studied the power consumptions of the fiber optical backhaul and the conventional microwave backhaul
- Built up a generic model of the base station power consumption and applied to various base station architectures.
- Further investigated the power consumptions of the ADCs using bandpass sampling in the digitized RF-over-fiber transmission scheme

1.5 Publications

1. Y. Yang, P.A. Gamage, C. Lim, and A. Nirmalathas, “Demonstration and Performance Analysis of an Uplink based on Digitized RF-over-fiber Signal Transport”, Asia-Pacific Microwave Photonics Conference (APMP), 2009.
2. Y. Yang, C. Lim, P.A. Gamage, and A. Nirmalathas, “Demonstration of SCM Signal Transmission based on Digitized Radio-over-Fiber Technique”, IEEE International Topical Meeting on Microwave Photonics (MWP), 2009.
3. Y. Yang, C. Lim, P.A. Gamage, and A. Nirmalathas, “Performance Evaluation of Digitized RF-over-Fiber Transport Link”, Photonics Society Annual Meeting (LEOS), 2009.

4. Y. Yang, C. Lim, P.A. Gamage, and A. Nirmalathas, “Experimental Demonstration of a Downlink Multi-Channel Hybrid Fiber-Radio using Digitized RF-over-Fiber Technique”, IEEE MTT International Microwave Symposium (IMS), 2010.

5. Y. Yang, C. Lim, P.A. Gamage, and A. Nirmalathas, “18 GHz RF Transport based on Digitized Radio-over-Fiber technique”, Asia-Pacific Microwave Photonics Conference (APMP), 2010.

6. Y. Yang, C. Lim, and A. Nirmalathas, “Multi-Channel Digitized RF-over-Fiber Transmission based on Bandpass Sampling and FPGA”, IEEE Journal of Lightwave Technology (JLT), 2010.

7. Y. Yang, C. Lim, and A. Nirmalathas, “Bit Resolution Enhanced Digitized RF-over-Fiber Link”, IEEE International Topical Meeting on Microwave Photonics (MWP), 2010.

8. Y. Yang, C. Lim, P.A. Gamage, and A. Nirmalathas, “Experimental Demonstration of Multi-Channel Hybrid Fiber-Radio System using Digitized RF-over-Fiber Technique”, submitted to IEEE Journal of Lightwave Technology (JLT).

9. Y. Yang, C. Lim, and A. Nirmalathas, “Energy consumptions on radio-over-fiber techniques”, accepted by The Optical Fiber Communication Conference and Exposition (OFC) 2011.

10. Y. Yang, C. Lim, and A. Nirmalathas, “Enhanced Digitized RF-over-Fiber Technique,” submitted to JLT.

11. Y. Yang, C. Lim, and A. Nirmalathas, “Energy consumption of Integrated Optical-Wireless Access Networks,” submitted to JLT.

12. A. Nirmalathas, P.A. Gamage, C. Lim, D. Novak, R.B. Waterhouse and Y. Yang, "Digitized RF over Fiber Transport," Microwave Magazine, vol. 10, pp. 75-81, 2009.

13. C. Lim, A. Nirmalathas, M. Bakaul, P. Gamage, K.L. Lee, Y. Yang, D. Novak and R. Waterhouse, "Fiber-wireless networks and microwave photonics subsystem technologies" (Invited Tutorial), OFC/NFOEC2009, Mar. 2009.

14. C. Lim, A. Nirmalathas, P. Gamage, Y. Yang, D. Novak, and R.B. Waterhouse, "High Performance Radio-over-Fiber Links," LEOS, 2009.

15. C. Lim, A. Nirmalathas, Y. Yang, D. Novak, and R.B. Waterhouse, "Radio-over-Fiber Systems," OSA/ACP, 2009.

16. A. Nirmalathas, P.A. Gamage, Y. Yang, C. Lim, D. Novak, and R.B. Waterhouse, "Digitized RF over Fiber Transport: Enabling Cost-Effective Integration of Optical and Wireless Access Networks," (invited) APMP 2009.

17. A. Nirmalathas, P.A. Gamage, Y. Yang, C. Lim, D. Novak, and R.B. Waterhouse, "Cost-effective Optical Backhaul for Broadband Wireless," (invited) LEOS 2009.

18. C. Lim, A. Nirmalathas, Y. Yang, D. Novak, and R.B. Waterhouse, "Radio-over-Fiber Systems," (invited) Proc. SPIE, 2009.

19. C. Lim, A. Nirmalathas, M. Bakaul, P. Gamage, K. L. Lee, Y. Yang, D. Novak, and R. Waterhouse, "Fiber-Wireless Networks and Subsystem Technologies," Journal of Lightwave Technology, Volume 28, Issue 4, pp: 390 – 405, 2010

20. C. Lim, Y. Yang, and A. Nirmalathas, "High Performance Radio-over-Fiber Links using Digitized Wireless Transport," (invited) APMP 2010.

1.6 Reference

[1.1] S. Z. Pinter, and X. N. Fernando, “Fiber-Wireless Solution for Broadband Multimedia Access,” IEEE Canadian Review (summer), 2005.

[1.2] A. Nirmalathas, P. A. Gamage, C. Lim, D. Novak, R. Waterhouse, “Digitized Radio-Over-Fiber Technologies for Converged Optical Wireless Access Network,” Journal of Lightwave Technology, vol. 28, Issue: 16, pp. 2366-2375, 2010.

[1.3] Scott Bloom, and W. Seth Hartley, “The last-mile solution: hybrid FSO radio,” Whitepaper, AirFiber Inc, 2002.

[1.4] Jeffrey A. Tompkins, Jeffrey R. Jacobs, and Jane Li, “Bridging The Last Mile Access Network Wireline Architectures,” Whitepaper, Corning Inc, 2001.

[1.5] X. Fernando, “Broadband access networks,” IEEE International conference on signal processing, communications and networking, 2008.

[1.6] Uyless Black, Residential broadband networks xDSL, HFC and fixed wireless access, Prentice Hall PTR, Upper Saddle River, New Jersey.

[1.7] X. Fernando, “Radio over Fiber in Multimedia Access Networks,” Proceedings of the 1st international conference on Access networks, 2006.

[1.8] Chang-Hee Lee, Wayne V. Sorin, and Byoung Yoon Kim, “Fiber to the Home Using a PON Infrastructure,” Journal of Lightwave Technology, vol. 24, Issue: 12, 2006.

[1.9] Paul W. Shumate, “Fiber-to-the-Home: 1977–2007,” Journal of Lightwave Technology, vol. 26, Issue: 9, 2008.

[1.10] Xin Yao, Susanna Anderson, and Xin You, “What is holding back FTTH?” https://drachma.colorado.edu/dspace/bitstream/123456789/234/1/What+is+holding+back+FTTH.pdf .

[1.11] Christina Lim, Ampalavanapillai Nirmalathas, Masuduzzaman Bakaul, Prasanna Gamage, Ka-Lun Lee, Yizhuo Yang, Dalma Novak, and Rod Waterhouse, “Fiber-Wireless Networks and Subsystem Technologies” Journal of Lightwave Technology, vol. 28, Issue: 4, 2010.

[1.12] Christina Lim, Ampalavanapillai Nirmalathas, Yizhuo Yang, Dalma Novak, and Rod Waterhouse, “Radio-over-Fiber Systems,” Communications and Photonics Conference and Exhibition (ACP), 2009.

[1.13] T. Kurniawan, and A. Nirmalathas, “Performance Analysis of Optimized Millimetre-Wave Fibre Radio Links,” IEEE Transaction on Microwave Theory Technology, vol. 54, Issue: 2, 2006.

[1.14] D. Novak and A. Nirmalathas, “Fibre-radio: challenges and possible solutions,” IEEE International Topical Meeting on Microwave Photonics, 2003.

[1.15] U. Gliese, S. Norskow, and T. N. Nielsen, “Chromatic Dispersion in Fiber-Optic Microwave and Millimetre-Wave Links,” IEEE Transaction on Microwave Theory Technology, vol. 44, Issue: 10, 1996.

[1.16] Philip M. Wala, “A new microcell architecture using digital optical transport,” IEEE Vehicular Technology Conference, 1993.

[1.17] A. M. J. Koonen, M. Garcia Larrode, A. Ng’oma, K. Wang, H. Yang, Y. Zheng, and E. Tangdiongga, “Perspectives of Radio over Fiber Technologies,” Conference on Optical Fiber communication/National Fiber Optic Engineers Conference OFC/NFOEC, 2008.

[1.18] A. Nirmalathas, C. Lim, D. Novak, and R. B. Waterhouse, “Progress in Millimeter-Wave Fiber-Radio Access Networks,” Annals of Telecommunications, vol. 56, no. 1-2, pp. 27-38, 2001.

[1.19] L. Luic and D. Glumac, “The role of ICT technology in the knowledge society,” 9th International Conference on Telecommunication in Modern Satellite, Cable, and Broadcasting Services, 2009.

[1.20] A. J. Cooper, “Fiber/Radio for the provision of cordless/mobile telephony services in the access network,” Electron. Letters, vol. 26, no. 24, pp. 2054-2056, 1990.

[1.21] Chun-Ting Lin, Jason Chen, Peng-Chun Peng, Cheng-Feng Peng, Wei-Ren Peng, Bi-Shiou Chiou, and Sien Chi, “Hybrid Optical Access Network Integrating Fiber-to-the-Home and Radio-Over-Fiber Systems,” IEEE Photonics Technology letters, vol. 19, no. 8, 2007.

[1.22] Ken-ichi Kitayama, Toshiaki Kuri, Hiroyuki Toda, and J.J. Vegas Olmos, “Radio over Fiber: DWDM Analog/digital Access Network and its Enabling Technologies,” The 20th Annual Meeting of the IEEE Lasers and Electro-Optics Society LEOS, 2007.

[1.23] Rujian Lin, “Next Generation PON in Emerging Networks,” Conference on Optical Fiber communication/National Fiber Optic Engineers Conference OFC/NFOEC, 2008.

Chapter 2

Radio-Over-Fiber Techniques

2.1 Introduction

It is well-established that the integration of wireless broadband access and the optical access network infrastructure via a common backhaul network can lead to significant benefits to network operators through savings in operational and capital expenditure associated with the broadband deployment. Radio-over-fiber has long been studied as a way of realizing ultra-high-speed, high-quality, and multi-service backhaul networks that connect radio base stations with the central office and simplify the architecture of remote base stations via an optical feeder network [2.1, 2.2]. In chapter 1, we have briefly discussed the significance and advantages of deploying radio-over-fiber systems for future mobile and fixed wireless communications. Some of the benefits are listed below.

High bandwidth: Optical fibers offer enormous bandwidth and consequently high transmitting capacity. There are three main transmission windows, which offer low attenuation for optical fiber: 850 nm, 1310 nm, and 1550 nm wavelengths. The combined bandwidth of the three windows for single mode fiber is more than 50 THz [2.3]. In addition, some signal processing that may be difficult or impossible to do in electronic system can be resolved by the high bandwidth of optical system [2.5].

Low Attenuation: The electrical distribution of high-frequency microwave signals either in free space or through transmission lines is problematic and costly. Optical fiber offers

much lower loss [2.4]. Commercially available standard single-mode fibers have attenuation losses about 0.2-dB/km and 0.5-dB/km in the 1550 nm and the 1300 nm windows respectively. Optical fibers employed in RF transmission will increase the transmission distance dramatically, and reduce the required transmission powers greatly.

Immunity to EMI: Another attractive property of fiber optical communication is the immunity to Electromagnetic Interference (EMI). This is also because signals are transmitted in the form of light through the fiber. This property also leads to eavesdropping immunity, which provides privacy and security [2.6].

Low Power Consumption: In radio-over-fiber systems, most of the complex functions are implemented at the central office. It reduces the equipments in remote antenna unit, and leads to low power consumption of each base station. The energy consumed by central office is shared by large numbers of remote units. As a result, the total energy consumption per user will be low.

Multiple service operation: In radio-over-fiber systems, subcarrier multiplexing (SCM) and wavelength division multiplexing (WDM) can be used to distribute multiple radio signals over one single optical fiber [2.7, 2.8]. It is expected that radio over fiber incorporating these multiplexing techniques can further enhance the infrastructure sharing and lead to greater economic benefits.

This chapter presents a comprehensive literature review of radio-over-fiber techniques. In Section 2.2, a variety of fiber-radio system configurations are introduced encompassing three analog and two digital systems including their advantages and disadvantages. In Section 2.3, we review the implementation issues and previous research in this area. RF signal generation is an important topic in radio-over-fiber techniques whereby three RF generation techniques will be discussed. It is well-established that nonlinear distortion and chromatic dispersion are two crucial issues in the radio-over-fiber systems and we will review the various schemes

and solutions to overcome these impairments. The linearization techniques, such as optical modulator configuration, nonlinear predistortion and post compensation, are also reviewed. Then, base station simplification techniques are discussed in detail and catalogued into four groups. The first is to use a dual-functional electro-absorption modulator (EAM) transceiver to reduce the optoelectronic devices in the base station; the second is to reuse the downlink optical carrier for uplink transmission without using an extra light source in the base station; the third is to remotely delivery the LO signal from the central office and remove the needs for a physical LO in the base station; the last category uses photonics frequency downconversion technique which employs an optical switching-encoding scheme that does not need a LO. In Section 2.4, the review on multiplexing techniques incorporating radio-over-fiber systems, such as WDM, SCM, and multi-band transmission are presented. The last section of this chapter focuses on the power consumption and energy-efficient solutions in access networks with FTTH based on PON architecture being the most energy efficient in the wired access networks. In the wireless access networks, the base station accounts for the large power consumption, and has the most energy-saving potential.

2.2 Analog and Digital RoF Schemes

Most of the conventional optical networks employ digital signal transmission. However, the typical radio-over-fiber system is fundamentally an analog transmission system. The analog signal transmitted over the optical fiber can either be radio frequency (RF) signal, intermediate frequency (IF) signal or baseband (BB) signal. In the optical transmitter, the RF/IF/BB signal can be modulated onto the optical carrier by using either direct or external modulation of the laser light. Ideally the output signal from the optical link will be an exact replica of the input signal free from additional distortion or noise. Signal distribution as RF-over-fiber has the advantage of a simplified BS design, but it is susceptible to fiber chromatic dispersion that severely limits the transmission distance as well as the requirement of high

speed optical modulation and detection techniques [2.9]. For IF and BB transmission cases, the BS should have additional functions, such as frequency up- and down- conversion from IF\BB signal to RF band and from RF band to IF\BB. In IF-over-Fiber scheme, the effect of fiber chromatic dispersion on the distribution of IF signals is much reduced. However, this means the antenna base stations implemented for the radio-over-fiber system to incorporate IF-over-fiber transport will require additional electrical hardware such as radio-frequency local oscillators and mixers for frequency up- and down-conversion. In the baseband over fiber transmission, the impact of the fiber dispersion is negligible, but the BS configuration is the most complex [2.10]. Comparing the three analog radio-over-fiber transmission schemes (shown in Fig. 2.1), there is a trade-off between the base station complexity, the dispersion immunity and the optoelectronic interface [2.11].

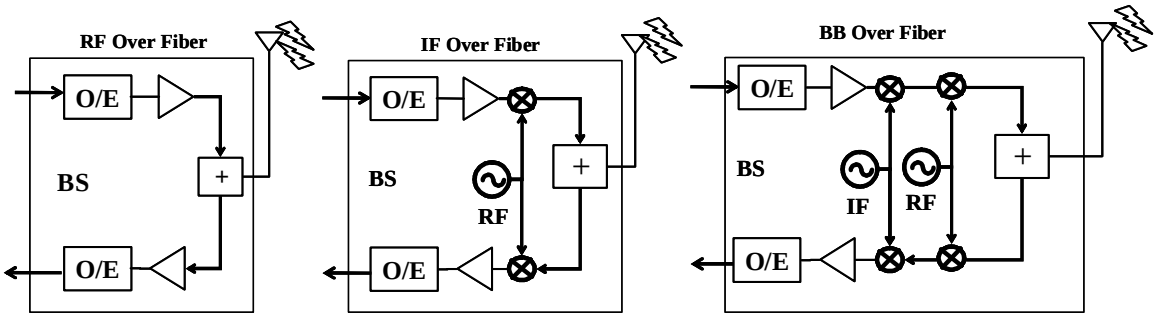

Fig.2.1 BS configurations of different frequency bands transmission

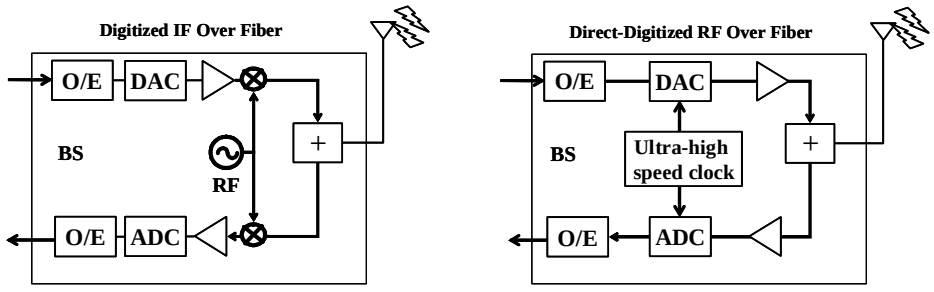

Fig.2.2 BS configurations for digital optical links

The transmission of analogue signals requires high-quality performance on the linearity and dynamic range of the optical link. Moreover, there are a number of distortions arising from the non-linear characteristics and frequency response limitations associated with the laser or the external modulator as well as the effect of fiber dispersion. Many of the problems associated with analog modulation could be circumvented if it is possible to first digitize the information signal and then transport it digitally. Therefore, radio-over-fiber taking advantage of the digital optical link by using analog-to-digital/digital-to-analog converters (ADC and DAC) has attracted more attention in recent years [2.12, 2.13]. A direct digitized RF solution has been proposed by ADC Telecommunications [2.140], where the A/D and D/A conversion functionalities are located in both base transceiver station site and remote unit for up and down links. However, in direct-digitized RF-over-fiber link (shown in Fig. 2.2), extremely high sampling rate ADCs and DACs are required for high frequency radio signal transmissions, and it severely increases the implementation cost and difficulty. In digitized IF-over-fiber approach (shown in Fig. 2.2), the frequency up- and down-conversion is the same as in analog IF-over-fiber link, but the BS configuration will be even more complex due to the additional electronic devices [2.20].

Two specifications for open base station architectures have emerged recently, Common Public Radio Interface (CPRI) [2.21] and Open Base Station Architecture Initiative (OBSAI) [2.22]. The open base station architectures have recently been introduced in wireless infrastructure networks for distributing and decentralizing Base Transceiver Stations (BTS). The BTS is an integral part of the radio access network and is the bridge between the handset and the wireless infrastructure core network. In a distributed BTS network architecture, a digitized and serial interface is descript between a digital base station (DBS) containing the baseband processing functions and a remote radio head (RRH) containing the radio functions of a traditional base station, and the links connecting the DBSs and RRHs use a standardized digital optical interface [2.24]. Although CPRI and OBSAI both specify the use of digital

transmission links between DBS and RRH, it is likely that such links will be very expensive if high bit-rate capability is incorporated [2.23].

2.3 Issues and Previous Research on Radio-over-Fiber

Though the radio-over-fiber technology has been well-suited for microwave and millimeter-wave applications, it is not straightforward. There are also some implementing issues in radio-over-fiber systems. Some of them have been studied for years; some of them still need further investigations.

2.3.1 RF signal generation

The simplest scheme for transporting wireless signals via an optical fiber network is to directly transport the RF signals over fiber without any frequency conversion required in the base stations. However, as the wireless carrier frequency increases, the requirement for high-speed optical sources, modulators and photodetectors may pose as a cost-constraint to the overall link. In addition, the impact of fiber chromatic dispersion on the transported wireless signals becomes more pronounced with increasing wireless carrier frequency [2.25]. As a result, IF over Fiber scheme, which places the RF signal generation as well as the RF-to-IF down-conversion in the base stations, has attracted much attention. However, it will also increase the complexity and cost of the base stations. Therefore, the RF signal generation technique at the base station is an important topic in mitigating the required specification of both photonic and RF devices, especially for millimeter wave (MMW) signals [2.14] [2.15].

Conventional approaches to generate microwave or mm-wave signals using electronic circuitry with many stages of frequency doubling to achieve the desired frequency are complicated and costly. The microwave or mm-wave signals generation in the optical domain based on optical heterodyning may be an ideal solution. Two optical waves of different wavelengths are delivered from the central office to the base station, and beat at a

photodetector within the base station. An electrical beat signal is then generated at the output of the photodetector with a frequency corresponding to the wavelength spacing of the two optical waves [2.26]. The stability of the generated signal depends on the instantaneous frequency difference between the two optical carriers being mixed. Therefore, it is necessary to control the instantaneous frequency difference accurately. Given that the laser emission frequency is highly sensitive to temperature variations, phase noise and other effects, techniques to maintain the required frequency offset and phase noise performance have to be used. There are several methods for controlling the frequency offset between the two lasers, such as optical frequency-locked loop (OFLL), optical phase-locked loop (OPLL), optical injection locking (OIL), and optical injection phase-locked loop (OIPLL) [2.16-2.19]. Microwave signals can also be generated using a dual wavelength laser source with the two wavelengths separated at a desired frequency [2.31]. Due to the fact that the two wavelengths are generated from the same cavity, the phase correlation between the two wavelengths is better than that using two free-running laser sources, and the system is simpler with no need for a microwave reference source, which can reduce the system cost.

The easiest way for the generation of two phase correlated frequencies is the external modulation of a continuous wave (CW) by a Mach-Zehnder modulator (MZM) [2.27]. This MZM is driven at the non-linear regime and generates a double-sideband suppressed-carrier (DSSC) signal. The upper band and lower band act as two phase correlated optical signals, and the frequency of the driving local oscillator signal is only half of the wireless carrier frequency. As shown in Fig. 2.3, a Mach–Zehnder modulator is biased at the minimum transmission point of the transfer function to suppress the even-order optical sidebands. Due to the square-law process of the photodetector (PD), a stable, low-phase noise mm-wave signal at twice the frequency of the RF drive signal is generated at the receiver. In [2.28-2.30], frequency quadrupling and upconversion techniques are realized. The optical millimeter wave carriers are generated with four times the frequency of the driving local

oscillator signal. Fig. 2.4 shows the frequency quadrupling scheme using cascaded MZMs, which are both biased at the minimum transmission to completely suppress the even-order optical sidebands and a π/2 shift in applied to the RF modulated signals. In [2.32] and [2.33], the MZM is driven to generate harmonics around the carrier with a frequency separation that corresponds to the modulation frequency. The sidebands are generated up to the order of 6, and stimulated Brillouin scattering is used at the receiver to amplify the harmonic at the desired frequency.

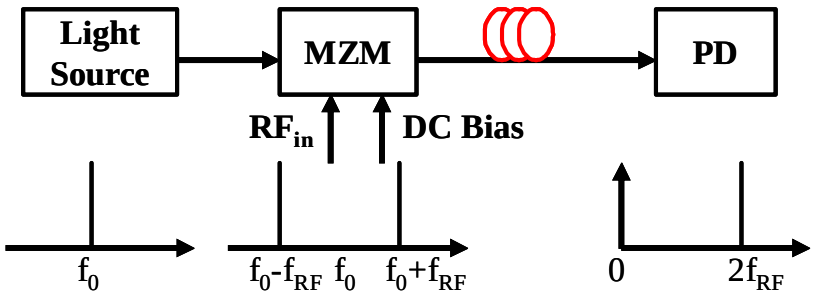

Fig.2.3 Frequency doubling using MZM

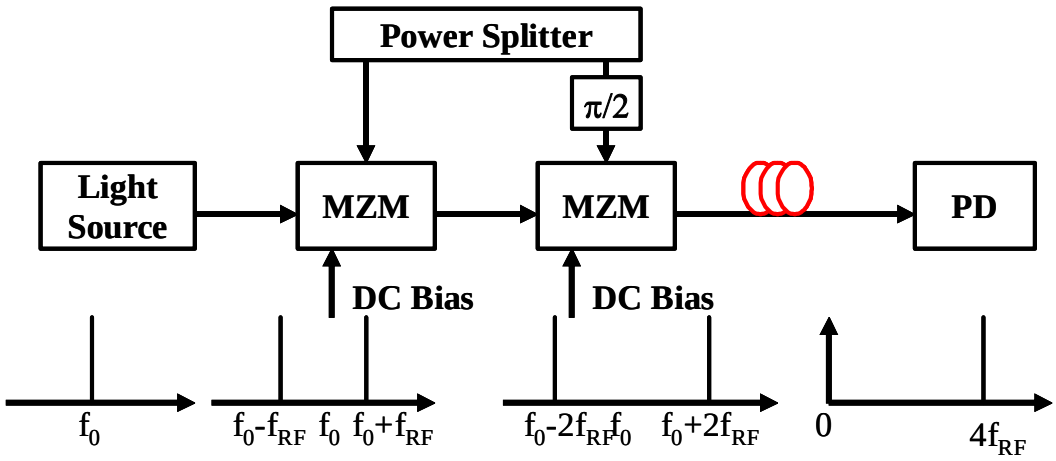

Fig.2.4 Frequency quadrupling using cascaded MZMs

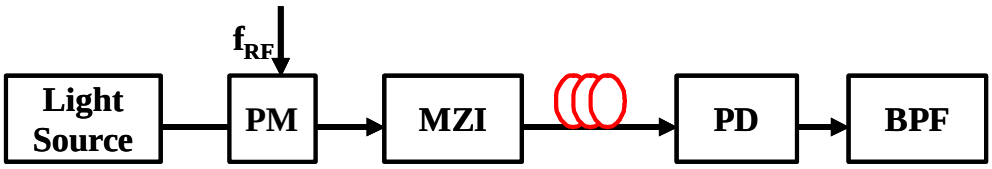

Fig.2.5 Microwave signal generation using a phase modulator

The approach using an MZM for microwave signal generation can produce a high-quality frequency-tunable microwave or mm-wave signal with a simple system structure. However, the MZM must be biased at the minimum or maximum point of the transfer function, which would cause bias-drifting problem, leading to poor system robustness or a sophisticated control circuit has to be employed to minimize the bias drift [2.34]. Another method for high frequency RF signal generation is by taking advantages of an optical phase modulator to generate a frequency comb and a narrow band optical notch filter is used to select the two desired bands to beat at the photodetector for the microwave signal generation. The key advantage of using an optical phase modulator is that no dc bias is required, which eliminates the bias-drift issue. There are various methods that have been used to realize the optical filter, such as a fiber Mach Zehnder Interferometer (MZI) filter [35,36], a fiber Fabry-Perot filter [2.37], and a fiber Bragg grating (FBG) filter [2.38, 2.39]. Fig. 2.5 shows the radio-over-fiber system employing an optical phase modulation with a MZI periodic filter.

2.3.2 Nonlinear distortion and dynamic range limitation

Analog optical links employing radio-over-fiber techniques inherently suffer from the cumulative effects of noise and distortions induced by the nonlinearity of both optical fiber and components of the optical link [2.40]. When optical communication systems are operated

at high bit rates, high transmitted power, or using WDM, the nonlinear effects can become more severe [2.41]. For optical links employing MZMs, it is found that the nonlinear distortions generated in MZMs such as harmonic distortions and intermodulation distortions is the limiting factor of the overall link performance [2.41]. Spurious free dynamic range (SFDR) is one of the key measures that characterize the performance of a radio-over-fiber link, and it is severely limited by the nonlinear effects, especially the third-order intermodulation distortion, from the optical link [2.42, 2.43]. The issue of linearity of radio-over-fiber systems has been widely investigated, and numerous techniques have been proposed to combat the nonlinear distortions.

The optical modulator configurations such as dual parallel MZMs [2.44-2.46], cascaded MZM architectures [2.47], and suboctave linearized modulators [2.48] have been proposed to linearize the transfer function of the optical modulator in an analogue optical link. A linearization technique for DFB laser diode based on a light-injection technique using cross-gain modulation effect is proposed in [2.49, 2.50]. Nonlinear distortions in single-sideband modulation schemes have also been investigated [2.51-2.53]. In [2.52] a technique is proposed to improve the optical front-end linearity by the removal of the optical components that contribute most to the third-order IMD in the RF domain, and in [2.53] a balanced radio-over-fiber system is used to suppress the even order nonlinear distortions. In [2.54, 2.55] a frequency allocation algorithm is proposed to assign the frequencies in a proficient way to minimize the distortion components falling onto the channel carriers, and thus improve the signal quality. All these above techniques improve the system linearity at the expense of the transmitter complexity.

Nonlinear predistortion techniques are also commonly used in radio-over-fiber systems. In [2.56], a look-up table based adaptive predistortion scheme is proposed to enhance the radio-over-fiber link linearity. There are two major issues in this approach. First, the total power into the laser must be known beforehand and the second is getting the feedback path for table

generation. A higher order adaptive filter based modeling and predistortion scheme is proposed in [2.57]. The filter is adapted from the distortions of vector modulated symbols, so that no in-depth information of physical link parameters is needed. But the power handling capability of the laser diode is the upper limit in this approach. Apart from that analog predistortion circuits have also been designed for the linearization of radio-over-fiber systems [2.58-2.61]. In this approach the RF signal is split into two parts. One part goes through the nonlinearity generation circuit (nonlinear path), while the other part goes through a time delay. Phase shifters and amplifiers are used in the nonlinear path to adjust the phase and magnitude of the generated third-order intermodulation products (IMD3). These two paths are then recombined to generate the IMD3 pre-added RF signal.

Another group of linearization method for radio-over-fiber systems is categorized as the post compensation scheme. In [2.62-2.65], the transmitter feedforward compensation based on distortion cancellation is widely investigated and found to be a promising technique for system linearization and dynamic range improvement, though in this technique the physical parameters of the system have to be known. In [2.66-2.69], signal processing based method has been investigated using various algorithms to estimate channel nonlinearity in radio-over-fiber systems, and the post compensations are carried out based on the channel estimation results. Both optical and wireless channels are considered in this method. Most of the radio-over-fiber systems use asymmetric compensation: predistortion for the downlink transmission and post compensation for the uplink transmission. It is because that this scheme allows for most of the signal processing to be done at the central station which is an important characteristic of radio-over-fiber technology.

2.3.3 Chromatic dispersion and compensation

The standard intensity modulation of optical carrier generates double-sideband (DSB) with carrier modulation format where the sidebands are located at the wireless carrier frequency

on either side of the optical carrier. Thus, due to the chromatic dispersion effects, each optical sideband propagates in the fiber at a different speed. Consequently, on arrival at the base station, the sidebands are phase shifted relative to the carrier. Since the base station's photodetector is a quadratic detector, the recovered power level of the signal is a function of this phase shift (Eq. 2.1). Thus, it suffers from periodical fading depending on the fiber length and on the square of the modulation frequency. For a radio-over-fiber link using an optical fiber with a length of L and a dispersion parameter of D, the power distribution as a function of microwave frequency is given by Eq. 2.2, where λ is the wavelength of the optical carrier, f_{RF} is the microwave frequency, and c is the velocity of light in vacuum [2.41]. Fig. 2.6 shows the power distribution of a double-sideband modulated signal in a single mode fiber, where the fiber dispersion parameter is 17-ps/nm.km, and the RF frequencies are 18 GHz, 36 GHz and 60 GHz respectively.

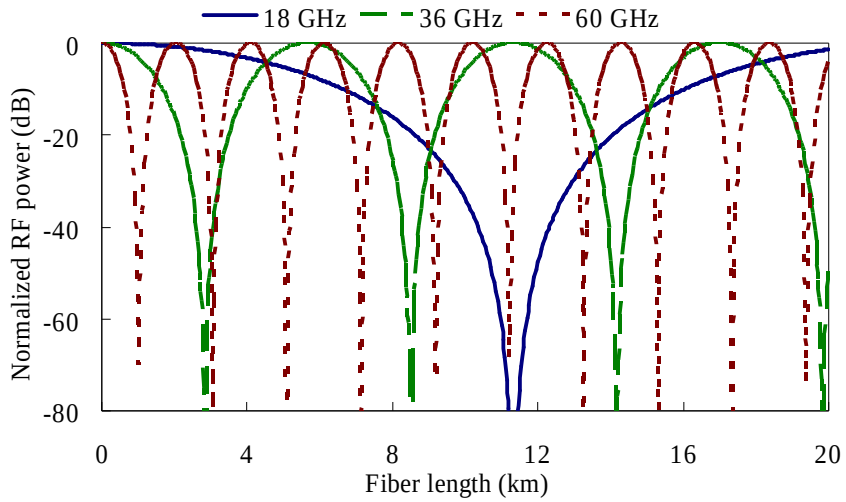

Fig.2.6 Power distribution as a function of transmission distance

$$\Phi = \frac{\pi L D \lambda^2 f_{RF}^2}{c} \tag{2.1}$$

$$P_{RF} \propto \cos^2\left(\frac{\pi L D \lambda^2 f_{RF}^2}{c}\right) \tag{2.2}$$

The straightforward way for dispersion compensation is by using a length of dispersion compensating fiber. But to maintain the cost effectiveness of radio-over-fiber technology, various techniques have been proposed and demonstrated to overcome dispersion effects. Chirped FBGs are commonly used for dispersion compensation in optical transmission systems, which provide higher equalization ratios [2.70-2.72]. Another technique is to compensate using optical phase conjugation [2.73-2.77], which is based on four-wave mixing (FWM) introduced in the dispersion-shifted fiber [2.74, 2.75] or the semiconductor optical amplifier (SOA) [2.76, 2.77]. This technique can also reduce the effects of fiber-induced self-phase modulation (SPM) [2.73].

The recent research on fiber-wireless issues have reported that the power fading drawback can be eliminated by transmitting a single-sideband signal [2.78]. Optical single-sideband (OSSB) generation has previously been achieved using the double modulation of a dual-electrode MZM [2.79] biased at quadrature or using a source integrating two electro-absorption modulators (EAM) [2.80]. Another effective solution for generating SSB signals relies on the suppression of one of the sidebands of a DSB signal by means of optical filtering, such as fiber gratings [2.81, 2.82] and arrayed waveguide gratings (AWG) [2.83]. In [2.84, 2.85], tunable optical filters are realized to suppress one sideband for dispersion compensation. However, a fixed 6-dB penalty is incurred in the generation of SSB. An optical double sideband signal with carrier suppressed also shows the characteristic of dispersion tolerance. In [2.86], an intensity-modulated two-tone optical signal is investigated and shows high tolerance to the fiber dispersion with a drawback that the linearity is limited by the sinusoidal transfer function of the MZM. In [2.87], the author generates the carrier suppressed signal by biasing the electro-optical modulator at the minimum transmission point and mitigates the impact of fiber dispersion. Similarly, in [2.88] the optical carrier suppression modulation scheme was employed by using a dual-electrode MZM in the central

office, combined with a same optical carrier remotely delivered to the base station for the uplink transmission.

2.3.4 Base station simplification

As we mentioned before, the most attractive characteristic of radio-over-fiber technique is the centralization of the processing functionalities in the central offices and the maximization of the equipments' sharing to minimize the cost per user, as well as the deployment of the simple, compact base stations to achieve cost and energy efficiencies.

To simplify the base station by reducing the component counts, a dual-functional electro-absorption modulator (EAM) transceiver has been introduced to replace the laser and the photodiode at the base station antenna unit in the radio-over-fiber link and hence produces the potential of cost reduction. The EAM transceiver partially absorbs the light coming from the central office, and allowing the remaining light passes through. Therefore, the EAM act as a photodiode for the downlink transmission and as a laser for the uplink transmission. Single-source bidirectional systems are demonstrated in [2.89] and [2.90] (Fig. 2.7). However, in both cases, the electrical bias has to be adjusted to achieve either efficient optical modulation or detection. This requires a bias control circuitry at the base station and only allows for half-duplex transmission which is bi-directional but not simultaneous. The first full duplex operation of an EA device that can be used as a photodetector and as a modulator simultaneously is demonstrated in a frequency division multiplexed (FDM) analog system using separate forward and reverse RF bands [2.91, 2.92]. A 1.55-μm InGaAsP/InP EA MQW waveguide device is presented and shown to be an attractive solution for full-duplex fiber-optic transmission using dual-function modulator/photodetector in [2.93, 2.94]. A dual-lightwave approach is used in conjunction with an EA transceiver (EAT) to simultaneously achieve optimum modulation and detection performances (Fig. 2.8). The full-

duplex transmission is demonstrated in a point-to-point fiber-optic link using SCM, as well as in a point-to-multipoint fiber-optic ring network using WDM.

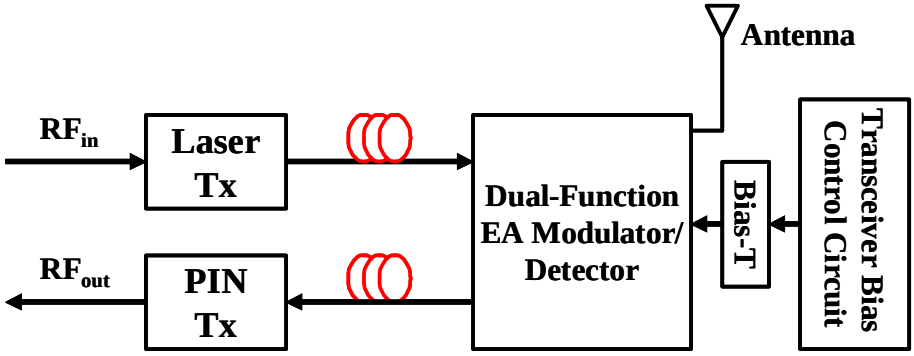

Fig.2.7 Single-source half-duplex scheme

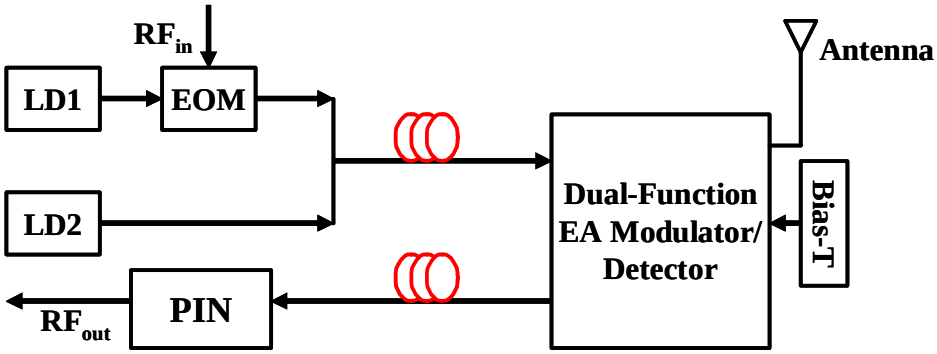

Fig.2.8 Dual-lightwave full-duplex scheme

The EAM transceiver does not only simplify the O/E interface, but also realizes the wavelength reuse in the base station by using the unabsorbed downlink optical signal as the uplink optical carrier. The simplification of base station by removing the light source from

the uplink using wavelength reuse technique can also be implemented by using MZMs. In [95, 96], two wavelength reuse configurations are introduced using optical single sideband with carrier (OSSB+C) modulation format. In the first design, the incoming downstream signal is split equally by a 50:50 optical coupler. One part of the signal is then input into a PD, which converts the signal into an electrical downstream signal. The other part of the downstream optical signal is injected into a custom designed FBG having a transmission profile where the transmission at the wavelength corresponding to the downstream modulation sideband is close to zero and the transmission elsewhere is close to 100%. The downstream modulation sideband is reflected while the optical carrier is passed through to be reused for the upstream transmission. The second design is based on an optical circulator in conjunction with an FBG filter. The downstream signal is injected into Port 1 of the optical circulator. The signal output from Port 2 of the circulator is then passed through FBG, which has 50% reflectivity at the wavelength corresponding to the downstream optical carrier. The reflected carrier (50%) is collected at Port 3 of the circulator and then reused for the upstream, and the passing through signal is used to recover the RF signal. Another approach is to take advantage of optical interleaving, which also makes it easily cooperate with WDM/DWDM systems [2.97, 2.98]. As shown in Fig. 2.9, an MZM is biased at the minimum operation point driving by a push-pull sinusoidal electrical clock signal to realize the carrier suppression and generate two sidebands [2.98]. Then the two sidebands are separated by an optical interleaver. The lower band is modulated to carry the downlink data, while the upper band is directly delivered to the base station. In the base station, another optical interleaver is employed to separate the two bands for signal detection and wavelength reuse purposes respectively.

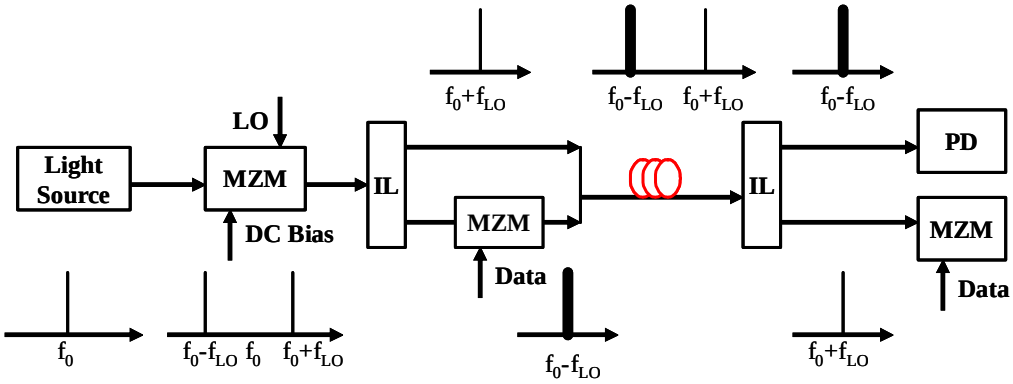

Fig.2.9 Wavelength reuse via optical interleaver

As we discussed before, the impact of fiber chromatic dispersion becomes more severe when the transmitting RF frequency is higher. If transmitting IF or BB signals to overcome dispersion, the frequency up/down conversion has to be implemented in the base station. As a result, the base station will become complex with the additional requirement of mixers and LOs. The remote delivering of the LO signal is considered as a way to simplify the base station as well as to reduce the link cost. In [2.99, 2.100], the LO signal is modulated on an optical carrier and delivered together with the downlink data, and in the base station the local oscillator signal is separated by a bandpass filter and used for frequency up/ down conversion.

Wavelength reuse and LO free techniques can be combined for further base station simplification, and it is first realized in [2.101]. The optical carrier is modulated with a radio signal and a LO signal. In the base station, part of the signal is photodetected to regenerate the radio signal. The remaining part of the optical signal is modulated by the uplink radio signal, and a number of frequency components in optical domain are generated including the downconverted uplink signal which will be extracted using optical bandpass filter and then used for uplink transmission. In this technique, only frequency downconversion for uplink is

realized and it is done in the optical domain using an MZM. In [2.102, 2.103], the optical source carrying both the IF signal and the local oscillator signal is transmitted to the base station. Similarly part of the optical carrier signal is filtered out for uplink wavelength reuse, and the other part is photodetected to recover both the IF signal and the LO signal. Then, the LO signal is use to upconvert the IF signal to the desired wireless carrier frequency for downlink wireless transmission as well as to downconvert the received upstream RF signal to an IF signal before optical transmission. In this case, the frequency conversion functionality is realized in the electrical domain and it is applicable for both downlink and uplink.

Recently, a photonic frequency downconversion method using bandpass sampling [2.104, 2.105] is proposed to realize low-cost base station without mixers and LOs [2.15, 2.106]. It uses direct optical switching-encoding scheme to sample the optical signal, which can spread the signal over the entire optical spectrum and enabling frequency downconversion to be established. The uplink transmission scheme is given in Fig. 2.10. In the base station, the optical signal is directly modulated by the radio signal, and then launched into an MZM. The MZM is modulated by on-off pulse sequence and acts as a photonic sampler. In the central office, the signal is detected and filtered to obtain the IF band image and recover the data.

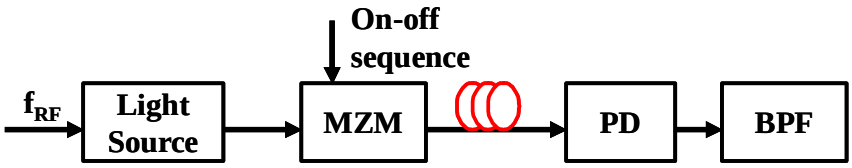

Fig.2.10 Frequency downconversion using photonic sampling

However, external modulation using MZMs in the base station is not desirable because it has no significant performance benefits and of much higher cost. A simple and straightforward intensity-modulation and direct-detection (IM-DD) system, as well as low cost optoelectronics devices are always preferred for a compact low-cost base station

configuration. Great dynamic range and high linearity are required for the optical devices to guarantee a good system performance and to avoid channel crosstalk and nonlinear effects. In the last few years the new generation of semiconductor lasers, the vertical cavity surface emitting lasers (VCSEL) has proven to be competitive to the conventional, high performance edge emitting communication lasers [2.107, 2.108]. VCSELs produced in research labs have been reported with SFDR values of up to 100dB.Hz$^{2/3}$ [2.109], and proved to have sufficient link performance and great economic benefits. Moreover, VCSELs are recognized as promising candidates for picocell radio-over-fiber networks for in-building wireless transmissions, which requests a large number of antenna base stations [2.35, 2.110, 2.111].

2.4 Multiplexing techniques

In order to meet the increasing demand of bandwidth and to maximize the sharing of the existing fiber optical infrastructure to achieve cost efficiency, it becomes necessary to increase spectrum efficiency, centralize multiple services in a single base station, as well as enabling co-existence of wired and wireless optical network. Multiplexing techniques, such as WDM, SCM and multi-band (BB, IF and RF) transmission, have been long considered as solutions to these issues.

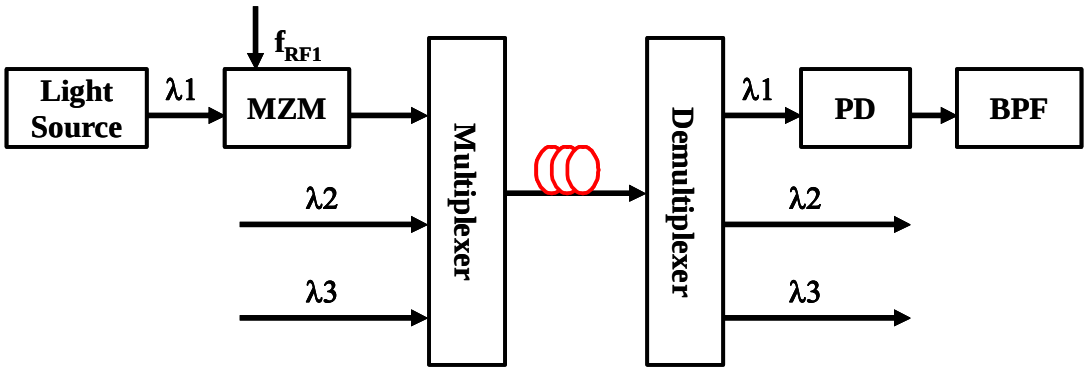

Fig.2.11 Schematic of WDM fiber-wireless networks

The transmission of radio-over-fiber signals is seen to be spectrally inefficient as the modulation bandwidth is only a small fraction of the optical carrier signal frequency. WDM technology is able to improve the spectral usage for radio-over-fiber and enables efficient exploitation of the fiber network's bandwidth. The distribution of radio-over-fiber signals over WDM networks has gained more importance recently, since it can significantly improve the spectrum efficiency and the number of base stations supported by one central office. Fig. 2.11 shows a schematic of a WDM fiber-wireless architecture incorporating OSSB+C modulation format to overcome fiber chromatic dispersion. Carriers modulated with RF signals are added to a fiber using multiplexers. The multiplexed signals are then transported to the remote nodes (RN), where the individual optical mm-wave signals are demultiplexed and sent to their corresponding base stations. The optical add/drop multiplexing technique plays an important role in the seamless integration of radio-over-fiber networks with WDM networks, and many research has been carried out to realize the WDM optical interface for fiber radio antenna base stations [2.112-2.115].

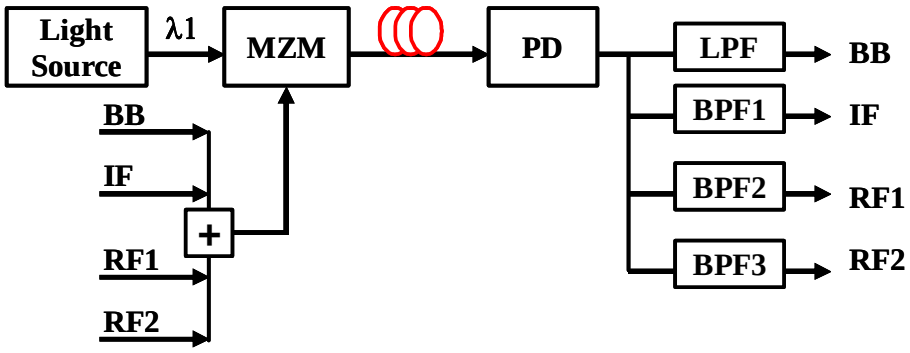

Fig.2.12 Schematic of SCM fiber-wireless networks

With various last-mile solutions emerging, it is a trend for radio-over-fiber technologies to coexist with other optical access technologies within the existing infrastructure, and to support multiple wireless services' simultaneous transmission. SCM is a cost effective

approach to implement the multi-band transmission, including BB, IF and RF, simultaneously, while co-existing with other access technologies. This technique has the potential for future FTTH access networks combined with wireless access supported by an RoF wireless feeder. As shown in Fig. 2.12, signals at different bands are electrically combined before modulating the optical carrier, and then transmitted over a single fiber. At the receiver side, filters are used after the photodetector to obtain different signal bands. 3G signals distribution based on PON using SCM technique is successfully demonstrated in [2.116, 2.117]. In [2.118], the multi-band modulation and fiber-optic transmission of a 2.5 Gb/s baseband signal, a 3.5–12.0 GHz microwave signal, and a 60 GHz millimeter wave signal are reported. In [2.138] and [2.139], subcarrier modulated multimode fiber links are demonstrated for local area networks (LANs) with multimode fibers (MMF) already installed. In addition, the system can be further simplified using WDM in conjunction with SCM [2.119, 2.120], where a different WDM channel can feed each BS and different SCM channels can carry different wireless services within one BS.

2.5 Green access networks

In the last decade, global warming has become an increasingly important item on the global political agenda. In December 2008, the European Commission (EC) decided to cut greenhouse gas emissions by 20%, to establish a 20% share for renewable energy, and to improve energy efficiency by 20% [2.121]. Information and communication technology (ICT) has a profound impact on the environment, and the energy consumption of ICT is currently becoming a social and political issue [2.122]. Within ICT, the telecommunication sector, with a rapid increasing due to the growth of traffic demanding, plays a significant role in developing energy-efficient (“green”) solutions for future ICT with environmental sustainability. The modern telecommunication network can be generally divided into three parts, namely the access network, the core network and the transmission network. The energy

consumptions of these three parts are extremely different. The access network, known as the ‘last mile’ of telecommunication network, is the main contributor since it contains large numbers of active elements. The proportion of access network in the modern telecommunication network varies from 50% to 70% as a result of different operating environments [2.123], and it will continue to consume a major portion of overall internet energy consumption during the next decade with the ever-increasing demand for bandwidth [2.124].

In order to increase the bit rates in access environment, a lot of efforts were concentrated on high-capacity fiber-based optical transmission in fixed access networks. Consequently, energy consumptions of these networks have attracted enormous attention from researchers around the world. Energy consumption models have been built for a number of competing high-speed technologies including PON, fiber to the node (FTTN), FTTH and point-to-point (PtP) optical systems as well as for traditional DSL and HFC technologies [128, 129]. The FTTH technology based on PON has a clear energy advantage. Results show that the customer modem or optical network unit (ONU) consumes over 65% of the total power in the access network. This implies that the power consumption of the access network could be significantly reduced through the use of automated sleep modes in customer premises network equipment [2.130].

In wireless access networks, the wireless base station accounts for up to 70% of the total power consumption in a number of mobile operators, and it is found to have the most feasible energy-saving potential [2.123]. In recent years, there are many researchers dedicated in ‘greening’ the wireless base station and can be catalogued into three groups according to the different approaches used in reducing the energy waste. The first approach is to simplify the base station architecture by eliminating the active elements and improving the energy efficiency of base station components. At present, radio frequency power amplifier (PA) accounts for 40% of the power consumption of a 3G wireless base station. Various RF

amplifier design techniques are proposed to increase the amplifier efficiency [2.125, 2.131, 2.132]. In addition, digital pre-distortion processor is widely used in 3G base stations to maximize the efficiency and linearity of the power amplifiers [2.133, 2.134]. An alternative option of base station energy-saving is to reduce the energy waste of the feeder, which leads to about on average a 50% loss of power at a typical site and has a significant impact on the coverage ability of a particular base station site. This problem can be solved by deploying distributed base station architecture and through the design of smaller base stations. A baseband unit (BBU) + remote radio unit (RRU) solution is proposed to mitigate the feeder loss, as the RRU is mounted on top of buildings near the antenna and connected with BBU via optical fiber [2.135]. Meanwhile, new base station controller with boosted capacity is developed to simplify the base station sites [2.136], and more and more small size base stations such as pico-cell or femto-cell are used for efficient coverage expansion.

The second approach is to reduce energy waste during idle time and build up an energy aware network [2.122]. Traffic levels and demands for service within the busy and idle time of the mobile network are not evenly distributed. The most effective energy saving technology is the based on “base station turn-off” technology. The high frequency site is switched off in low-traffic periods and re-powered to on-status when the traffic level pick up based on a predetermined demand threshold. The turning-off of a base station in period of low or zero demand results in significant power consumption savings. Energy-aware design techniques and routing protocols are also very attractive in reducing energy waste. Different mathematical models are proposed to balance the power consumption, performance and robustness of the whole network [2.122, 2.137].

The third approach is targeted at the base station cooling system. Innovative cooling techniques as well as new air-conditioning solutions are widely investigated to achieve the energy efficiency [2.126, 2.127].

2.6 Summary

A comprehensive literature review on the investigation of the radio-over-fiber technologies has been presented in this chapter. Section 2.1 introduced the radio-over-fiber systems and their benefits in terms of high bandwidth, low attenuation, immunity to EMI, low power consumption and multi-service operation ability. Section 2.2 presented three conventional analog radio-over-fiber schemes (BBoF, IFoF and RFoF) and two novel digital radio-over-fiber schemes (Digitized IFoF, Direct-Digitized RFoF), and discussed their advantages as well as disadvantages. In section 2.3, various implementation issues and previous research were reviewed. In 2.3.1, three RF generation techniques were discussed. In 2.3.2, linearization techniques were reviewed. In 2.3.3, chromatic dispersion and various compensation solutions were presented. In 2.3.4, base station simplification techniques were discussed in details. Section 2.4 presents the multiplexing techniques incorporating radio-over-fiber systems, such as WDM, SCM, and multi-band transmission. The last section of this chapter focuses on the power consumption and energy-efficient solutions in access networks.

2.7 Reference

[2.1] R J. E. Mitchell, “Techniques for Radio over Fiber Networks,” Annual Meeting of the IEEE Lasers an Electro-Optics Society (LEOS), pp. 346-347, 2006.

[2.2] I. Dayoub, “Radio over Fiber networks: Low cost solution for different applications and emerging technologies,” Information and Communication Technologies, vol. 2, pp. 2537-2542, 2006.

[2.3] D. K. Mynbaev, L. L. Scheiner, “Fiber Optic Communications Technology”, 2001.

[2.4] D. Novak, “Fiber Optics in Wireless Applications”, Conference on Optical Fiber communication/National Fiber Optic Engineers Conference OFC/NFOEC, Short Course 217, 2004.

[2.5] J. Capmany, B. Ortega, D. Pastor, and S. Sales, “Discrete-Time Optical Processing of Microwave Signals”, Journal of Lightwave Technology, vol. 23, no. 2, 2005.

[2.6] Anthony Ng’oma, Radio-over-Fibre Technology for Broadband Wireless Communication Systems, Ph.D thesis, 2005.

[2.7] W. Chen and W. Way, "Multi-channel signal-sideband SCM/DWDM transmission systems," J. Lightw. Technol., vol. 22, no. 7, pp. 1679-1693, Jul. 2004.

[2.8] C. Lim, A. Nirmalathas, M. Attygalle, D. Novek, and R. Waterhouse, "On the merging of millimeter-wave fiber-radio backbone with 25 GHz WDM ring networks," J. Lightw. Technol., vol. 21, no. 10, pp. 2203-2210, Oct. 2003

[2.9] U. Gliese, S. Norskow, and T. N. Nielsen, "Chromatic Dispersion in Fiber-Optic Microwave and Millimetre-Wave Links," IEEE Trans. Microwave Theory Tech., vol. 44, no. 10, pp. 1716.1724, Oct. 1996.

[2.10] Christina Lim, Ampalavanapillai Nirmalathas, Dalma Novak, and Rod Waterhouse, "Millimeter-Wave Broad-Band Fiber-Wireless System Incorporating Baseband Data Transmission over Fiber and Remote LO Delivery," Journal of Lightwave Technology, vol. 18, no. 10, 2000.

[2.11] Christina Lim, Ampalavanapillai Nirmalathas, Masuduzzaman Bakaul, Prasanna Gamage, Ka-Lun Lee, Yizhuo Yang, Dalma Novak, and Rod Waterhouse, "Fiber-Wireless Networks and Subsystem Technologies" Journal of Lightwave Technology, vol. 28, no. 4, 2010.

[2.12] E. I. Ackerman and C. H. Cox, "RF Fiber-Optic Link Performance," IEEE Microwave, pp. 50-58, 2001.

[2.13] P. M. Wala, "A new microcell architecture using digital optical transport," in Proc. 43rd IEEE Trans. Veh. Technol. Conf., pp. 585-588, 1993.

[2.14] D. Novak and A. Nirmalathas, "Fibre-radio: challenges and possible solutions," IEEE International Topical Meeting on Microwave Photonics, 2003.

[2.15] T. Higashino, K. Tsukamoto, and S. Komaki, "Proposal of Photonic Frequency-Conversion Method Using Bandpass Sampling in Multicarrier Operated Radio-on-Fiber Link," IEEE Transactions on Microwave Theory and Technologies, vol. 54, no. 2, 2006.

[2.16] O'Reilly J, "Optical Generation and Delivery of Modulated mm-waves For Mobile Communications," in Analogue Optical Fibre Communications, pp.229 – 256, 1995.

[2.17] L. N. Langley, "Packaged Semiconductor Laser Optical Phase-Locked Loop (OPLL) for Photonic Generation, Processing and Transmission of Microwave Signals," IEEE Trans. On Microwave Theory and Techniques, pp.1257 – 1264, July 1999.

[2.18] Y. J. Wen, D. Novak, Y. Ogawa, "Millimeter-Wave Signal Generation From a Monolithic Semiconductor Laser via Subharmonic Optical Injection," IEEE Photonics Tech. Letters, pp.1058 – 1060, 2000.

[2.19] L. A. Johansson, and A. J. Seeds, "36 GHz 140 –Mb/s Radio-Over-Fibre Transmission Using an Optical Injection Phase-Lock Loop Source," IEEE Photonics Technology Letters, pp.893 – 895, 2001.

[2.20] D.Wake, M.Webster, G.Wimpenny, K.Beacham, and L.Crawford, “Radio over fiber for mobile communications,” IEEE International Topical Meeting on Microwave Photonics, 2004.

[2.21] CPRI Specification v4.0 at www.cpri.info

[2.22] OBSAI Specification v2.0 at www.obsai.com

[2.23] David Wake, Silvia Pato, Joao Pedro, Esther Lopez, Nathan Gomes, and Paulo Monteiro, “A Comparison of Remote Radio Head Optical Transmission Technologies for Next Generation Wireless Systems,” Annual Meeting of the IEEE Lasers an Electro-Optics Society (LEOS), 2009.

[2.24] Christian F. Lanzani, “OBSAI RP3-01 6.144 Gbps Interface Implementation,” at http://www.obsai.org/obsai/latest_news

[2.25] Christina Lim, Ampalavanapillai Nirmalathas, Yizhuo Yang, Dalma Novak, and Rod Waterhouse, “Radio-over-Fiber Systems,” Communications and Photonics Conference and Exhibition (ACP), 2009.

[2.26] U. Gliese, T. N. Nielsen, S. Norskov, and K. E. Stubkjaer, “Multifunctional fiber-optic microwave links based on remote heterodyne detection,” IEEE Transactions on Microwave Theory and Technologies, vol. 46, no. 5, 1998.

[2.27] J. J. OReilly, P. M. Lane, R. Heidemann, and R. Hofstetter, “Optical generation of very narrow linewidth millimetre wave signals,” Electronics Letters, vol: 28 , Issue: 25, 1992.

[2.28] J. Yu, Z. Jia, T.Wang, and G. K. Chang, “Centralized lightwave radio-over-fiber system with photonic frequency quadrupling for high-frequency millimeter-wave generation,” IEEE Photon. Technol. Lett., vol. 19, no. 19, pp. 1499–1501, Oct. 2007.

[2.29] J. Zhang, H. Chen, M. Chen, T. Wang, and S. Xie, “A photonic microwave frequency quadrupler using two cascaded intensity modulators with repetitious optical carrier suppression,” IEEE Photon. Technol. Lett., vol. 19, no. 14, pp. 1057–1059, Jul. 2007.

[2.30] Hao Chi, and Jianping Yao, “Frequency Quadrupling and Upconversion in a Radio Over Fiber Link,” Journal of Lightwave Technology, vol. 26, no. 15, 2008.

[2.31] Xiangfei Chen, Zhichao Deng, and Jianping Yao, “Photonic generation of microwave signal using a dual-wavelength single-longitudinal-mode fiber ring laser,” IEEE Transactions on Microwave Theory and Techniques, vol. 54, no. 2, pp. 804-809, 2006.

[2.32] Markus Junker, Thomas Schneider, Max J. Ammann, Andreas T. Schwarzbacher, Kai-Uwe Lauterbach, Ronny Henker, and Steffen Neidhardt, “32 GHz Carrier Generation and 200 Mbit/s Error Free Data Transmission in a Radio Over Fibre System,” IET Irish Signals and Systems Conference, 2008.

[2.33] Markus Junker, Thomas Schneider, Kai-Uwe Lauterbach, and Ronny Henker, “High Quality Millimeter Wave Generation via Stimulated Brillouin Scattering,” Conference on Lasers and Electro-Optics (CLEO), 2007.

[2.34] Jianping Yao, “Microwave Photonics,” Journal of Lightwave Technology, vol. 27, no. 3, 2009.

[2.35] A. M. J. Koonen, and M. García Larrodé, “Radio-Over-MMF Techniques—Part II: Microwave to Millimeter-Wave Systems,” Journal of Lightwave Technology, vol. 26, no. 15, 2008.

[2.36] A. Ng’oma, A.M.J. Koonen, I. T.Monroy, H. P. A. Boom, and G. D. Khoe, “Using optical frequency multiplication to deliver a 17 GHz 64 QAM modulated signal to a simplified radio access unit fed by multimode fiber,” Optical Fiber Communication Conference (OFC/NFOEC), 2005.

[2.37] K.Yiannopoulos , K. Vyrsokinos, E. kehayas, N. Pleros, K. Vlachos, H. Avramopoulos, and G. Guekos, “Rate Multiplication by Double Passing Fabry-Perot Filtering,” Photonics Technology Letters, vol. 15, Issue: 9, pp. 1294-1296, 2003.

[2.38] P. Petropoulos, M.lbsen, M.N.Zervas, and OJ. Richardson, "Generation of a 40-GHz pulse stream by pulse multiplication with a sampled fiber Bragg grating," Optics Letters, vol. 25, Issue: 8, pp. 521-523, 2000.

[2.39] Guohua Qi, Jianping Yao, Joe Seregelyi, Stéphane Paquet, and Claude Bélisle, “Optical generation and distribution of continuously tunable millimeter-wave signals using an optical phase modulator,”Journal of Lightwave Technology, vol. 23, no. 9, 2005.

[2.40] T. Kurniawan, and A. Nirmalathas, “Performance Analysis of Optimized Millimetre-Wave Fibre Radio Links,” IEEE Transaction on Microwave Theory Technology, vol. 54, Issue: 2, 2006.

[2.41] R. Ramaswami, “Optical Networks: a practical perspective,” 2rd edition, 2001.

[2.42] Philip M. Wala, “A new microcell architecture using digital optical transport,” IEEE Vehicular Technology Conference, 1993.

[2.43] T. Tsucluya, T. Shiraishi and J. Arata, “An estimation of input dynamic range and CA characteristic on the design of optical fibre for mobile communication,” Fibre Network for Telephony and CATK SPIE, 1991.

[2.44] S. K. Korotky and R. M. DeRidder, “Dual parallel modulation schemes for low-distortion analogue optical transmission,” IEEE J. Sel. Areas Commun., vol. 8, pp. 1377-1380, 1990.

[2.45] J. L. Brooks, G. S. Maurer, and R. A. Becker, “Implementation and evaluation of a dual parallel linearization system for AM-SCM video transmission,” Journal of Lightwave Technology, vol. 11, no. 1, pp. 34-41, 1993.

[2.46] A. Djupsjobacka, “A linearization concept for integrated-optic modulators,” IEEE Photon. Technology Letters, vol. 4, no. 8, 1992.

[2.47] H. Skeie and R. V. Johnson, “Linearization of electro-optic modulators by a cascade coupling of phase modulating electrodes,” Proc. SPIE, vol. 1583, pp. 153-164, 1991.

[2.48] G. E. Betts, “Microwave Analog Optical Links Using Suboctave Linearized Modulators,” IEEE Photonics Technology Letters, vol. 8, no. 9, 1996.

[2.49] Sang-Hoon Lee, Jeung-Mo Kang, In-Hyuk Choi, and Sang-Kook Han, “Linearization of DFB Laser Diode by External light injected cross gain modulation for radio overf fiber link,” IEEE Photonics Technology Letters, vol. 18, no. 14, 2006.

[2.50] Sang-Hoon Lee, Jeung-Mo Kang, Yong-Yuk Won, Hyuk-Choon Kwon, and Sang-Kook Han, “Linearization of RoF optical source by using light injected gain modulation,” International Topical Meeting on Microwave Photonics, 2005.

[2.51] Caiqin Wu and Xiupu Zhang, “Impact of Nonlinear Distortion in Radio Over Fiber Systems With Single-Sideband and Tandem Single-Sideband Subcarrier Modulations,” Journal of Lightwave Technology, vol. 24, no. 5, 2006.

[2.52] C.Lim, and A. Nirmalathas, “Intermodulation Distortion Improvement for Fiber–Radio Applications Incorporating OSSB+C Modulation in an Optical Integrated-Access Environment,” Journal of lightwave technology, vol. 25, no. 6, 2007.

[2.53] Biagio Masella, and Xiupu Zhang, “Novel Single Wavelength Balanced System for Radio Over Fiber Links,” Journal of lightwave technology, vol. 18, no. 1, 2006.

[2.54] W. I. Way, “Optical fibre based microcellular systems: An overview,” IEICE Transaction on Communication., pp. 1091–1102, 1993.

[2.55] C. K. Chan, and L. K. Chen, “Efficient frequency assignment scheme for intermodulation distortion reduction in fibre-optic microcellular systems,” Electronics Letters, vol. 30, no. 22, 1994.

[2.56] Xavier N. Fernando, “Look-up table based adaptive predistortion for DR enhancement in a radio over fibre link,” IEEE Pacific Rim Conference on Communications, Computers and Signal Processing, 1999.

[2.57] Xavier N. Fernando, and Abu B. Sesay, “Higher order adaptive filter Characterization of Microwave fibre Optic link Nonlinearity,” Proceedings of Optical Pulse and Beam Propagation, SPIE Conference, 2000.

[2.58] A.R. Shah, and B. Jalali, “Adaptive equalisation for broadband predistortion linearisation of optical transmitters,” IEE Proceedings on Optoelectronics, vol. 152, Issue. 1, 2005.

[2.59] L. Roselli, V. Borgioni, F. Zepparelli, F. Ambrosi, M. Comez, P. Faccin, and A. Casini, “Analog laser predistortion for multiservice radio-over-fiber systems,” Journal of lightwave technology, vol. 21, no. 5, pp. 1211-1221, 2003.

[2.60] Yiming Shen, Bouchaib Hraimel, Xiupu Zhang, Glenn E. R. Cowan, KeWu, Fellow, and Taijun Liu, “A Novel Analog Broadband RF Predistortion Circuit to Linearize Electro-Absorption Modulators in Multiband OFDM Radio-Over-Fiber Systems,” IEEE Transactions on Microwave Theory and Technologies, vol. 58, no. 11, 2010.

[2.61] Shingo Tanaka, Noritaka Taguchi, Tsuneto Kimura, and Yasunori Atsumi, "A Predistortion-Type Equi-Path Linearizer Designed for Radio-on-Fiber System," IEEE Transactions on Microwave Theory and Technologies, vol. 54, no. 2, 2006.

[2.62] R. S. Tucker, "High speed modulation of semiconductor lasers," Journal of lightwave technology, pp. 1180-1192, 1985.

[2.63] P. Raziq and M. Nagakawa, "Semiconductor laser's nonlinearity compensation for DS-CDMA optical transmission system by post nonlinearity recovery block," IEICE Transaction on Communications, 1996.

[2.64] L. S. Fock and R. S. Tucker, "Simultaneous reduction of intensity noise and distortion in semiconductor laser by feed forward compensation," Electronic Letters, pp. 1297–1298, July 1991.

[2.65] Tabassam Ismail, Chin-Pang Liu, John E. Mitchell, and Alwyn J. Seeds, "High-dynamic-range wireless-over-fiber link using feedforward linearization," Journal of lightwave technology, pp. 3274-3282, 2007.

[2.66] Xavier N. Fernando, and Abu B. Sesay, "Nonlinear channel estimation using correlation properties of PN sequences," Canadian Conference on Electrical and Computer Engineering, 2001.

[2.67] Stephen Z. Pinter, and Xavier N. Fernando, "Estimation and Equalization of Fiber-Wireless Uplink for Multiuser CDMA 4G Networks," IEEE transactions on communications, vol. 58, no, 6, 2010.

[2.68] Carlos A. R. Fernandes, Alain Kibangou, G´erard Favier, and Jo˜ao C. M. Mota1, "Identification of Nonlinear MIMO Radio Over Fiber Uplink Channels," International Telecommunications Symposium, 2006.

[2.69] Hongwen Tang, and Guangxi Zhu, "Nonlinear Channel Estimation for the Radio over Fiber Uplink," 4th International Conference on Wireless Communications, Networking and Mobile Computing, 2008.

[2.70] H. Sun, M. Kardakli, and K. Feng, "Tunable RF power fading compensation of multiple channel double-sideband SCM transmission using a non-linearly chirped FBG," IEEE Photonics Technolology Letters, vol. 12, no. 5, pp. 546-548, 2000.

[2.71] J. Marti, D. Pastor, and M. Tortola, "On the use of tapered linearly chirped gratings as dispersion-induced distortion equalizers in SCM systems," Journal of lightwave technology, vol. 15, no. 2, pp. 179-187, 1997.

[2.72] S. Chandra, A. Vishnu Vardhanan, and R. Gangopadhyay, "Compensation of chromatic dispersion-induced power fading using optimised chirped fibre Bragg grating for millimetre-wave radio-over-fibre system," IET Circuits Devices and Systems, vol. 2, no. 1, pp. 123-127, 2008.

[2.73] S. Watanabe, and M. Shirasaki, "Exact compensation for both chromatic dispersion and Kerr effect in a transmission fiber using optical phase conjugation," Journal of lightwave technology, vol. 14, pp. 243-248, 1996.

[2.74] R. M. Jopson, and A. H. Gnauck, “Compensation of fibre chromatic dispersion by spectral inversion,” Electronics Letters, 1993.

[2.75] F. Ramos, J. Marti, and V. Polo, “Compensation of Chromatic Dispersion Effects in Microwave/Millimeter-Wave Optical Systems Using Four-Wave-Mixing Induced in Dispersion-Shifted Fibers,” IEEE Photonics Technology Letters, vol. 11, no. 9, 1999.

[2.76] Ken-ichi Kitayama and Hideyuki Sotobayashi, “Fading-free fiber-optic transport of 60GHz-optical DSB signal by using in-line phase conjugator,” Conference on Optical Fiber communication/National Fiber Optic Engineers Conference OFC/NFOEC, 1999.

[2.77] M.C. Tatham, G. Sherlock, and L.D. Westbrook, “Compensation fibre chromatic dispersion by optical phase conjugation in a semiconductor laser amplifier,” Electronics Letters, vol. 29, Issue: 21, pp. 1851-1852, 1993.

[2.78] C. Lim, A. Nirmalathas, M. Bakaul, P. Gamage, K. L. Lee, Y. Yang, D. Novak, and R. Waterhouse, “Fiber-Wireless Networks and Subsystem Technologies,” Journal of lightwave technology, vol. 28, no. 4, 2010.

[2.79] G. H. Smith, D. Novak, and Z. Ahmed, “Overcoming chromatic-dispersion effects in fiber-wireless systems incorporating external modulators,” IEEE Transactions on Microwave Theory and Technologies, vol. 45, pp. 1410-1415, 1997.

[2.80] E. Vergnol, F. Devaux, D. Tanguy, and E. Pénard, “Integrated lightwave millimetric single side-band source: Design and issues,” Journal of lightwave technology, vol. 16, pp. 1276-1284, 1998.

[2.81] J. Park, W. V. Sorin, and K. Y. Lau, “Elimination of the fibre chromatic dispersion penalty on 1550 nm millimetre-wave optical transmission,” Electron. Letters, vol. 33, no. 6, pp. 512–513, 1997.

[2.82] K. Yonenaga and N. Takachio, “A fiber chromatic dispersion compensation technique with an optical SSB transmission in optical homodyne detection systems,” IEEE Photonics Technology Letters, vol. 5, no. 8, pp. 949-951, 1993.

[2.83] J. Capmany, D. Pastor, P. Munoz, S. Sales, B. Ortega, and A. Martinez, “WDM-SSB generation and dispersion mitigation in radio over fiber systems with improved performance using an AWG multiplexer with flat top resonances,” International Topical Meeting on Microwave Photonics, 2003.

[2.84] E. Vourch, D. Le Berre, and D. Herve, “Lightwave single sideband wavelength self-tunable filter using InP:Fe crystal for fiber-wireless systems,” IEEE Photonics Technology Letters, vol. 14, no. 2, pp. 194–196, 2002.

[2.85] M. V. Drummond, R. N. Nogueira, P. Monteiro, M. A. Violas, C. Stemer, and P. Fonjallaz, “Tunable Optical Dispersion Compensator Based on Power Splitting Between Two Dispersive Media,” Journal of lightwave technology, vol. 28, no. 8, 2010.

[2.86] R. A. Griffin, P. M. Lane, and J. J. O’Reilly, “Dispersion-tolerant subcarrier data modulation of optical millimetre-wave signals,” Electronic Letters, vol. 32, no. 24, pp. 2258-2260, 1996.

[2.87] J. M. Fuster, J. Marti, and J. L. Corral, “Chromatic dispersion effects in electro-optical upconverted millimetre-wave fibre optic links,” Electronic Letters, vol. 33, no. 23, pp. 1969-1970, 1997.

[2.88] Z. Jia, J. Yu, and G.-K. Chang, “A full-duplex radio-over-fiber system based on optical carrier suppression and reuse,” IEEE Photonics Technology Letters, vol. 18, no. 16, pp. 1726–1728, Aug. 2006.

[2.89] R.B. Welstand, S.A. Pappert, C.K. Sun, J.T. Zhu, Y.Z. Liu, and P.K.L. Yu, “Dual-function electroabsorption waveguide modulator/detector for optoelectronic transceiver applications,” Photonics Technology Letters, vol. 8, Issue: 11 , 1996.

[2.90] T. H. Wood, E. C. Carr, B. L. Kasper, R. A. Linke, C. A. Burrus, and K. L, Walker, “Bidirectional fibre-optical transmission using a multiple-quantum-well (MQW) modulator/detector ,” Electronics Letters, vol. 22 , Issue: 10, 1986.

[2.91] L.D. Westbrook, and D.G. Moodie, “Simultaneous bi-directional analogue fibre-optic transmission using an electroabsorption modulator,” Electronics Letters, vol. 32, Issue: 19, 1996.

[2.92] L. D. Westbrook, L. No¨el, and D. G. Moodie, “Full-duplex, 25 km analogue fiber transmission at 120 Mbytes/s with simultaneous modulation and detection in an electroabsorption modulator,” Electronic Letters, vol. 33, no. 8, pp. 694–695, 1997.

[2.93] Andreas Stohr, Ken-ichi Kitayama, and Dieter Jager, “Error-free full-duplex optical WDM-FDM transmission using an EA-transceiver,” International Topical Meeting on Microwave Photonics, 1998.

[2.94] Andreas Stohr, Ken-ichi Kitayama, and Dieter Jager, “Full-Duplex Fiber-Optic RF Subcarrier Transmission Using a Dual-Function Modulator/Photodetector,” IEEE Transactions on Microwave Theory and Technologies, vol. 47, no. 7, 1999.

[2.95] A. Nirmalathas, C. Lim, D. Novak, and R. Waterhouse, “Optical Interfaces without Light Sources for Base-Station Designs in Fiber-Wireless Systems Incorporating WDM,” International Topical Meeting on Microwave Photonics, 1999.

[2.96] A. Nirmalathas, D. Novak, C. Lim, and R. Waterhouse, “Wavelength Reuse in the WDM Optical Interface of a Millimeter-Wave Fiber-Wireless Antenna Base Station,” IEEE Transactions on Microwave Theory and Technologies, vol. 49, no. 10, 2001.

[2.97] Lin Chen, Xiaoyan Lei, and Shuangchun Wen, “A novel radio over fiber system with DWDM mm-wave generation and wavelength reuse for upstream data connection,” Optics Express, vol. 15, no. 9, 2007.

[2.98] Zhenbo Xu, Xiupu Zhang, and Jianjun Yu, “A Simplified Wavelength Reuse and Dispersion Tolerance Scheme for Radio-Over-Fiber System,” IEEE International Topical Meeting on Microwave Photonics, 2007.

[2.99] C. Lim, A. Nirmalathas, D. Novak, R. Waterhouse, and G. Yoffe, “Millimeter-Wave Broad-Band Fiber-Wireless System Incorporating Baseband Data Transmission over Fiber and Remote LO Delivery,” Journal of lightwave technology, vol. 18, no. 10, 2000.

[2.100] A. Kaszubowska-Anandarajah, and L. P. Barry, "Remote downconversion for the radio/fiber uplink connection," 31st European Conference on Optical Communication, 2005.

[2.101] T. Kuri, K. Kitayama, and Y. Takahashi, "Simplified BS without light source and RF local oscillator in full duplex millimeter-wave radio-on-fiber system based upon external modulation technique," International Topical Meeting on Microwave Photonics, 1999.

[2.102] A. Kaszubowska, L. Hu, and L. P. Barry, "Remote Downconversion with Wavelength Reuse for the radio fiber uplink connection," Photonics Technology Letters, vol. 18, no. 4, 2006.

[2.103] M. Haider Raza, S.M. Hassan Zaidi, M. Ramzan, and K. Zaidi, "Bidirectional Radio-over-Fiber Architecture based on Frequency up and down conversion with lightsource and LO source free BS," International Conference on Emerging Technologies, 2008.

[2.104] R. G. Vaughan, N. L. Scotto, and D. R. White, "The theory of bandpass sampling," IEEE Transaction on Signal Processing, vol. 39, no. 9, pp. 1973-1984, 1991.

[2.105] A. J. Coulson, R. G. Vaughan, and M. A. Poletti, "Frequency-shifting using bandpass sampling," IEEE Transaction on Signal Processing, vol. 42, no. 6, pp. 1556-1559, 1994.

[2.106] T. Higashino, K. Tsukamoto and S. Komaki, "Proposal of Frequency Conversion and Routing Method for Multi-band RF Signal Transmission Using Direct Optical Switching-Encoding Scheme in Fiber-Optic Radio Highway," International Topical Meeting on Microwave Photonics, 2005.

[2.107] D.Wake, M.Webster, G.Wimpenny, K.Beacham and L.Crawford, "Radio over fiber for mobile communications," International Topical Meeting on Microwave Photonics, 2004.

[2.108] T. Marozsak, A. KovAcs, E. Udvary, and T. Berceli, "Direct Modulated Lasers in Radio Over Fiber Applications," International Topical Meeting on Microwave Photonics, 2002.

[2.109] C. Carlsson, H. Martinsson and A. Larsson, "High performance microwave link using a multimode VCSEL and a high bandwidth multimode fiber," International Topical Meeting on Microwave Photonics, 2001.

[2.110] M. Sauer, A. Kobyakov, and J. George, "Radio over Fiber for Picocellular Radio over Fiber for Picocellular," Journal of lightwave technology, vol. 25, no. 11, 2007.

[2.111] A, Nkansah, A. Das, N. J. Gomes, P. Shen, and D. Wake, "VCSEL-based Single-mode and multimode Fiber Star/Tree Distribution Network for Millimeter-wave Wireless Systems," International Topical Meeting on Microwave Photonics, 2006.

[2.112] M. Bakaul, A. Nirmalathas, and C. Lim, "Multifunctional WDM optical interface for millimeter-wave fiber-radio antenna base station," Journal of lightwave technology, vol. 23, no. 3, pp. 1210-1218, 2005.

[2.113]H. Toda, T. Yamashita, T. Kuri, and K. Kitayama, "25-GHz channel spacing DWDM multiplexing using an arrayed waveguide grating for 60-GHz band radio-on-fiber systems International Topical Meeting on Microwave Photonics, 2003.

[2.114]M. Bakaul, A. Nirmalathas, C. Lim, D. Novak, and R. B. Waterhouse, "Efficient multiplexing scheme for wavelength-interleaved DWDM millimeter-wave fiber-radio systems," IEEE Photonics Technology Letters, vol. 17, no. 12, pp. 2718-2720, 2005.

[2.115]C. Marra, A. Nirmalathas, D. Novak, C. Lim, L. Reekie, J. A. Besley, C. Weeks, and N. Baker "Wavelength-Interleaved OADM's incorporating optimized multiple phase-shifted FBG's for fiber-radio systems," Journal of Lightwave Technology, vol. 21, no. 1, pp. 32-39, 2003.

[2.116]Hugues Le Bras, and Maryse Moignard, "Distribution of 3G Base Stations on Passive Optical Network Architecture," International Topical Meeting on Microwave Photonics, 2006.

[2.117]A. Brizido, M. Lima, R. Nogueira, P. Andre, A. Teixeira, " 3G radio distribution based on directly modulated lasers over passive transparent optical networks," SBMO/IEEE MTT-S International Microwave and Optoelectronics Conference, 2007.

[2.118]K. Ikeda, T. Kuri, K. Kitayama, "Simultaneous three-band modulation and fiber-optic transmission of 2.5-Gb/s baseband, microwave-, and 60-GHz-band signals on a single wavelength," Journal of Lightwave Technology, vol. 21 , Issue: 12, 2003.

[2.119]C. Lim, A. Nirmalathas, M. Attygalle, D. Novak, and R. B. Waterhouse, "On the merging of millimeter-wave fiber-radio backbone with 25 GHz WDM ring networks," Journal of Lightwave Technology, vol. 21, no. 10, pp. 2203-2210, 2003.

[2.120]M. Bakaul, A. Nirmalathas, C. Lim, D. Novak, and R. Waterhouse, "Hybrid multiplexing of multiband optical access technologies towards an integrated DWDM network," IEEE Photon. Technology Letters, vol. 18, no. 21, pp. 2311-2313, 2006.

[2.121]"Climate change: Commission welcomes final adoption of Europe's climate and energy package," EC press release Dec. 2008.

[2.122]P. Chowdhury, M. Tornatore, S. Sarkar, and B. Mukherjee, "Building a Green Wireless-Optical Broadband Access Network (WOBAN)," Journal of Lightwave Technology, vol. 28, pp. 2219-2229, 2010.

[2.123]"Improving energy efficiency, Lower CO2 emission and TCO," Whitepaper, Huawei energy efficiency solution, Oct. 2009.

[2.124]C. Lange, and A. Gladisch, "On the energy consumption of FTTH access networks," Conference on Optical Fiber communication/National Fiber Optic Engineers Conference OFC/NFOEC, 2009.

[2.125]V. Bassoo, K. Tom, A.K. Mustafal, E. Cijvat, H. Sjoland, and M. Faulkner, "Potential Architecture for Future Generation `Green' Wireless Base Station," 4th International Symposium on Wireless Pervasive Computing (ISWPC 2009), pp. 1-5, 2009.

[2.126]"The power play: Reducing the build and power consumption costs of WiMAX base stations," Whitepaper, Motorola new design for WiMAX base stations, 2009.

[2.127]Y. Maeda, Y. Seshimo, and T. Okazaki, "Study of a cooling system for the telecommunication base site. Discussion," ASHRAE transactions, vol. 111, pp. 746-755, 2005.

[2.128]J. Baliga, R. Ayre, K. Hinton, W. V. Sorin, and R. S. Tucker, "Energy Consumption in Optical IP Networks," Journal of Lightwave Technology, vol. 27, no. 13, 2009.

[2.129]C. Lange, M. Braune, and N. Gieschen, "On the Energy Consumption of FTTB and FTTH Access Networks," Conference on Optical Fiber communication/National Fiber Optic Engineers Conference OFC/NFOEC, 2008.

[2.130]M. Gupta, S. Grover, S. Singh, "A feasibility study for power management in LAN switches," Proceedings of the 12th IEEE International Conference on Network Protocols, 2004.

[2.131]M. Vasic, etc., "High Efficiency Power Amplifier for High Frequency Radio Transmitters," Twenty-Fifth Annual IEEE Applied Power Electronics Conference and Exposition (APEC), 2010.

[2.132]G. Liu, P. Haldi, T. K. Liu, and A. M. Niknejad, "Fully Integrated CMOS Power Amplifier with Efficiency Enhancement at Power Back-Off," IEEE Journal of Solid-State Circuits, vol. 43, Issue: 3, 2008.

[2.133]"Designing a High-Efficiency WCDMA BTS Using TI GC5322 Digital Pre-Distortion Processor," Application Report, Texas Instrument, 2010.

[2.134]"Optichron Second-Generation Digital Pre-Distortion Processor Provides Wide-Band, Class 1 Performance for Multi-Protocol Base stations," Optichron, 2009.

[2.135]"ZTE's BBU+RRU Solution," ZTE technologies, 2007.

[2.136]"Base station controller reduces power consumption by 80%," Nokia Siemens Networks, 2010.

[2.137]J. Chabarek, etc., "Power Awareness in Network Design and Routing,"

[2.138]E. J. Tyler, M. Webster, A. Wonfor, R. V. Penty, and I. H. White, "Transmission of a single 2.5 Gb/s subcarrier modulated channel over 300 m of 62.5 μm multimode fibre," IEEE Lasers and Electro-Optics Society 2000 Annual Meeting (LEOS), 2000.

[2.139]E. J. Tyler, M. Webster, R. V. Penty, and I. H. White, "Penalty free subcarrier modulated multimode fiber links for datacomm applications beyond the bandwidth limit," Photonics Technology Letters, vol. 14, Issue: 1, pp. 110, 2002.

[2.140]http://adce13.adc.com/adcindia/site_images/carrier/wireless/Digivance%20LRCS.pdf, ADC Telecommunication.

Chapter 3

Digitized Radio-Over-Fiber Technique

3.1 Introduction

Wireless network based on radio-over-fiber (RoF) technologies is a promising solution to meet the ever increasing demand for larger transmission bandwidth. Such architecture moves most of the processing, routing and switching functionalities to a centralized location with optical fiber backhaul providing high speed interconnection to a large number of antenna base stations. Extensive research has been carried out to simplify the architecture of these remote antenna base stations and to realize high-performance backhaul networks that connect these base stations to a central office via an optical feeder network [3.1].

Though this approach has been well-suited for microwave and millimeter-wave applications; it still demands highly linear optical links with sufficient link gains to accommodate for antenna emitting over a wide area. Optical transport of the wireless signals in a radio-over-fiber system inherently suffers from inter-modulation distortion arising from the nonlinearility of both microwave and optical components within the link. For radio-over-fiber links employing Mach-Zehnder modulators (MZM), it has been shown that the nonlinear characteristics of the MZMs are the major source of performance degradation [3.2]. For a highly linear optical transport link, it will require special techniques for linearizing the transfer function of the components within the link. Despite the many linearization techniques that have been introduced to combat the linearity issue of analog optical link [3.3-3.6], these techniques may end up introducing more complexity and additional noise into the

transmission link, thus reducing the cost-effectiveness of the RoF systems. Meanwhile, it has also been shown that the dynamic range of an analog optical link decreases linearly with the transmission distance due to the signal attenuation in the optical fiber [3.7]. Furthermore, radio-over-fiber links have to be designed with good frequency response to accommodate for the highest RF frequency component of the signal. Thus, they often require optoelectronic devices with wide bandwidth. Such considerations often demand for the customization of optoelectronic components specific to a particular application to accommodate for their RF signals. Because of these factors, the deployment of a dedicated fiber-optic backhaul network or the system-specific design of radio-over-fiber link can be less competitive than wireless and free-space optics alternatives for the backhaul.

The transmission of digitized RF signals [3.8] can be a better alternative to analog radio-over-fiber implementation. First of all, the digital optical link has a better performance and is easy to implement using intensity-modulation and direct-detection (IM-DD) with less stringent requirements of the optoelectronic devices. Secondly, in a digital signal transport scheme, the signal is immune to the nonlinear effects arising from the optical link and the overall system dynamic range is independent of the fiber transmission distance unless the signal amplitude falls below the sensitivity of the link [3.9]. Thirdly, the advancement in analog-to-digital converter (ADC) and digital-to-analog converter (DAC) technologies has made it possible to push the ADC and DAC functions from the central office to the base station and allowing some of the base station functionalities to be performed in digital domain. . In addition, it can also take advantage of the direct digitized RF distribution to realize simpler base stations and the use of existing optical access and metro network infrastructures as the backhaul network. However, direct digitized RF-over-fiber scheme requires ADC and DAC with extremely high sampling rate, at least twice the wireless carrier frequency for exact signal reconstruction. Based on the current ADC technology, higher sampling rates lead to higher cost and instable operation. Though digitized IF-over-fiber can overcome this issue, additional RF devices

such as mixers and local oscillators (LOs) are required in the base station. Furthermore, in most of the currently available wireless services (WiMAX, 3G, etc.), only small fractional bandwidths are used to carry data relative to their carrier frequencies. Consequently, bandpass sampling [3.10] could be used to digitize the RF signals very effectively to produce digital baseband signals, where the sampling frequency is dependent on message bandwidth of the signal rather than at least twice the wireless carrier frequency in accordance to the Nyquist sampling theory. Moreover, bandpass sampling technique downconverts the RF band signal to IF band and thus simplifying the architecture of the base stations by eliminating additional devices required for frequency conversion, such as mixers and LOs [3.12]. Based on bandpass sampling and the maturity of analog-to-digital conversion technique, it is becoming more practicable to realize digitized transmission in RoF technology.

Digitized RF transmission over fiber based on the bandpass sampling theory and digital optical link has been proposed as a better alternative to analog radio-over-fiber in [3.11] and [3.13]. In this chapter, we have designed a digitized radio-over-fiber system, comprehensively analysed the digitized RF link using a theoretical model considering all noise sources, and compared the signal-to-noise ratio (SNR) and dynamic range between digitized and analog links. An uplink experimental demonstration is realized using a commercially available field-programmable gate array (FPGA) board, and the results have confirmed that digitized RF-over-fiber links can support extended reach well in excess over 60 km and can easily be integrated with any digital optical transmission technologies. We also experimentally investigate the link performance of digitized RF-over-fiber transport with different ADC resolutions, different carrier frequencies, different symbol rates and different sampling rates.

3.2 Digitized RF-over-fiber technique

We have proposed a digitized RF-over-fiber (DRoF) technique based on bandpass sampling technique [13]. The digitization of an RF signal produces a sampled digital signal in a serial form that can then be directly modulated on an optical carrier.. Modulation of the digital signal onto an optical carrier minimizes the nonlinear effects originating from the optical-to-electrical conversion function. The optically modulated signal can then be transmitted over an optical fiber link and the digital data can be recovered using direct detection. By doing so, a minimal set of hardware components is needed in the transceiver of the base station, leaving all signal processing functions to be located in the central office. With the intermodulation distortion arising from nonlinear electrical to optical conversions minimized, an optical link employing digitized radio-over-fiber transmission can maintain its dynamic range independent of the fiber transmission distance until the received signal goes below the sensitivity of the link. As a result, the transmission of digitized radio-over-fiber can be based on low-cost digital transmitters and receivers with a high dynamic range that can be sustained over a long distance in comparison to that of analog optical links. Simplified base stations with digitized RF interfaces can be an effective pathway for building a unified backbone network incorporating both wired and wireless services.

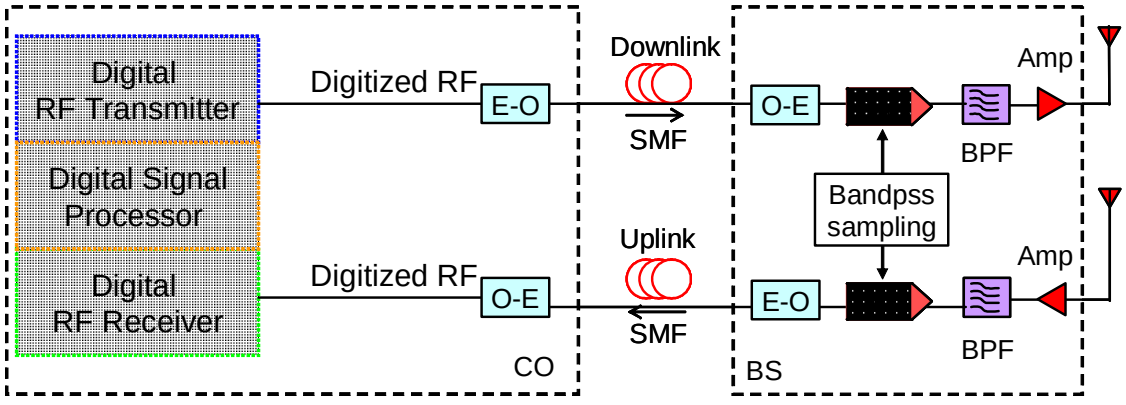

Fig.3.1 Digitized RF-over-fiber scheme

Fig. 3.1 illustrates an optical fiber link based on the DRoF technique. To accurately reconstruct the signal and prevent any spectral aliasing, the sampling rate for bandpass sampling should strictly follow the rules given in [3.12]. In the uplink transmission, the RF wireless signal received at the base station is sampled and quantized by an ADC with a sampling rate chosen based on bandpass sampling theory. After an IM-DD optical link, the digital data is detected in the central office and the uplink wireless signal is reconstructed and recovered using a DAC, in conjunction with a bandpass filter (BPF). The downlink transmission incorporing DRoF technique is also carried out in a similar manner.

3.3 Bandpass sampling theory

Bandpass sampling offers an attractive alternative solution to reduce the sampling rate for digitization process. It is a special form of undersampling method that alias a high frequency bandpass signal to a lowpass version in the vicinity of the zero frequency. The classic bandpass sampling theory states that for uniform sampling the signal can be reconstructed if the sampling rate is at least twice of the information bandwidth [3.10]. Real signals have Fourier spectra which is symmetrical around the zero frequency which also indicates that they have a negative-frequency spectrum that is a mirror image of the positive-frequency spectrum. Bandpass sampling can effectively shift both sides of the spectrum by multiples of the sampling frequency, as shown in Fig. 3.2.

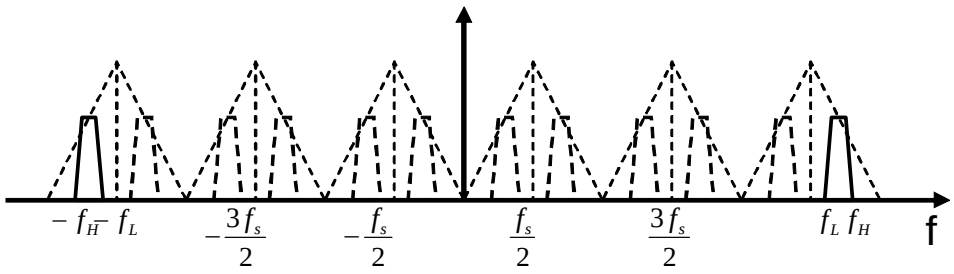

Fig.3.2 Spectral images after bandpass sampling

3.3.1 Principle of frequency relocation

To investigate how bandpass sampling relocates the various images, we investigate and study the sampling scheme analytically. Now, let *g(t)* be a complex baseband signal with a bandwidth of B_{RF}, and carrying the data of a bandpass radio signal *r(t)* represented by Eq. 3.1, where f_{RF} is the centre frequency.

(3.1) $$r(t) = \mathrm{Re}\left\{g(t)e^{i2\pi f_{RF}t}\right\}$$

The rectangular sampling function $s_{uni}(t)$ with a regular interval T_S is given by the convolution of an impulse train and a unit pulse function, which is represented by Eq. 3.2, where *p(t)* is the impulse train with unit amplitude and an interval of T_S, and *s(t)* is the unit pulse function with an amplitude of 1.

(3.2) $$s_{uni}(t) = p(t) * s(t) = \sum_{k=-\infty}^{+\infty} p(t - kT_S)$$

We can represent the spectra of *s(t)*, *p(t)* and $s_{uni}(t)$ by *S(f)*, *P(f)* and $S_{uni}(f)$, respectively. $S_{uni}(f)$ is calculated using the Fourier transform and it is given by Eq. 3.3, where *P(f)* is the envelope function.

(3.3) $$S_{uni}(f) = P(f) \cdot S(f)$$

The equivalent low-pass signal spectrum sampled by $s_{uni}(t)$, is represented by Eq. 3.4.

(3.4) $$R'(f) = R(f) * S_{uni}(f) = G(f) * (P(f) \cdot S(F))$$

The spectrum of the uniform sampling function $S_{uni}(f)$ is governed by Eq. 3.5, where d is the sampling rectangular pulse width to sequence period ratio, and δ is the Dirac delta function. Let f_S denote the sampling rate, which is a reciprocal of T_S. The frequency spectrum of the bandpass sampled RF signal has the evenly located alias components whose amplitude is determined by the sinc function [3.14].

$$S_{uni}(f) = d\sum_{n=-\infty}^{+\infty}(\sin(n\pi d)/n\pi d)\delta(f - n/T_S) \tag{3.5}$$

3.3.2 Determining the sampling frequency

The criterion to avoid spectral aliasing is to ensure that none of these shifted copies of the spectrum overlapped. For a bandpass signal, with lower and upper band limits f_L and f_U we have to ensure that after bandpass sampling with a sample rate of f_S, both lower and upper bands should be relocated in the first Nyquist zone as represented in Eq. 3.6 and Eq. 3.7.

$$0 \le f_L - \frac{nf_S}{2} \le \frac{f_S}{2} \tag{3.6}$$

$$0 \le f_U - \frac{nf_S}{2} \le \frac{f_S}{2} \tag{3.7}$$

Based on Eq. 3.6 and Eq. 3.7, we can derive Eq. 3.8, where n is an integer number. In bandpass sampling, Eq. 3.8 is sampling rate constrain to ensure exact reconstruction of the bandpass signal and to prevent spectral aliasing.

$$\frac{2f_U}{n+1} \le f_S \le \frac{2f_L}{n} \tag{3.8}$$

From both Fig. 3.2 and Eq. 3.5, we can see that the bandpass signal is repeated at integer multiples of half the sampling frequency. The image replicas of the original signal occupy the entire frequency band and by using appropriate filtering the RF signal can be recovered from any of these images. Therefore bandpass sampling is able to perform downconversion without the use of mixers and LO which greatly simplifies the hardware in the uplink base station architecture. The bandpass sampling theory is also transparent to modulation formats and can be applied to bandpass signals at any RF carrier. The high cost of ADC with high sampling rate has made it difficult to be implemented in commercial communication systems. Therefore bandpass sampling technique using ADC with lower sampling rate is more cost-efficient and is an attractive alternative for future commercial deployment. However, bandpass sampling requires the analog bandwidth of the ADC to be large enough to accommodate for the wireless signals before the digitization process. Current commercially available ADCs with low sampling rates generally do not have a large analog bandwidth as there is no requirement for such combination until now. This can be easily achieved as the analog bandwidth of an ADC with low sampling rate can be increased practically with reasonable cost. Therefore, bandpass sampling is a potential alternative solution which not only simplifies the base stations but also offers a cost effective scheme for wireless signal processing in a RoF environment.

3.4 SNR analysis on digitized RF-over-fiber link

Analog and digital transmission links have different noise sources, which induce different signal-to-noise ratios (SNR) in analog and digital transmission. Intensity noise from the laser is typically very small comparing with other noise sources, so it is ignored in the following analysis.

3.4.1 Noise and loss in analog transport

In analog transmission links, the main noise sources are inter-modulation distortion and photo-detector noise.

1. **Inter-modulation distortion**

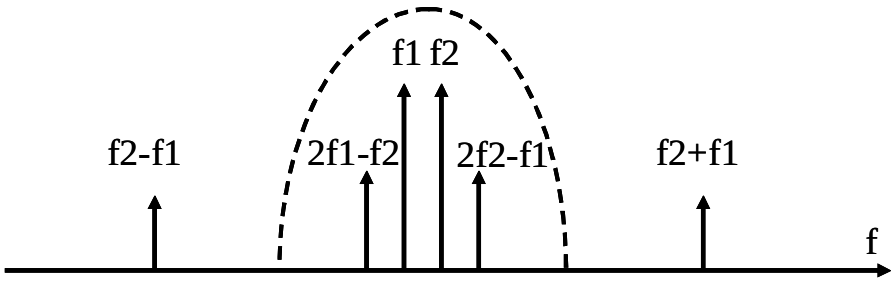

Fig.3.3 2nd and 3rd order two-tone inter-modulation products

In analog optical links, the RF modulation is inherently nonlinear and consequently introduces inter-modulation distortion that degrades the link performance. When two sufficiently strong signals are applied to the input of a nonlinear system, they will mix to create spurious signals known as inter-modulation products. The second-order and third-order inter-modulation distortions are the most common occurrence. The two-tone test spectrum showing the various inter-modulation products is shown in Fig. 3.3.

The second-order two-tone inter-modulation distortion can be removed easily using RF bandpass filters. However the third-order inter-modulation distortion is more troublesome since the spurious products fall in-band with the desired channels and cannot be easily removed via filtering. The third-order inter-modulation distortion of two strong signals will produce the third-order products at (2f1 - f2) and (2f2 - f1) with both located in-band with the desired RF signals. In recent years, the intercept point (IP) has become a popular method for

characterizing the inter-modulation distortion performance of many electronic components as well as radio transceivers [3.15]. The third-order inter-modulation product and the SNR due to the third-order inter-modulation with equivalent input power are given in Eq. 3.9 and Eq. 3.10, where P_{in} is the input signal power, *IP* is the intercept point, *IM* is the power of inter-modulation product, and SNR_{IM} is the signal-to-noise ration due to inter-modulation distortion.

(3.9) $$IM\,(dBm) = 3P_{in} - 2IP$$

(3.10) $$SNR_{IM}\,(dB) = 2IP - 2P_{in}$$

2. Photo receiver noise

The noise processes from the photo receiver are originated from thermal noise from the electronic circuitry and shot noise from the random arrival of photons [3.16]. The thermal noise, shot noise and total photo receiver noise are given in Eq. 3.11-3.13, where I_d is the dark current, $\Delta f = B_{DR}/2$ is the bandwidth, B_{DR} is the data rate, R_L is the load resistor to convert output current to a voltage signal, R is the responsivity of the photo-detector, η is the efficiency quantum, and F_n is the receiver noise figure.

(3.11) $$N_s^2 = 2q(I_d + I_p)\Delta f\ ,\ I_p = RP_{in}\ ,\ R = \eta q / h\nu$$

(3.12) $$N_{th}^2 = 4k_B T F_n \Delta f / R_L$$

(3.13) $$N_p^2 = N_{th}^2 + N_s^2$$

Since we are using direct-detection scheme, the SNR due to the photo receiver noise can be described as Eq. 3.14.

(3.14) $$SNR_{PD} = R^2 P_{in}^2 / (4k_B T F_n \Delta f / R_L + 2qRP_{in}\Delta f)$$

3. SNRs in analog links

Since the inter-modulation distortion and the photo receiver noise are independent, we can calculate the total noise generated in the analog link and then the total SNR. The total SNR is given by Eq. 3.15.

(3.15) $$1/SNR = 1/SNR_{IM} + 1/SNR_{PD}$$

3.4.2 Noise and loss in digital transport

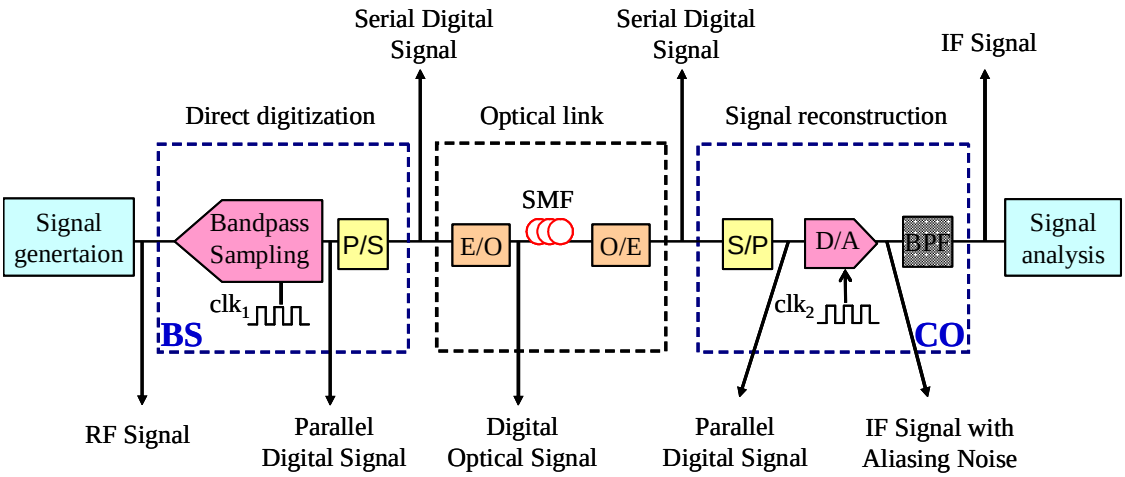

Fig.3.4 Digitized RF-over-fiber uplink

In the digitized RF-over-fiber transmission link, the noise processes are from traditional analog transmission links as no inter-modulation distortion is generated in the E/O and O/E

conversions. The uplink transmission scheme using digitized RF-over-fiber technique and the corresponding data format at each point are given in Fig. 3.4.

In the transmitter, the dominant noise is introduced during the ADC process. The ADC introduces jitter noise and quantization noise into the link. Jitter noise arises from the sampling clock jitter, while the quantization noise is determined by the ADC resolution. Although bandpass sampling technique enables lower sampling frequency to be used, this reduction leads to noise aliasing [3.17]. Also, the filter-induced noise before bandpass sampling needs to be considered. In the receiver, the photo-receiver introduces thermal noise and shot noise, and the DAC contributes to jitter noise. There are also additional noise processes from the filter, amplifier and modulator within the digitized RF link. These additional noise sources are common with the conventional analog photonic links and therefore to assess the performance of the DRoF link we will focus only on the noise sources that only originate from the DRoF link. Hence only ADC jitter noise, ADC quantization noise, pre-sampling filter noise, aliasing noise, DAC jitter noise, and photo-receiver noise are considered in the following analysis.

1. **Noise at the transmitter end**

Filter noise

Generally, a BPF is used prior to bandpass sampling or any signal processing to minimize any out-of-band noise, however the BPF itself also introduces noise to the signal. Under the assumption that the introduced thermal noise in a sampling device is an additive white Gaussian noise (AWGN) with zero-mean and the power spectral density (PSD) of the noise is a constant N_0, the noise introduced by BPF is $P_{Nth}=N_0B$ (B is the bandwidth of the filter). The corresponding SNR after BPF is given by Eq. 3.16, where P_S is the signal power.

$$SNR_F = P_S / P_{N_{th}} = P_S / N_0 B \tag{3.16}$$

Aliasing noise

As discussed previously, bandpass sampling generates image replicas of the original signal over the entire frequency spectrum as a result of spectral aliasing. The SNR of these images is generally poorer compared to the conventional analog system due to the noise aliasing from the bands between DC and the passband [3.10]. Again, assuming the introduced thermal noise in a sampling device is an AWGN with zero-mean with PSD a constant N_0, the corresponding SNR due to spectral aliasing in bandpass sampling is given by Eq. 3.17, where $m=B_{eff}/B$ is the total number of f_S bands within $[-B_{eff}, B_{eff}]$ and B_{eff} is the effective bandwidth of the sampling device, $(m-1)P_{Nth}$ represents the total out-of-band aliasing noise power.

(3.17) $$SNR_A = P_S/(m-1)P_{N_{th}} = P_S/(m-1)N_0B$$

ADC jitter noise

The jitter noise power of a sampled signal is given by Eq. 3.18, where y is the input signal, t_n is the ideal sampling time, and $t_n+\tau_n$ is the actual sampling time, ε_x is the error occurred due to jitter, N_J is the noise power during one sampling time, and n represents the order of the discrete sampled signal.

(3.18) $$N_J(n) = E[\varepsilon_\tau^2(n)] - E[\varepsilon_\tau(n)]^2,\ \varepsilon_\tau(n) = y(t_n+\tau_n) - y(t_n)$$

For a sinusoidal input signal $y(t)=A\sin(2\pi ft)$ and $2\pi f\tau_n<<1$, which can be satisfied by normal ADC in bandpass sampling, the corresponding average noise power is approximately given by Eq. 3.19, where σ_τ is the root mean square of the clock jitter. Therefore, considering the jitter noise only, the SNR can be expressed as Eq. 3.20.

(3.19) $$\overline{N_J} \approx 2\pi^2 f^2 \sigma_\tau^2 A^2$$

(3.20) $$SNR_J = P_S / 2\pi^2 f^2 \sigma_\tau^2 A^2 = 1/4\pi^2 f^2 \sigma_\tau^2$$

Quantization noise

ADCs provide the vital transformation of analog signals into digital code, which is an inherently nonlinear process. This nonlinearity manifests itself as wideband noise in the ADC's binary output, called quantization noise, limiting an ADC's dynamic range. It is a rounding error between the analog input voltage to the ADC and the output digitized value. Signal-to-quantization noise ratio is defined as the ratio of the root mean square value of the input analog signal to the root mean square value of the quantization noise [3.19]. The error due to quantization is $e_q(n)=y_q(n)-y(n)$, where $y(n)$ is the input signal and $y_q(n)$ is the quantized signal. In an ideal ADC the quantization error is uniformly distributed between −1/2 LSB (least significant bit) and +1/2 LSB, and the root mean square value of the error signal is given in Eq. 3.21, where Q is the bit resolution of the ADC.

(3.21) $$RSM_{e_q(n)} = \sqrt{2^{Q-1}\int_{-1/2^Q}^{1/2^Q} e_q^2(n)} = \frac{1}{\sqrt{3}2^Q}$$

When the signal has a uniform distribution ($RSM_{x(n)} = 3^{-1/2}$) covering all quantization levels, the signal-to-quantization noise ratio (SNR) is given in Eq. 3.22.

(3.22) $$SNR_Q = 20\log_{10}\left(3^{-1/2}\sqrt{3}2^Q\right) = 6.0206Q(dB)$$

When the input signal is an M-ary QAM signal, the distribution of the signal is not uniform, and the root mean square value of the error signal can be calculated using Eq. 3.23. The corresponding SNR equation will be Eq. 3.24.

$$RSM_{x(n)} = \left((\sqrt{M}+1)/(3\sqrt{M}-3)\right)^{\frac{1}{2}} \tag{3.23}$$

$$SNR_Q = 20\log_{10}\left(\left(\frac{\sqrt{M}+1}{3\sqrt{M}-3}\right)^{\frac{1}{2}}\sqrt{3}2^Q\right) = 6.02Q + 10\log\left(\frac{\sqrt{M}+1}{\sqrt{M}-1}\right)(dB) \tag{3.24}$$

2. Noise at the receiver end

Photo receiver noise

In digital transport, the sources of photo-detector noise are the same as in the analog transport. So, the SNR of the detector can be described using the same equation as Eq. 3.14.

DAC Jitter noise

The sampling clock jitter also has an effect on the SNR of DACs, and the effect is more pronounced for for high speed DACs [3.20] [3.21]. Ideally, digital-to-analog conversion extracts data samples from memory and converts them into an impulse train. Impulse train is not possible to generate in practice and to get around this; most DACs operate by holding the last value until next sample is received. This is called a zero-order hold, and it is equivalent to the sample-and-hold used during ADC. The zero-order hold can be mathematically described as the convolution of the impulse train with a rectangular pulse, having a width equal to the sampling period. In the frequency domain it is equivalent to multiplying the Fourier transform of the rectangular pulse (a sinc function). The ideal impulse train and the

zero-order hold signal have identical frequency spectra below the Nyquist frequency (half of the sampling rate). At higher frequencies, the zero-order hold signal contains same information but lower power comparing to impulse train.

After sampling, the SNR of the pulse train due to jitter noise is the same as it in ADC (Eq. 3.25). The composite SNR_{J_DAC} function (Eq. 3.26) of the DAC can be obtained by multiplying the square sinc function (because power spectral densities are being examined) and Eq. 3.25.

(3.25) $$SNR_J = 1/4\pi^2 f^2 \sigma_\tau^2$$

(3.26) $$SNR_{J\_DAC} = (1/4\pi^2 f^2 \sigma_\tau^2) \times (\pi^2 f^2 / f_s^2 / \sin^2(\pi f / f_s)) = 1/4\sigma_\tau^2 f_s^2 \sin^2(\pi f / f_s)$$

The original analogue signal can be perfectly reconstructed by passing the zero-order hold signal through a low-pass filter, with the cutoff frequency equal to one-half of the sampling rate. Here we employ a simple lowpass filter, and the frequency response is $1/(1+j\omega CR)$ with a cut-off frequency at $1/CR=\pi f_S$. After the lowpass filter, the SNR is rewritten as Eq. 3.27.

(3.27) $$SNR_{J\_DAC} = (1+2f/f_s)/(4\sigma_\tau^2 f_s^2 \sin^2(\pi f / f_s))$$

3. SNRs in digital links

Since all these noise sources listed above are weakly correlated and can be assumed to be independent, the SNR of the digitized RF-over-fiber link is governed by Eq. 3.28.

$$SNR_{Total}^{-1} = SNR_F^{-1} + SNR_A^{-1} + SNR_J^{-1} + SNR_Q^{-1} + SNR_{PD}^{-1} + SNR_{J\_ADC}^{-1} \quad (3.28)$$

Based on the above analysis and the parameters in a practical RoF link shown in Table 3.1, we calculate the noise power from all the additional noise sources in the digitized RF link. Since the ADC quantization noise is one of the dominant noise processes and is related to ADC resolution and signal modulation format, we calculate the link noise with different ADC resolutions and modulation formats and the results are shown in Fig. 3.5.

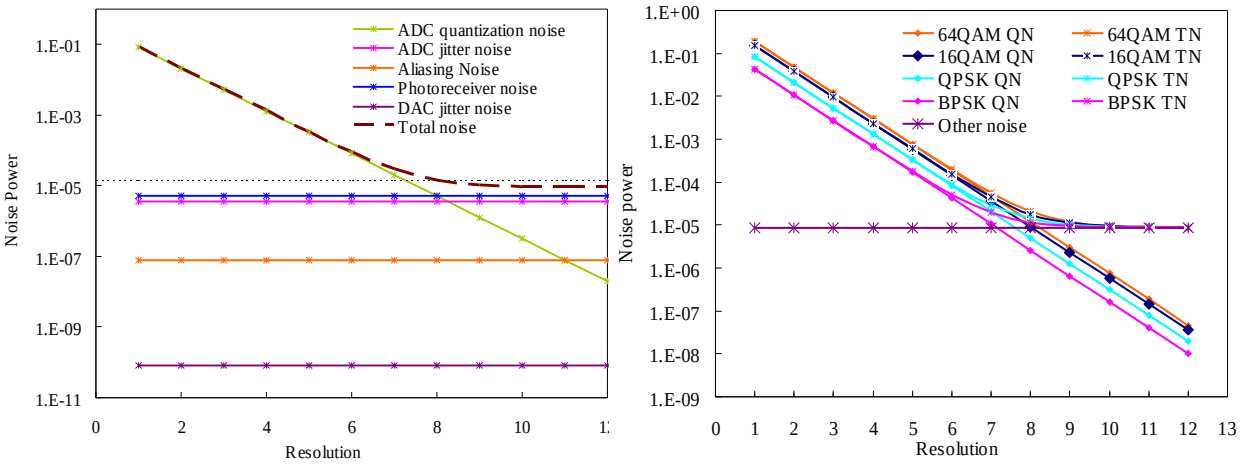

(a) (b)

Fig.3.5 (a) Various noise powers at different ADC resolutions (using QPSK modulation), and (b) Quantization noise and total link noise using different modulation formats.

In Fig. 3.5a, it is clearly shown that the quantization noise decreases exponentially with the increase of ADC resolution, while the other noise processes have no distinct relationship with ADC resolution. When the resolution is smaller than 8 bits, the quantization noise is the main noise source in the digitized RF link; when the resolution goes larger than 8 bits, ADC jitter

noise and photo-receiver noise start to dominate; bandpass sampling aliasing noise and DAC jitter noise are negligible in the digitized RF link. The total noise power in the digitized RF link decreases with ADC resolution before levelling off at a resolution > 8 bits.. These results indicate that the ADC resolution has to be > 8 bits optimize the noise performance in a digitized RF link. Since the total bit rate in the optical link increases with ADC resolution, in order to construct a high-performance cost-effective digitized RF link, the ADC resolution is best to maintain at no larger than 8 bits based on our analysis.

Table 3.1 Parameters used in computing the total SNR

Parameter	**Value**
Output RF signal power	-9 dBm
Sampling frequency of ADC	5 MSamples/s
Room temperature	290 K
Jitter (AD9433 and DAC904)	0.3 pS
RF carrier frequency	1 GHz
Resolution	8
M = 4 for QPSK	4
Noise figure of the PIN receiver	6 dB
Load resistor of the PIN receiver	100 Ω
Photo-detector responsivity	0.8 A/W
DAC clock frequency	100 MHz
Intercept point(IP)	15dBm
Fiber loss	0.25dB/km

Fig. 3.5b illustrates the impact of modulation formats on quantization noise (QN) and total link noise (TN) of the DRoF link as a function of ADC bit resolution.. It is shown that higher order modulation formats introduce higher quantization noise power in the digitized RF link, and hence leads to a larger total link noise power. Higher order modulated signals also require a larger ADC resolution to achieve the same link performance as the lower order modulated signals.

3.4.3 SNR comparison

Next we investigate the impact of laser launched power on the SNR of analog and digital links as a function of fiber transmission distance. Fig. 3.6a-d illustrate the SNRs of analog and digital links when the laser launched powers are -5, 0, 5 and 10 dBm respectively. We take Fig. 3.6c for instance, which shows the calculated SNR as a function of fiber transmission distance (L) for both analog and digital links with an optical launch power of 5 dBm. It is evident from Fig. 3.6c that the system SNR has a significant improvement using digitized RF transport. Initially, the SNR for the analog link increases and reaching a maximum at L=40km before it starts decreasing steadily with transmission length. The analog link performance is limited by nonlinear effects which increases with the launch power and also signal attenuation which is dependent on the transmission distance. The trend in Fig. 3.6c is due to the interplay between these two parameters. In contrast, the digitized RF optical link maintains a constant SNR for L < 60 km and this SNR is determined by the quantization noise. For L > 60 km, receiver noise starts to dominate as a result of the increased fiber loss. In this case, the receiver noise dominates over the quantization noise and limits the overall link performance.

Based on the calculated SNR curves in Fig. 3.6c, we are able to calculate the corresponding received error-vector-magnitude (EVM). Fig. 3.7 shows the calculated EVM as a function of L for both analog and digital links for a launch power of 5 dBm. When L <

60 km, the EVM in both links maintains at a low level (<1 %), which means both analog and digital links perform well; but when L > 60 km, the EVM in the analog link increases drastically while the EVM in the digital link still maintains at a relatively low level until L > 120 km.

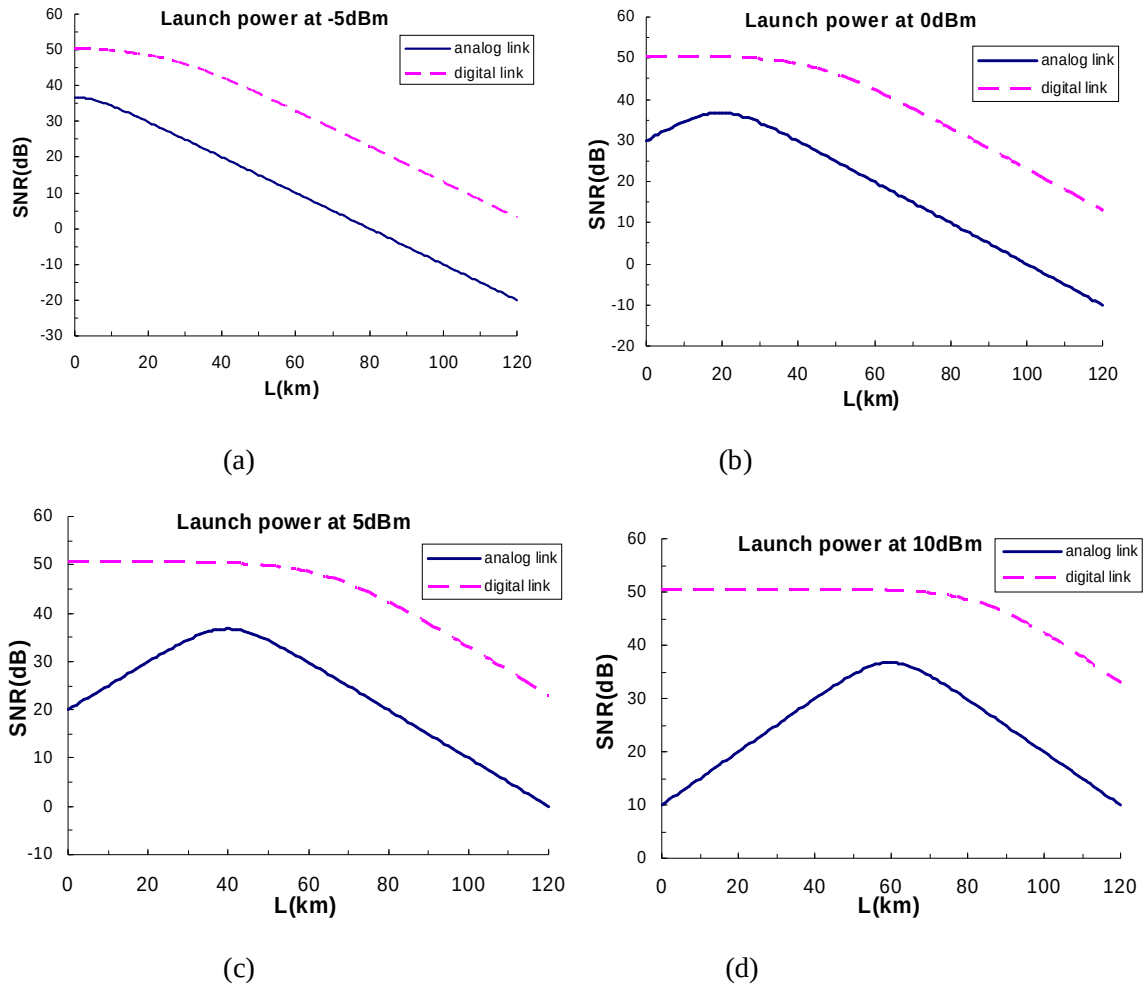

Fig.3.6 SNR comparisons at different launch powers

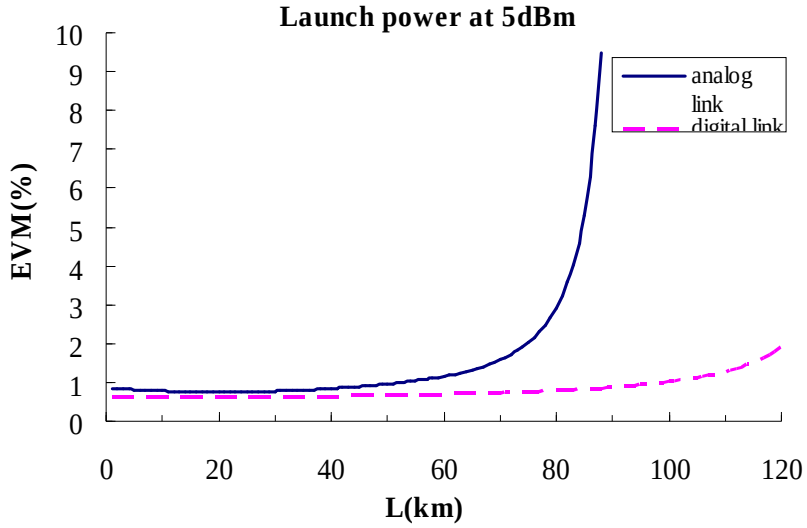

Fig.3.7 EVM in both digital and analogue links

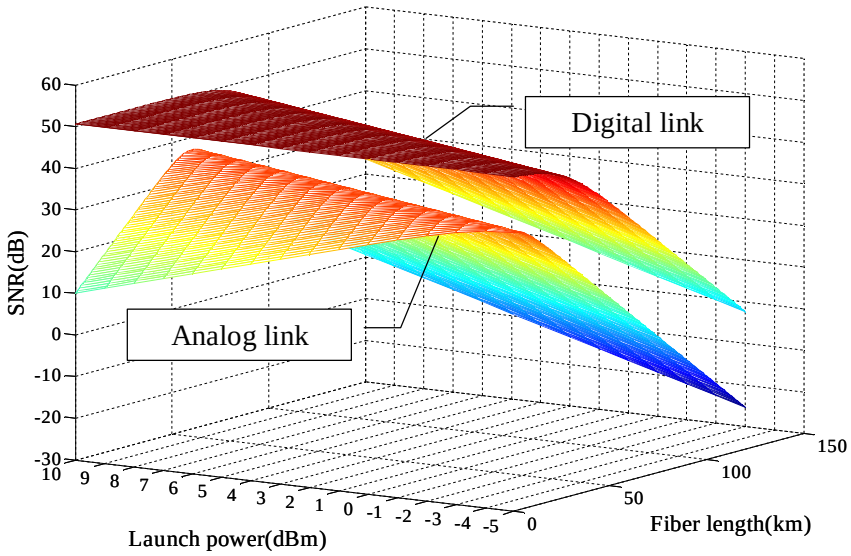

Fig.3.8 SNR Vs. launch power Vs. fiber length

Fig. 3.8 shows the three dimensional figure of the calculated SNR as a function of the fiber transmission distance (L) and the laser launched power for both analog and digital links. It is evident that the system SNR has a significant improvement due to the digitized RF-over-fiber technique. The analog link performance is limited by the nonlinear effects which increase

with the received optical power, and also by the signal attenuation which is dependent on the transmission distance. In contrast, the digitized RF-over-fiber link maintains a constant SNR determined by the quantization noise before the receiver noise dominates due to the signal attenuation. In addition, the increase of the laser launched power results in the transmission distance increasing in the digital link, but no evident improvement in the analog link due to the nonlinearity of O/E and E/O conversions.

3.5 Dynamic range analysis

The performance of wireless communications is governed by the dynamic range of the entire system. Therefore a wide dynamic range is critical as the capacity of the wireless signal is always on the rise. Hence it is obvious that dynamic range is also one of the key performance measures that characterize the performance of a radio-over-fiber link. The dynamic range of a system is defined as the range of input signal levels over which the system is usable. Various criteria have been used to define the upper and lower limits for this usable range.

3.5.1 Dynamic range of an analog RoF link

In the analog RoF link, spurious-free dynamic range (SFDR) is commonly used to measure the system performance, and it is defined as the range between the minimum and the maximum detectable signals. The SFDR is determined by the 3rd-order input intercept point (IP3) of the system, the receiver noise figure (NF), and the RF bandwidth [3.18] [3.22]. In analog optical link using direct detection, the minimum detectable signal is relative to receiver noise figure and RF or IF bandwidth following Eq. 3.29 and Eq. 3.30, where P_L is lower power limit of dynamic range in dBm, P_U is upper power limit of dynamic range in dBm, -174 dBm is thermal noise power in a 1-Hz bandwidth at room temperature, 3 dBm is the noise floor, *NF* is noise figure of receiver in dB, *B* is RF bandwidth in Hz, and *IP* is

receiver 3rd-order input intercept point in dBm of this link [3.14]. Then, the SFDR is given by Eq. 3.31. Using the parameters in Table 3.1, the SFDR can be computed as Eq. 3.32.

(3.29) $$P_L = -174 + 3 + NF + 10\log B \ (dBm)$$

(3.30) $$P_U = 1/3(-174 + 3 + NF + 10\log B) + 2/3(IP)(dBm)$$

(3.31) $$SFDR = P_U - P_L = 2/3(IP - NF - 10\log B + 171)(dBm)$$

(3.32) $$SFDR = P_U - P_L = 2/3[15 - 6 - 10\log(10^9) + 171] = 60(dBm)$$

The electrical power is proportional to the square of the photo current and also to the square of the optical power. Therefore, the contribution of fiber loss in the electrical domain will be twice of the optical loss in dB [3.9]. Now, we consider an L km direct-detection optical link with fiber loss of 0.25dB/km, the dynamic range of analog transport is given by Eq. 3.33.

(3.33) $$SFDR_L = P_U - P_L = \frac{2}{3}(IP - NF - 10\log B + 171 - 0.25 \times L \times 2) = 60 - \frac{1}{3}L(dBm)$$

3.5.2 Dynamic range of a digitized RoF link

Unlike analog systems, link noise and losses have no severe impact on the digital RF transport because of the discrete nature of the digitized RF signal. In the digital domain, a noisy ‘1’ is still a ‘1’ and a noisy ‘0’ is still a ‘0’ unless the noise power is comparable with signal power which leads to the synchronization loss in the transmission link. In the digital RF transport over fiber, as long as the signal is detectable, the digitized RF signal can be transported successfully. Therefore, the dynamic range in a digitized RF link is constant until

the signal goes beyond the link sensitivity where by the link dynamic range will reduce drastically.

To analyze the dynamic range in digitized links, we assume that a RF signal shows the following characteristics: the weakest signal is –100 dBm and strongest signal is –40 dBm. Before transmission over an RF transport system, the dynamic range of the signal is therefore 60 dB. Now we calculate the lowest detectable power using Eq. 3.34, below which the system synchronization will be lost, for this digital link by using the previous parameters.

$$P_{L_D} = -174 + 3 + NF + 10\log B_D = 2.5\times 10^{-12} \ (mW) \tag{3.34}$$

In a digital transport system over fiber, the dynamic range will maintain at 60 dB until the optical power difference between 1 and 0 goes below the lowest detectable power (-116 dBm) due to the fiber attenuation. In our case with extinction ratio at 0.9 and launch power at -10 dBm, the power difference is -20 dBm. The threshold would be [-20-(-116)]/0.25=384 (km).

3.5.3 Dynamic range comparison

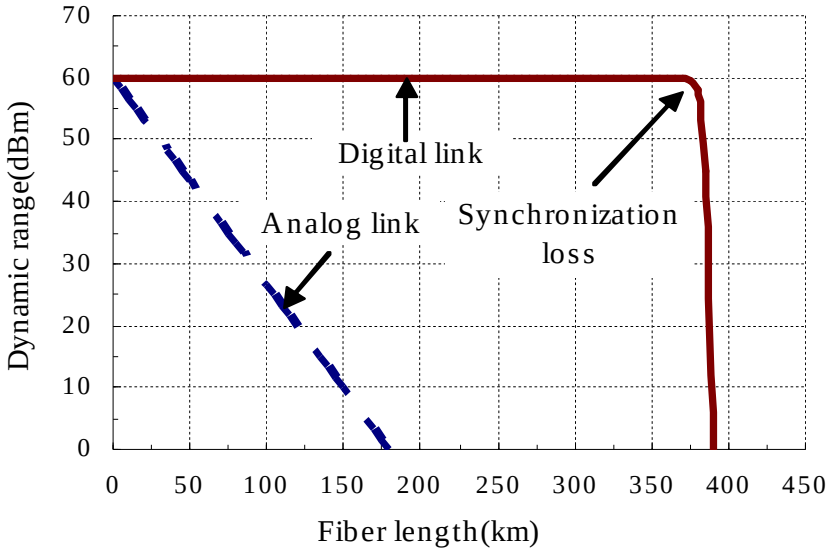

Fig.3.9 Dynamic range in both digital and analogue links

Fig. 3.9 shows the relationships between the system dynamic range and the transmission distance for both digital and analog links. The dynamic range in the analog link decreases steadily with the fiber length; while in the digital link, it remains constant until the transmission distance reaches a certain length. It is evident that the digitized RF transport offers a distinct advantage over the analog link.

Table 3.2 Comparison of loss in dynamic range

Source of loss/noise	**Loss of dynamic range in analog transport**	**Loss of dynamic range in digital transport**
Optical combiner loss	3 dB loss per 2:1 split	None
Optical transport loss	2 dB per 1 dB attenuation	None
Optical connector loss	2 dB per 1 dB attenuation	None
Optical transport noise	2 dB per 1 dB noise	None
RF noise	1 dB per 1 dB attenuation	1 dB per 1 dB attenuation

In an analogue RF transport system, the link losses and noise are the dominant limitations of the system dynamic range. Every splitter, combiner, and connector adds to the overall loss. Likewise, every additional component will generate noise in the system. But this has no severe impact on the digital RF transport. Table 3.2 compares the impact of losses and noise in analog and digital RF transports. In all analog RF transport systems, the losses and noise generated in the link are directly added to the RF signal and the noise is cumulative and cannot be removed from the signal. Digitized RF-over-fiber technique demonstrates the advantage in the system dynamic range, since the system is immune to degradation caused by

the noise processes in the transport that affect analog RF transport systems. The corresponding large dynamic range will allow both strong and weak signals to be transported simultaneously, which translates into improved quality of service.

3.6 Experimental demonstration

3.6.1 Experimental setup

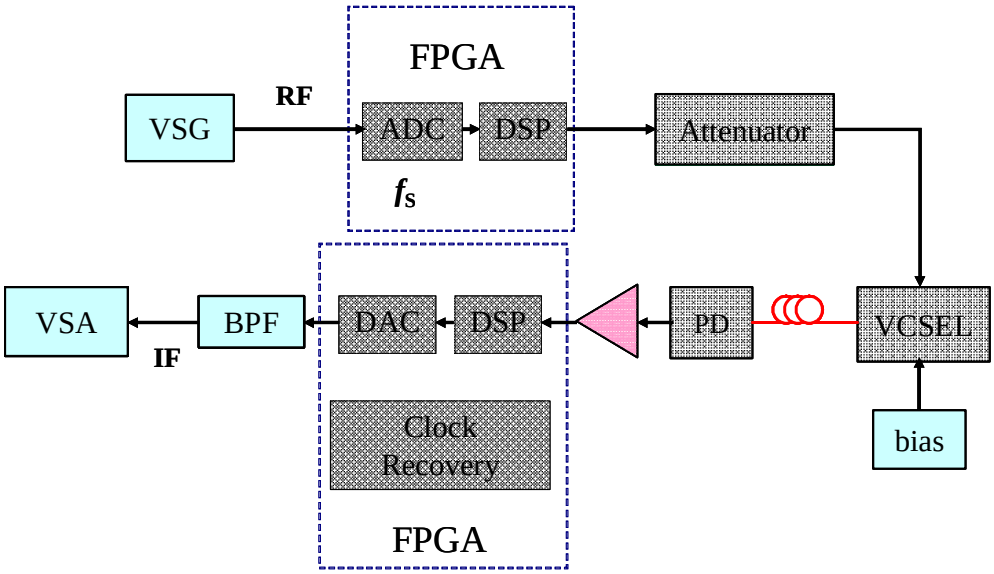

Fig.3.10 Experimental setup for uplink digitized transmission

Fig. 3.10 illustrates the experimental setup for an uplink digitalized RF-over-fiber transport based on a commercially available Field-Programmable Gate Array (FPGA) to establish the digitization interface. Fig. 3.11 shows the layout of the FPGA board and some of the key parameters. In this demonstration, we used a vector signal generator (VSG) and a vector signal analyser (VSA) as the RF transmitter and receiver, respectively.

The VSG is able to generate RF signals at different carrier frequencies, with different symbol rates and modulation schemes in this experiment. We used an Altera Stratix II DSP

Development FPGA board to sample and digitize the RF signal, to perform signal processing functionalities such as parallel-to-serial conversion and clock management. The output of the FPGA was attenuated before directly modulating a VCSEL. The optically modulated signal was then transmitted over 9.9 km of SMF.

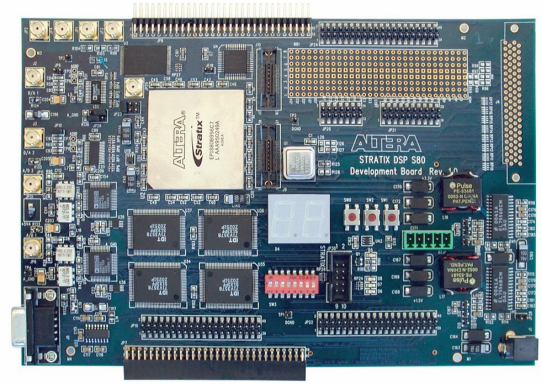

Parameters of AD9433	
Input frequency	Up to 350 MHz
Bit resolution	12 bits
Sampling rate	Up to 125 Msps
SFDR	72 dB
Jitter	0.25 ps

Fig.3.11 FPGA board and key parameters

In the receiver, a PIN detector was used to detect the signal. The received signal was amplified before entering the FPGA board. The FPGA was used to recover the clock, locate the most significant bit of the digital data stream and convert serial signal to parallel signal. The parallel data stream was then launched into the DAC to reconstruct the samples at IF frequency before the link performance was measured using the VSA.

3.6.2 Experimental results

Due to the limitation of the ADC input bandwidth (AD 9344) on the FPGA board [23] [24], the frequency of the RF signal in this demonstration was set to be 21 MHz. We used QPSK modulation scheme with symbol rates at 100 kS/s and 200 kS/s. The sample rate of the ADC was fixed at 5 MHz.

Fig. 3.12a and Fig. 3.12b show the measured EVM as a function of the received optical power for the symbol rate of 100 kS/s and 200 kS/s, respectively. From these results it is evident that EVM remains <2% and virtually constant at high received optical power before it increases when the received optical power decreases below -27 dBm. As a comparison we have also measured the EVM for an analog link as shown in Fig. 3.13. In the analog transmission, the measured EVM was ~ 1.5% when the received power was -17dBm. However the EVM increases when decreasing the received optical power. For a received power of -20 dBm, the EVM for analog link increases to ~ 4.5%.

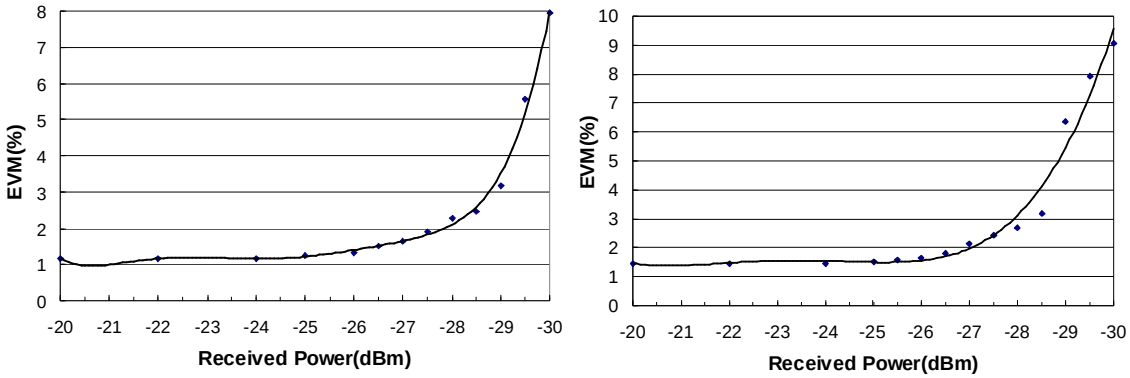

(a) (b)

Fig.3.12 (a) EVM curve with symbol rate at 100 kS/s and (b) 200 kS/s after digitized RF-over-fiber transmission

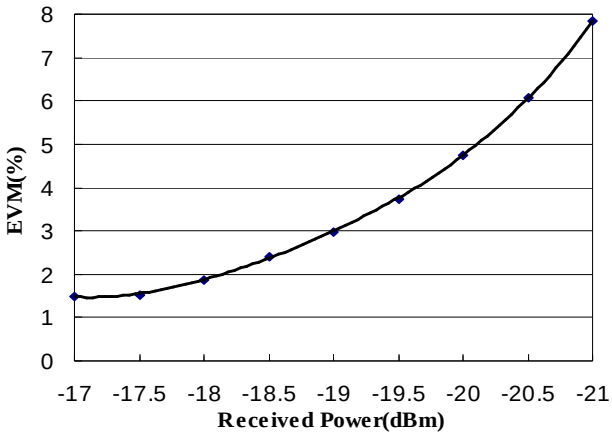

Fig.3.13 EVM for analog link with symbol rate of 100 kS/s

3.6.3 Performance Evaluation

We further extend our investigation of the digitized RF-over-fiber transport technique to evaluate and quantify the link performance in terms of the error vector magnitude (EVM), as a function of different digitization resolutions, carrier frequencies, symbol rates and sampling frequencies. The experimental results show that: the EVM decreases when increasing symbol rate and carrier frequency, but has no distinct relationship with the sampling rate; and the ADC quantization resolution of 8 bits is sufficient to provide a desired received SNR and a satisfactory optical bit rate in the digitized RF link.

1. **ADC resolution selection**

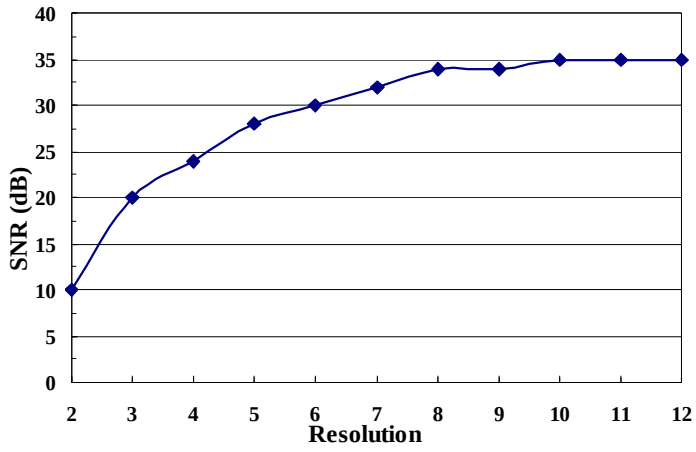

Fig.3.14 SNR vs. Resolution

Based on our previous analysis, the quantization noise from ADC is one of the dominate noise sources in the digitized RF transport link, and it is determined by the bit resolution of the ADC. However, higher resolution translates to higher optical bit rate in the digitized RF transport link which requires larger transmission bandwidth. To balance the trade-off between the link performance and the optical bit rate, we experimentally investigated the effects of the ADC resolution on the link performance, with RF carrier at 20 MHz, sampling

rate at 5 MHz, and symbol rate at 100 kS/s. Fig. 3.14 illustrates the relationship between the ADC resolution and the received SNR. It is clearly shown that when the resolution is greater than 8 bits, the SNR is relatively constant at a value of 35 dB. Therefore, in digitized RF transport scheme, the ADC resolution of 8 bits is sufficient to achieve satisfactory performance and an acceptable bit rate.

2. Impacts of carrier frequency and symbol rate

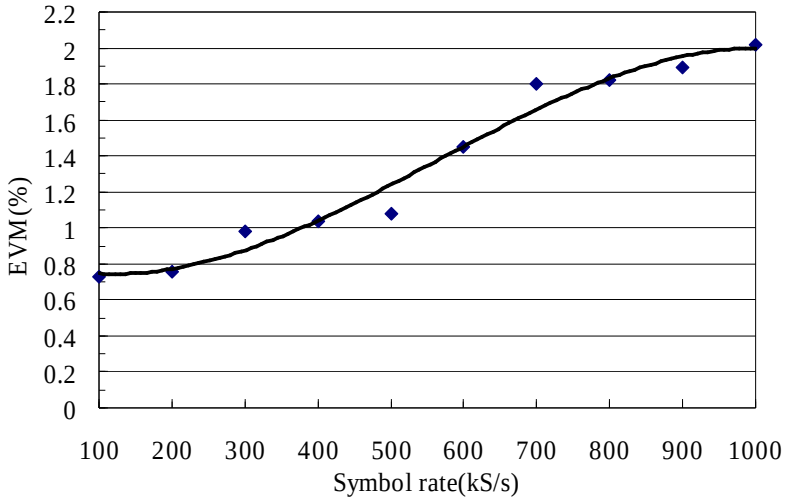

Fig.3.15 Symbol rate vs. EVM

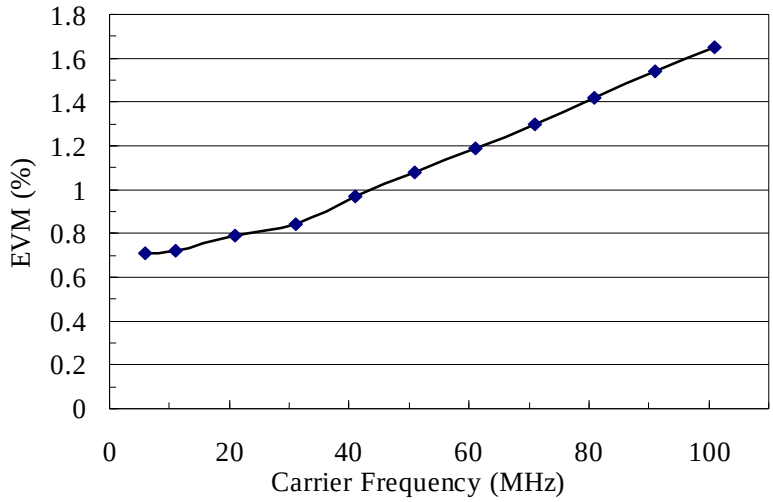

Fig.3.16 Carrier frequency vs. EVM

By fixing the ADC resolution at 8 bits, received power at -20 dBm, and sampling rate at 5 MHz, we measured the EVM performances at different symbol rates and carrier frequencies. Fig. 3.15 and Fig. 3.16 show that the EVM increases almost linearly with the carrier frequency and the symbol rate. This increment is mainly attributed to the increasing noise level as both the carrier frequency and the symbol rate are increasing within the digitized RF-over-fiber link.

3. Impacts of sampling rate

Fig. 3.17 shows the EVMs with different sampling rates, when symbol rates are fixed at 1 MS/s and 100 kS/s respectively. From the results it can be clearly seen that the EVMs for both symbol rates are relatively constant over the different sampling rates under investigation. This indicates that the link performance of the digitized RF transport is not affected very much by the sampling rate provided that the sampling rate satisfies the limitation imposed by the bandpass sampling theory.

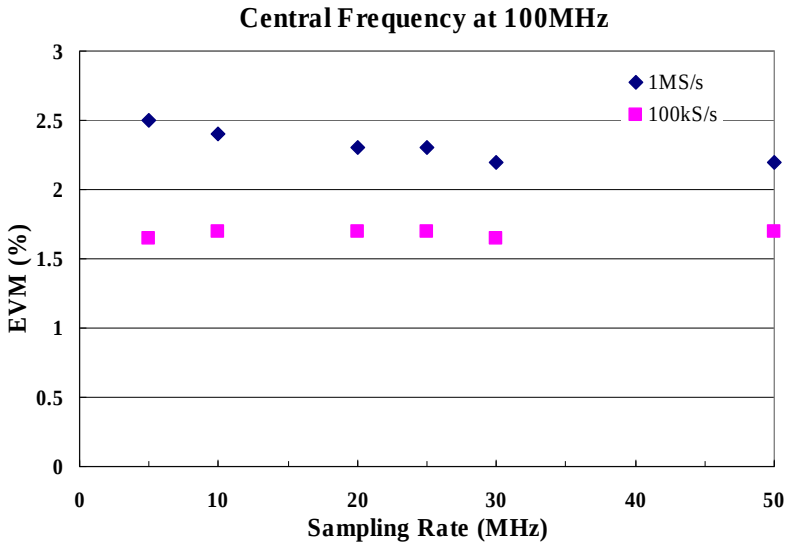

Fig.3.17 Sampling rate vs. EVM

3.7 Summary

In this chapter, we first introduced the digitized RF-over-fiber technique based on the bandpass sampling theory and commercial-available ADCs/DACs. It takes advantages of the higher performance digital optical links, the benefits of direct RF distribution to realize simpler base stations, and the use of existing optical access and metro network infrastructures.

Secondly, we have theoretically analysed the digitized RF-over-fiber link in terms of different noise sources, such as ADC jitter noise, ADC quantization noise, bandpass sampling aliasing noise, DAC jitter noise, and photo-receiver noise. Comparisons of SNR and dynamic range between digitized and analog RF-over-fiber links were carried out. For the digitized link, the increase of the laser launched power has no evident impact on the SNR value, but increases the transmission distance. However, in the analog link, the transmission distance does not increase with the laser launched power due to the system nonlinearity. The dynamic range in the analog link decreases steadily with the fiber length; while in a digital link, it remains constant until the transmission distance reaches a certain length where the signal goes below the link sensitivity. The high dynamic range of the digitized RF transport offers a distinct advantage over analog RoF links.

Finally, we experimentally demonstrated a low-cost digitized RF-over-fiber uplink transmission using commercially available FPGA boards. Our studies have confirmed that digitized RF-over-fiber links can support extended reach well in excess over 60 km and can easily be integrated with any other digital optical transmission technologies. We also have experimentally investigated the link performance of the digitized RF over fiber transport for different ADC resolutions, different carrier frequencies, different symbol rates and different sampling rates. The results indicate that: (1) 8 bits resolution is sufficient to construct a high-performance cost-effective digitized RF over fiber link; (2) the link EVM performance improved almost linearly with the carrier frequency and the symbol rate; (3) the link

performance is nearly independent of sampling rate, as long as the sampling rate satisfies the bandpass sampling theory.

3.8 References

[3.1] R.E. Schuh, D.Wake, B. Verii, and M. Mateescu, "Hybrid Fiber Radio Access: A Network Operators Approach and Requirements," Proceedings of 10th Microcoll Conference, Microcoll 99, Budapest, Hungary, pp. 211-214, 1999.

[3.2] T. Kurniawan, and A. Nirmalathas, "Performance Analysis of Optimized Millimetre-Wave Fibre Radio Links," IEEE Transaction on Microwave Theory and Technologies, vol. 54, no. 2, pp. 921.928, 2006.

[3.3] Xavier N. Fernando, and Abu B. Sesay, "Higher order adaptive filter Characterization of Microwave fibre Optic link Nonlinearity," Proceedings of Optical Pulse and Beam Propagation, SPIE Conference, 2000.

[3.4] Shingo Tanaka, Noritaka Taguchi, Tsuneto Kimura, and Yasunori Atsumi, "A Predistortion-Type Equi-Path Linearizer Designed for Radio-on-Fiber System," IEEE Transactions on Microwave Theory and Technologies, vol. 54, no. 2, 2006.

[3.5] X. N. Fernando and A. B. Sesay, "Fibre-Wireless Channel Estimation using Correlation Properties of PN Sequences," Canadian Journal of Electrical and Computer Engineering, pp. 43 - 47, 2001.

[3.6] C.Lim, and A. Nirmalathas, "Intermodulation Distortion Improvement for Fiber–Radio Applications Incorporating OSSB+C Modulation in an Optical Integrated-Access Environment," Journal of lightwave technology, 2007.

[3.7] L. Meyer, "Using fibre optics with analogue RF signals," 39th IEEE Vehicular Technology Conference, San Francisco, pp. 398-400, 1989.

[3.8] P. M. Wala, "A new microcell architecture using digital optical transport," in Proc. 43rd IEEE Trans. Veh. Technol. Conf., pp. 585–588, May 1993.

[3.9] "The Advantage of Digital RF Transport for Distributing Wireless Coverage and Capacity," ADC Telecommunication, Inc.

[3.10] R. G. Vaughan, N. L. Scott, and D. R. White, "The theory of bandpass sampling," IEEE Transaction on Signal Processing, vol. 39, no. 9, pp. 1973-1984, Sep. 1991.

[3.11] P. Gamage, A. Nirmalathas, C. Lim, D. Novak, and R. Waterhouse, "Design and Analysis of Digitized RF-Over-Fiber Links," Journal of lightwave technology, vol. 27, Issue: 12, 2009.

[3.12] N. Wong, and Tung-Sang Ng, "An efficient algorithm for downconverting multiple bandpass signals using bandpass sampling," IEEE International Conference on Communications, 2001.

[3.13] A. Nirmalathas, P.A. Gamage, C. Lim, D. Novak, R.B. Waterhouse and Y. Yang, "Digitized RF over Fiber Transport," Microwave Magazine, vol. 10, pp. 75-81, June 2009.

[3.14] Paulo S. R Diniz, "Digital Signal Processing: System Analysis and Design," Cambridge University Press, 2010.

[3.15] Watkins-Johnson Company, "High Dynamic Range Receiver Parameters," Tech Notes, 1987.

[3.16] Govind P. Agrawal, "Fibre-optical communication systems," 3rd Edition.

[3.17] Y. Sun, "Nonuniform Bandpass Sampling in Radio Receivers," Microelectronics and Information Technology, 2004.

[3.18] B. H. Wang, P. Chiang, M. Kao, and W. Way "Large-Signal Spurious-Free Dynamic Range Due to Static and Dynamic Clipping in Direct and External Modulation Systems", Journal of lightwave technology, vol. 16, no. 10, pp. 1773-1785, Oct. 1998.

[3.19] John G. Proakis, "Digital Signal Processing - Principles, Algorithms and Applications," 4th Edition.

[3.20] Naoki Kurosawa, "Sampling clock jitter effects in digital-to-analogue converters," Elsevier Measurement, 2002.

[3.21] Paul Smith, "Little known characteristics of phase noise," www.rfdesign.com, 2004.

[3.22] J. Lerdworatawee, and W. Namgoong, "Revisiting Spurious-Free Dynamic Range of Communication Receivers", IEEE Transactions on Circuits and Systems , vol. 53, pp. 937-943, Apr. 2006.

[3.23] Altera Corporation, "Stratix II DSP Development Board Reference Manual." Aug. 2006.

[3.24] Analog Devices, Inc., "AD9433–SPECIFICATIONS," 2001.

Chapter 4

Multi-Channel Digitized RF-over-Fiber Transmission

4.1 Introduction

Radio-over-fiber has long been studied as a way of realizing ultra-high-speed, high-quality, and multi-service backhaul networks. Such radio-over-fiber system can take the advantage of subcarrier multiplexing (SCM) technique to further increase the optical bandwidth efficiency as well as hardware sharing in access networks [4.1, 4.2]. SCM is a scheme that multiplexes multiple signals in the RF domain which can then be transmitted using a single wavelength in a RoF environment. SCM has the advantage of exploiting the maturity of microwave devices and hardware. For instance, the stability of microwave oscillators and the sensitivity of electrical filters are more superior to their optical counterparts. Many different implementations of SCM have been demonstrated ranging from improving optical spectral efficiency to resilience against fiber chromatic dispersion to improve the performance of RoF systems, which include SSB modulation [4.3], hybrid multiplexing scheme [4.5], and tandem single-sideband (TSSB) modulation [4.4]. Most of these schemes rely heavily on optical Mach-Zehnder modulators (MZM) which have nonlinear characteristics. This may lead to an increase in the system nonlinear distortions comprising harmonic distortion (HD) and third-order intermodulation (IMD) when multiple radio frequency signals in SCM format are used to modulate the optical signal using an MZM. Apart from that, fiber nonlinearity such as cross-phase modulation (XPM) and four-wave mixing (FWM) may also generate a significant

amount of nonlinear crosstalks between adjacent channels that lead to further degradation of the system performance. Also, carrier fading due to polarization mode dispersion (PMD) can also affect the performance when a large number of subcarrier frequencies are presented [4.7]. Therefore, nonlinear distortions considerably reduce the receiver sensitivity and dynamic range, and compromise the performance of subcarrier-multiplexed-radio-over-fiber (SCM-RoF) systems [4.6]. To combat these nonlinear distortions, many different techniques effectively linearizing the transfer function of the analog optical link have been demonstrated [4.8]. However, these techniques introduce more complexity and can often reduce the cost-effectiveness of the RoF links.

In this chapter, we extend our study of the digitized RF-over-fiber technique and propose a multi-channel digitized radio-over-fiber transmission scheme based on multi-band bandpass sampling and realize frequency conversion of multiple channels using a single ADC and a single DAC. We thoroughly analyse the subcarrier multiplexed digitized RF-over-fiber (SCM-DRoF) link, and compare with the conventional analog links in terms of signal-to-noise ratio (SNR), dynamic range, and performance degradation with increasing channel number. We also experimentally demonstrate the SCM-DRoF link for multi-channel simultaneously transmission using commercially available FPGAs and ADCs. By appropriate selection of the sampling rate determined by the bandpass sampling theory, we downconvert all signal bands to the first Nyquist zone and recover the data. We also theoretically analyze the performance of the SCM-DRoF link to further investigate the cost-effectiveness of such a link.

4.2 Proposed Multi-Channel DRoF Scheme

As previously discussed in Chapter 3, based on the ideal sampling theorem, any sampled signals will ideally occupy the entire frequency spectrum with images of exact replica of the original signal located repeatedly in infinite Nyquist zones. In theory, any of the images can

be recovered to reconstruct the original signal. Based on this observation, we are able to establish frequency up- and down-conversion of the original signal by selecting the appropriate images. This theory is also applicable for multi-channel signals [4.9]. An appropriate sampling rate can be chosen to sample multi-channel signals ensuring no overlapping of the multiple frequency bands within each Nyquist window arising from the bandpass sampling scheme. Here we propose a multi-channel DRoF transmission link and the schematic is shown in Fig. 4.1. The proposed multi-channel DRoF scheme provides a practical solution to realize signal multiplexing, which also simplifies the architecture of the BSs by eliminating additional devices required in BSs for frequency conversion.

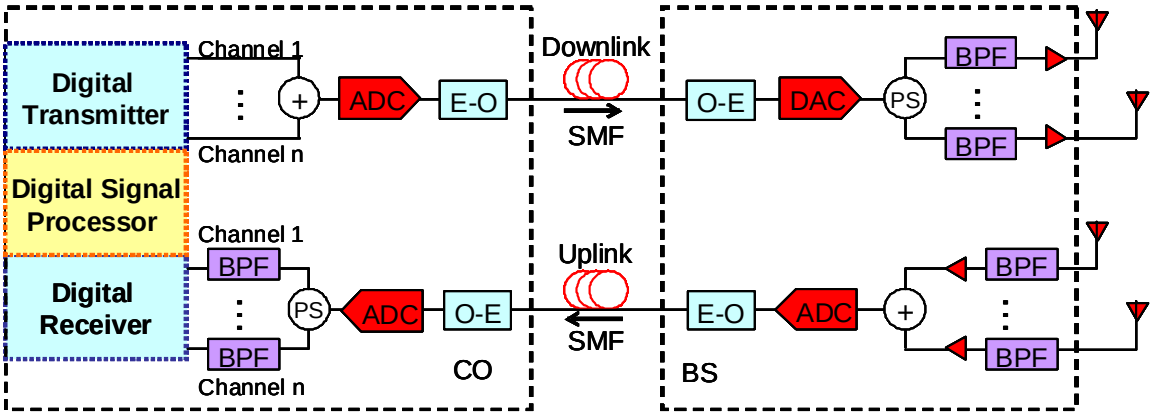

Fig.4.1 Scheme of Multi-Channel DRoF Transmission

In the uplink path, the BSs have three main functions. The first function is to receive, amplify and filter the multiple RF signals separately. The second function is to combine all the analog RF signals to a multi-band RF signal before sampling using an ADC with the sampling rate determined by the RF carrier frequencies. The last function of the BS is to provide parallel-to-serial conversion and electrical-to-optical conversion (E-O) before transmitting to the CO. In summary, the BS combines multiple RF signals before converting them to a baseband digital data stream and sending it optically via the optical fiber link. In

the CO, the detected digital data stream is converted back to a parallel digital data. A DAC is employed to convert the parallel digital signal to a multi-band analog signal. In the frequency domain, this analog signal contains the spectral replicas of each RF band in every Nyquist region without spectral overlapping. By taking advantages of bandpass filters, we are able to extract the IF spectrum replica of each RF band from the first-order Nyquist region which has the largest signal power. The data carried by each RF channel can then be recovered by demodulating its corresponding IF replica.

In the downlink path, wireless signals at different IF frequencies are electrically combined within the CO before digitized using an ADC. The sampling rate of the digitization process is selected according to the IF signal frequency using the Nyquist sampling theory. Upon digitization, the samples are processed digitally via digital signal processing (DSP) modules including parallel-to-serial conversion and clock management. The digitized data stream is modulated onto an optical carrier before transported over the optical link and recovered using a photodetector. In the BS, the analog signals are reconstructed using a DAC with a sufficient analog bandwidth in conjunction with DSP. The output of the DAC covers the entire RF spectrum with the image replicas of the original IF signals. To extract the wireless signals in a multiple-wireless environment, the analog signal is further divided using a power splitter (PS) and the wireless signal at the desired wireless frequency is extracted separately using a bandpass filter (BPF) and amplified before the air-interface. The wireless signals are essentially upconverted to the desired wireless frequencies (RF) without physical mixers and local oscillators.

4.3 Analysis on multi-channel DRoF link

4.3.1 SNR in multi-channel analog links

In Chapter 2, noise sources and their corresponding SNRs of a signal channel radio-over-fiber link have been discussed. Here we extend the analysis to incorporate multiple channels. The main difference between single channel and multiple channel transmission links is the nonlinear distortion arising from the optical modulator and the photo receiver. In this analysis, we assume that the third-order nonlinearity product dominates the nonlinear interference of the transmission system; the second-order nonlinear products are mitigated by band selective filters; the higher order distortions are assumed to be negligible for simplicity [4.10].

Assuming that an MZM is used at the transmitter front end, the mathematical expression of the transfer function is given by Eq. 4.1. After converting back to the electrical domain, the photocurrent governed by Eq. 4.2, where E_0 is the amplitude of the input optical carrier of the modulator; V_π is the switching voltage of the modulator; ω is the optical carrier frequency; ω_{RF} is the RF carrier frequency; V is the amplitude of the signal that drives the modulator; E_{out} is the optical field at the output of the modulator; R is the load resistance; and η is the photodetector responsivity.

$$E_{out} = \frac{E_0}{2}\left[\sin(\omega t + \pi/2) + \sin(\omega t + (V\pi/V_\pi \sin\omega_{RF} t)\right] \tag{4.1}$$

$$I_{out} = R\eta\left\{\frac{E_0}{2}\left[\sin(\omega t + \pi/2) + \sin(\omega t + (V\pi/V_\pi \sin\omega_{RF} t)\right]\right\}^2 \tag{4.2}$$

To quantify the intra-channel intermodulation distortion, we use a two-tone test with frequency carriers at ω_1 and ω_2 and substituting these into Eq. 4.2 to generate Eq. 4.3. The fundamental and the intra-channel intermodulation products are calculated as shown in Eq.

4.4 and Eq. 4.5, and the signal-to-interference ratio (SIR) is then given by (J_0^2/J_2^2). Here, ω_1 *and* ω_2 represent the RF frequencies used in the two-tone test; and J_n represents n[th] order product of the first kind Bessel function.

$$I_{out} = R\eta\left\{\frac{E_0}{2}\left[\sin(\omega t + \pi/2) + \sin(\omega t + (V\pi/V_\pi \sin\omega_1 t + V\pi/V_\pi \sin\omega_2 t)\right]\right\}^2 \quad (4.3)$$

$$2J_1J_0E_0^2R\eta \quad (4.4)$$

$$2J_1J_2E_0^2R\eta \quad (4.5)$$

Table 4.1 Three-tone test results at the transmitter side

	Fundamental		Intermodulation	
	Frequency	Amplitude	Frequency	Amplitude
Channel1	ω_1	$J_1J_0^2E_0^2R\eta/2$	$2\omega_2-\omega_3$	$J_0J_1J_2E_0^2R\eta/2$
Channel2	ω_2	$J_1J_0^2E_0^2R\eta/2$	$\omega_1+\omega_3-\omega_2$	$J_1J_1J_1E_0^2R\eta/2$
Channel3	ω_3	$J_1J_0^2E_0^2R\eta/2$	$2\omega_2-\omega_1$	$J_0J_1J_2E_0^2R\eta/2$

There are also inter-channel intermodulation distortions needed to be considered in multi-channel cases. To determine the inter-channel intermodulation products, we use a three-tone test, where the positive frequencies are denoted as ω_1, ω_2 and ω_3 ($\omega_1<\omega_2<\omega_3$), and the channel spacing is assumed to be consistent. The transfer function of the optical modulator and the received photo current can be expressed by Eq. 4.6 and Eq. 4.7. Considering only the

products falling in the signal channel, the fundamental products and inter-channel intermodulation products are listed in Table 4.1. The SIRs will be (J_0^2/J_2^2), (J_0^4/J_1^4), and (J_0^2/J_2^2) for these three channels respectively. If we consider both intra-channel and inter-channel intermodulation distortion, the SNRs for these three channels will be ($J_0^2/2J_2^2$), ($J_0^4/(J_1^4+J_0^2J_2^2)$, and ($J_0^2/2J_2^2$).

$$(4.6)\quad E_{out} = \frac{E_0}{2}\left[\sin(\omega t + \pi/2) + \sin(\omega t + (V\pi/V_\pi \sin\omega_1 t + V\pi/V_\pi \sin\omega_2 t + V\pi/V_\pi \sin\omega_3 t))\right]$$

$$\begin{aligned}(4.7)\quad I &= \frac{E_0^2}{4}R\eta(1+\sin(V\pi/V_\pi \sin\omega_1 t + V\pi/V_\pi \sin\omega_2 t + V\pi/V_\pi \sin\omega_3 t)) \\ &= \frac{E_0^2}{4}R\eta + \frac{E_0^2}{2}R\eta\sum_{n=1}^{\infty}J_{2n-1}\cos[(2n-1)\omega_1 t]\times \\ &\left[J_0 + 2\sum_{n=1}^{\infty}J_{2n}\cos(2n\omega_2 t)\right]\times\left[J_0 + 2\sum_{n=1}^{\infty}J_{2n}\cos(2n\omega_3 t)\right] \\ &-\frac{E_0^2}{2}R\eta\sum_{n=1}^{\infty}J_{2n-1}\cos[(2n-1)\omega_1 t]\times 2\sum_{n=1}^{\infty}J_{2n-1}\cos[(2n-1)\omega_2 t] \\ &\times 2\sum_{n=1}^{\infty}J_{2n-1}\cos[(2n-1)\omega_3 t] \\ &+\frac{E_0^2}{2}R\eta\sum_{n=1}^{\infty}J_{2n-1}\cos[(2n-1)\omega_2 t]\times\left[J_0 + 2\sum_{n=1}^{\infty}J_{2n}\cos(2n\omega_1 t)\right] \\ &\times\left[J_0 + 2\sum_{n=1}^{\infty}J_{2n}\cos(2n\omega_3 t)\right] \\ &+\frac{E_0^2}{2}R\eta\sum_{n=1}^{\infty}J_{2n-1}\cos[(2n-1)\omega_3 t]\times\left[J_0 + 2\sum_{n=1}^{\infty}J_{2n}\cos(2n\omega_1 t)\right] \\ &\times\left[J_0 + 2\sum_{n=1}^{\infty}J_{2n}\cos(2n\omega_2 t)\right]\end{aligned}$$

Assume that: subcarrier frequencies are 1.004 GHz, 1.008GHz and 1.012GHz; channel spacing is 5 MHz; laser output power is 0 dBm; modulator insert loss is 8 dB; switching voltage is 5 V; input resistance is 50 Ω; photodetector responsivity is 0.85 A/W; receiver noise floor is -70dBm; receiver load resistance is 50 Ω; amplifier gain is 50dB; amplifier noise figure is 3 dB; filter loss is 1dB; filter noise figure is 1dB; IIP3 of modulator is 5 dBm; IIP3 of receiver is 15 dBm. Using these parameters, we can calculate the SNR and SFDR

changes due to intermodulation distortions for the side channel (ω_1 and ω_3) and the central channel (ω_2) based on above solution and the analysis in the 3.4.1 and 3.4.2, which are illustrated in Fig. 4.2a and Fig. 4.2b. The results show that the reductions of SNR, SFDR and IIP3 in the three-channel system are 7 dB, 2.3 dB and 4.6 dB correspondingly.

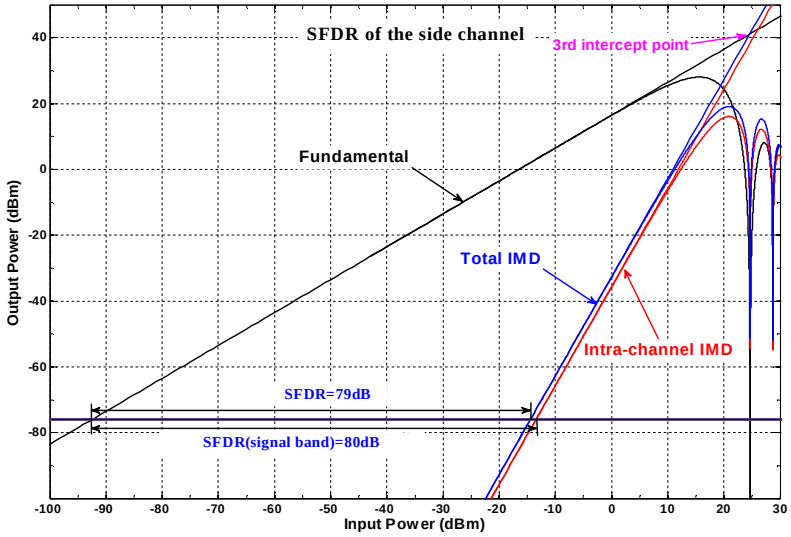

(a)

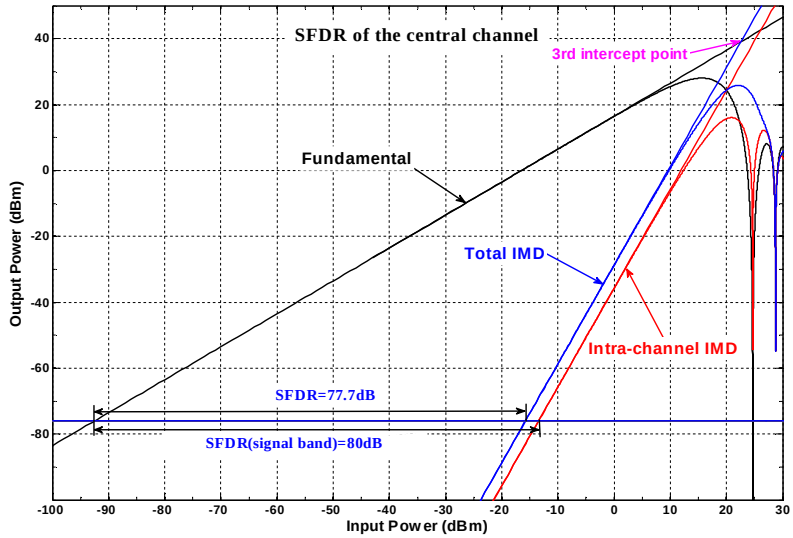

(b)

Fig.4.2 Input power vs. output power in (a) the side channel and (b) the central channel of a three-channel system

At the receiver end, the transfer function of a photo detector can be expressed as Eq. 4.8. $\beta=V\pi/V_\pi$ is the modulation index; k_1 is photo-receiver responsicivity; and k_2 and k_3 are determined by the 2nd-order and the 3rd-order input intercept points of the photo-receiver.

To quantify the intra-channel intermodulation distortion, again we use the two-tone on the photo detector. The fundamental product and the intra-channel intermodulation product are formulated as Eq. 4.9 and Eq. 4.10, and the SNR due to the intra-channel intermodulation is given in Eq. 4.11.

(4.8) $$I(t) = k_1 E(t)^2 + k_2 E(t)^3 + k_3 E(t)^4$$

(4.9) $$2\beta \times \frac{E_0^2}{8} k_1 + \left(4\beta + 4\beta^3 + 2\beta^3\right) \times \frac{3E_0^4}{8\times 16} k_3 = 2\beta \times \frac{E_0^2}{8} k_1$$

(4.10) $$\frac{3E_0^4}{8\times 16} k_3 \times 3\beta^3$$

(4.11) $$SNR = \left(32k_1 / 9E_0^2 \beta^2 k_3\right)^2$$

(4.12)
$$\begin{aligned} I &= \frac{E_0^2}{4} k_1 \cos(\omega t)^2 (1 + V\pi/V_\pi \sin\omega_1 t + V\pi/V_\pi \sin\omega_2 t + V\pi/V_\pi \sin\omega_3 t)^2 \\ &+ \frac{E_0^3}{8} k_2 \cos(\omega t)^3 (1 + V\pi/V_\pi \sin\omega_1 t + V\pi/V_\pi \sin\omega_2 t + V\pi/V_\pi \sin\omega_3 t)^3 \\ &+ \frac{E_0^4}{16} k_3 \cos(\omega t)^4 (1 + V\pi/V_\pi \sin\omega_1 t + V\pi/V_\pi \sin\omega_2 t + V\pi/V_\pi \sin\omega_3 t)^4 \\ &= \frac{E_0^2}{8} k_1 (1 + V\pi/V_\pi \sin\omega_1 t + V\pi/V_\pi \sin\omega_2 t + V\pi/V_\pi \sin\omega_3 t)^2 \\ &+ \frac{3E_0^4}{8\times 16} k_3 (1 + V\pi/V_\pi \sin\omega_1 t + V\pi/V_\pi \sin\omega_2 t + V\pi/V_\pi \sin\omega_3 t)^4 \end{aligned}$$

Similarly, three-tone test is used to determine the inter-channel intermodulation distortion. The output electrical signal can be expressed using Eq. 4.12. The received fundamental products and the inter-channel intermodulation products are listed in Table 4.2.

Table 4.2 Three-tone test results at the receiver side

	Fundamental		Intermodulation	
	Frequency	Amplitude	Frequency	Amplitude
Channel1	ω_1	$2\beta \times \frac{E_0^2}{8} k_1$	$2\omega_2 - \omega_3$	$\frac{3E_0^4}{8\times 16} k_3 \times 3\beta^3$
Channel2	ω_2	$2\beta \times \frac{E_0^2}{8} k_1$	$\omega_1 + \omega_3 - \omega_2$	$\frac{3E_0^4}{8\times 16} k_3 \times 6\beta^3$
Channel3	ω_3	$2\beta \times \frac{E_0^2}{8} k_1$	$2\omega_2 - \omega_1$	$\frac{3E_0^4}{8\times 16} k_3 \times 3\beta^3$

The SNRs due to the receiver inter-channel intermodulation distortion for these three channels are $(32k_1/9E_0^2\beta^2k_3)^2$, $(16k_1/9E_0^2\beta^2k_3)^2$, and $(32k_1/9E_0^2\beta^2k_3)^2$ respectively. If we consider both intra-channel and inter-channel intermodulation distortions, the SNRs for these three channels are calculated to be $(32k_1/9E_0^2\beta^2k_3)^2*1/2$, $(32k_1/9E_0^2\beta^2k_3)^2*1/5$ and $(32k_1/9E_0^2\beta^2k_3)^2*1/2$. Comparing the three-channel system with a single channel system, the reductions of SNR, SFDR and IIP3 at the receiver end are comparable to that at the transmitter frontend.

Assuming that the channel number is N and the input signal power is unified, based on the three-tone and two-tone tests, we can calculate the nonlinearity products for the i^{th} channel and the SNR degradation due to increasing channel number.

At the Tx:

Inter-channel IMD from higher frequency channels: $\left\lfloor {(N-i)}/{2} \right\rfloor {J_2^2}/{J_0^2}$

Inter-channel IMD from lower frequency channels: $\left\lfloor {(i-1)}/{2} \right\rfloor {J_2^2}/{J_0^2}$

Inter-channel IMD from both higher and lower channels: $(i-1)\,J_1^4/J_0^4$ **(**$i \le N+1/2$**)**

Total inter-channel IMD: $(N-2)\,J_2^2/J_0^2 + (i-1)\,J_1^4/J_0^4$

Intra-channel IMD: J_2^2/J_0^2

Total IMD: $(N-1)\,J_2^2/J_0^2 + (i-1)\,J_1^4/J_0^4 = (N-1+4\times(i-1))\,J_2^2/J_0^2$

SNR degradation at transmitter side $= \begin{cases} 10\log(3N-3) & \textbf{N is even} \\ 10\log(3N-5) & \textbf{N is odd} \end{cases}$

At the Rx side:

Inter-channel IMD from higher frequency channels: $\left\lfloor (N-i)/2 \right\rfloor (32k_1/9E_0^2\beta^2k_3)^{-2}$

Inter-channel IMD from lower frequency channels: $\left\lfloor (i-1)/2 \right\rfloor (32k_1/9E_0^2\beta^2k_3)^{-2}$

Inter-channel IMD from both higher and lower channels: $(i-1)(16k_1/9E_0^2\beta^2k_3)^{-2}$ **(**$i \le N+1/2$**)**

Total inter-channel IMD $(N-2)(32k_1/9E_0^2\beta^2k_3)^{-2} + (i-1)(16k_1/9E_0^2\beta^2k_3)^{-2}$

Intra-channel IMD: $\left(\frac{32k_1}{9E_0^2\beta^2k_3}\right)^{-2}$

Total IMD: $[(N-1)+(i-1)\times 4]\left(\frac{32k_1}{9E_0^2\beta^2k_3}\right)^{-2}$

SNR degradation at receiver side $= \begin{cases} 10\log(3N-3) & \textbf{N is even} \\ 10\log(3N-5) & \textbf{N is odd} \end{cases}$

Considering that the transmitter intermodulation products and the receiver intermodulation products are independent, the degradation in a multi-channel analog transport system can be expressed as Eq. 4.13.

(4.13) $$\begin{cases} 10\log(3N-3) & \textbf{N is even} \\ 10\log(3N-5) & \textbf{N is odd} \end{cases}$$

4.3.2 SNR in multi-channel DRoF links

In multi-channel DRoF links, according to the analysis in Chapter 2, only the bandpass sampling aliasing noise and ADC quantization noise are related to the channel number. To analyse the change of bandpass sampling aliasing noise, we assume that a bandpass signal is first fed into an ideal anti-aliasing filter, and then sampled at a sampling rate of f_s. In applying bandpass sampling to relocate a bandpass signal to a lower frequency location, the resulting SNR is poorer than that from an equivalent analog system, and the degradation is due to the noise aliasing from the bands between dc and the passband [4.11]. Under the assumption that the introduced thermal noise in a sampling device is an additive white Gaussian noise (AWGN) with zero-mean and the power spectral density (PSD) of the noise is a constant N_0, the corresponding SNR after bandpass sampling is given by Eq. 1.14 [4.12]. In a multi-channel case, the out-of-band thermal noise power from each channel contributes to the total thermal noise power. Therefore, the function of SNR after bandpass sampling in a multi-channel DRoF link can be rewritten as Eq. 4.15.

$$SNR_A = P_s / (P_{N_s} + N_0 B + (m-1) N_0 B) \tag{4.14}$$

$$SNR_A = P_s / (P_{N_s} + N N_0 B + N(m-1) N_0 B) \tag{4.15}$$

Here, P_S is the signal power; P_{Ns} is the input noise power of the anti-aliasing filter; B is the bandwidth of each channel; N_0B is the introduced thermal noise power in the anti-aliasing filter; m is the total number of f_S bands between dc and the passband; $(m-1)N_0B$ represents the total out-of-band thermal noise power; N is the channel number.

Signal-to-quantization noise ratio is defined as the ratio of the root mean square value of the input analog signal to the root mean square value of the quantization noise [4.13]. In an ideal ADC, where the quantization error is uniformly distributed between −1/2 LSB (least significant bit) and +1/2 LSB, and the root mean square value of the error signal is given in Eq. 4.16.

(4.16) $$RSM_{e_q(n)} = \sqrt{2^{Q-1}\int_{-1/2^Q}^{1/2^Q} e_q^2(n)} = \frac{1}{\sqrt{32^Q}}$$

For a full-amplitude, M-ary QAM modulated, N-channel signal, the root mean square value of the input analog signal follows Eq. 4.17.

(4.17) $$RSM_{x(n)} = \left(N\frac{\sqrt{M}+1}{\sqrt{M}-1} \right)^{\frac{1}{2}}$$

Therefore, the function of SNR due to the ADC quantization noise in the multi-channel DRoF link can be expressed as Eq. 4.18.

(4.18) $$SNR_Q = 20\log_{10}\left(\left(\frac{\sqrt{M}+1}{\sqrt{M}-1} \right)^{\frac{1}{2}} \sqrt{N}\,2^Q \right) = 6.02Q + 10\log\left(\frac{N\sqrt{M}+N}{\sqrt{M}-1} \right)(dB)$$

As shown in the previous chapter, an ADC resolution of 8 bits is sufficient to provide optimal link efficiency; the following results in multi-channel DRoF links are calculated using an ADC resolution of 8 bits. Based on Eq. 4.17 and Eq. 4.18, we can deduce that the SNR decreases by *10log(N)* dB as a result of aliasing noise and ADC quantization noise. No other noise sources are affected by the increasing channel numbers. Therefore the total SNR degradation ina multi-channel DroF link is no more than *10log(N)* dB. As quantization noise

and aliasing noise dominate this link, we can use *10log(N)* dB as the total SNR degradation in the multi-channel DRoF system.

4.3.3 Comparison on performance degradation of multi-band systems in both links

According to the previous analysis, we calculate the curves of SNR degradation vs. channel number in both analog and digitized RF links, and the results are plotted in Fig. 4.3. Both links show a gradual degradation in SNRs with increasing channel numbers but the SNR deterioration in the digitized RF link is at a much slower rate compared to the analog link. The green line denotes the degradation difference between these two links. It is evident that when the channel number is more than 10, the degradation difference remains constant at 4.5 dB. Therefore, the digitized RF transport has a more superior performance over the analog counterpart even in a multi-channel environment.

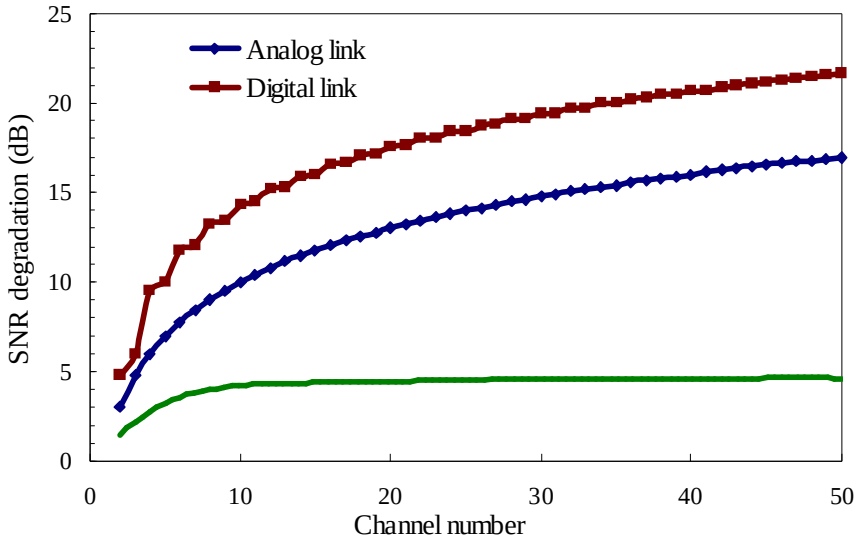

Fig.4.3 SNR degradation vs. channel number

In analog multi-band RF transmission links, the IP3 decreases with channel number while the nonlinearity products increase with channel number. The degradation of IP3 has been

quantified to be two third of the increase in the nonlinearity products [4.10, 4.14]. Fig. 4.4 takes a 3-channel system for example, and explains the IP3 reduction in multi-channel systems using the parameters in Table 3.1. And the RF bandwidth (B) in multi-band system is N-timed under the assumption that each channel carries the same amount of data. Consequently, the dynamic range degradation in an analog multi-band RF system is expressed as Eq. 4.19.

$$10\log(N)+\frac{2}{3}\times\begin{cases}10\log(3N-3)\,\mathbf{dB} & \mathbf{N\ is\ even}\\ 10\log(3N-5)\,\mathbf{dB} & \mathbf{N\ is\ odd}\end{cases} \tag{4.19}$$

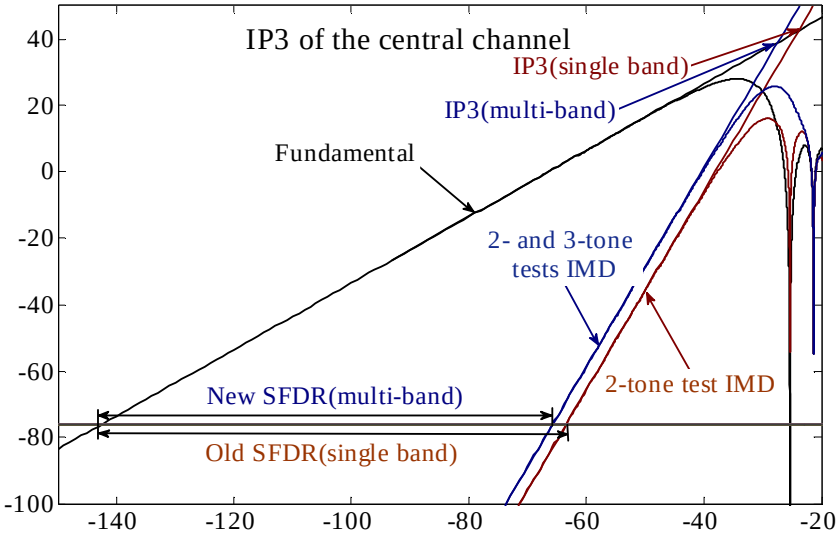

Fig.4.4 IP3 reduction in multi-band system

In digitized multi-band RF transmission links, no nonlinear effect is generated with increasing channel number as binary digital signals are transmitted in the optical link. The only factor resulting in dynamic range decreasing is the SNR degradation which has been quantified as *10log(N)* dB. Fig. 4.5 shows the dynamic range degradations in both links. It is evident that the dynamic range in both links decrease with increasing channel number, with the analog link decreases at twice the rate as the digital link.

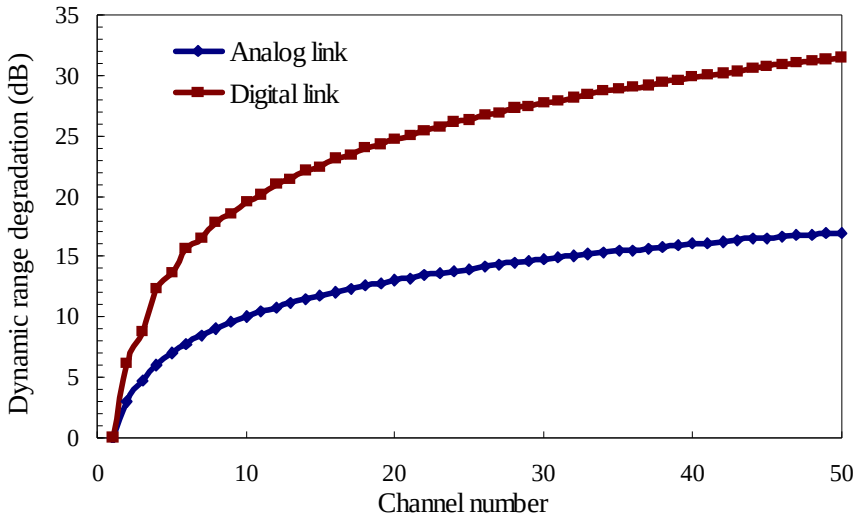

Fig.4.5 Dynamic range degradation vs. channel number

4.4 Experimental demonstration of multi-channel DRoF transport

4.4.1 Experimental setup

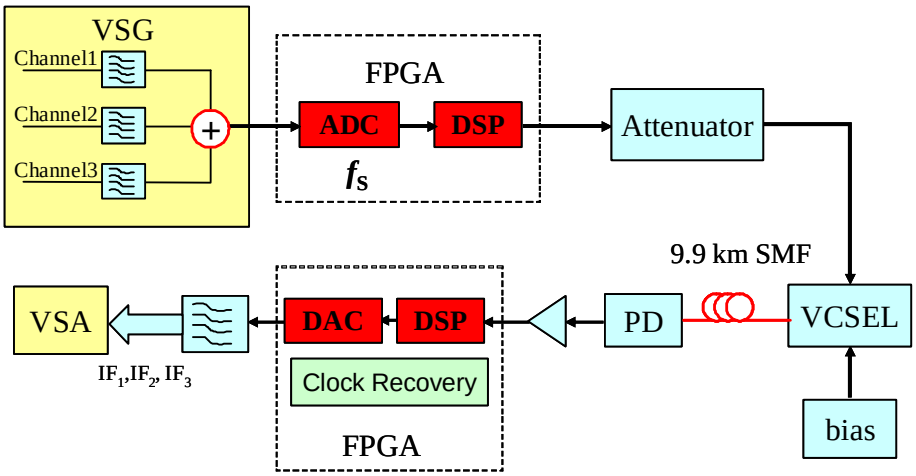

Fig.4.6 Experimental setup

Based on the DRoF transmission scheme given in Section 4.2, we experimentally demonstrated a DRoF link, which is shown in Fig. 4.6, using commercially available FPGA to establish the digitization interface. A vector signal generator (VSG) and a vector signal analyzer (VSA) were used as the RF transmitter and receiver respectively. Due to the bandwidth limitation of the ADC (AD9344) on the FPGA board, the carrier frequency of the RF signal generated by the VSG was set to around 20 MHz, the sample rate of the ADC was fixed at 5 MHz, and the symbol rate of each channel was fixed at 100 kS/s. We used an Altera Stratix II DSP Development FPGA board to digitize the RF signal including sampling, quantizing, and performing signal processing functionalities such as parallel-to-serial conversion and clock management. The resolution of quantization was fixed at 8 bits. The output of the FPGA was attenuated before directly modulating a 1.55 nm VCSEL. The optically modulated signal was then transmitted over 9.9 km of single mode fiber (SMF). In the receiver, a PIN detector was used to detect the signal. The received signal was amplified before entering the FPGA board. The FPGA was used to recover the clock, locate the most significant bit and convert the serial signal to a parallel signal. The parallel data stream was then launched into a DAC to reconstruct the signal at IF frequency. Bandpass filters were employed to separate multiple bands from the reconstructed signal before measured in the VSA.

4.4.2 Experimental results analysis

Fig. 4.7 shows the RF power spectra of a single-channel signal at 20.8 MHz (a) after the electrical back-to-back (B2B) transmission and (b) after the DRoF transmission. It clearly shows that after the DRoF transmission link the RF signal was reconstructed at its corresponding IF frequency in the first Nyquist zone. The noise power introduced in the DRoF link was -40 dBm, and contributed to a 20 dB loss in the SNR (decreasing from 60 dB to 40 dB). Fig. 4.8a shows the power spectra of the three-band RF signal generated by the VSG with the carrier frequencies at 20.4 MHz, 20.8 MHz and 21.2 MHz, respectively. Since

the sampling rate was set to 5 MHz, all these three bands were located in the fifth-order Nyquist region. Fig. 4.8c shows the power spectrum of the output signal from the DAC, which has replicas of the original signal in every Nyquist region. It also illustrates that the first-order Nyquist region has the largest power. Fig. 4.8b shows the filtered first spectrum replica for data recovery. In Fig. 4.8b, the central frequencies of the three recovered channels are 0.4 MHz, 0.8 MHz and 1.2 MHz respectively. Since the carriers of the original signal are located in the same Nyquist region, the channel spacing remains the same after the DRoF transmission.

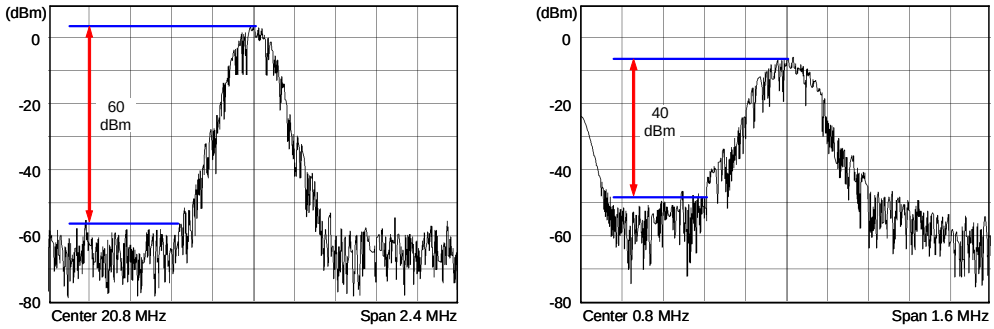

(a) (b)

Fig.4.7 Measured RF power spectrum of the single-channel signal in (a) electrical back-to-back transmission link and (b) digitized RF transmission link

By comparing Fig. 4.7a and Fig. 4.8a, we ascertain that the noise level and the interference level of the original signal are -60 dBm and -20 dBm respectively. Similarly, the comparison between Fig. 4.7b and Fig. 4.8b illustrates that the noise level and the interference level in the digitized signal are -40 dBm and -20 dBm respectively. It clearly shows that, although the DRoF transmission link increases the noise level from -60 dBm to -40 dBm, it is still significantly lower than the interference noise (-20 dBm). Therefore, for a channel spacing of 0.4 MHz and symbol rate of 100 kS/s, when implementing the multiple channel transmission

using DRoF technique, the noise and intermodulation levels do not have any adverse impact on the link performance.

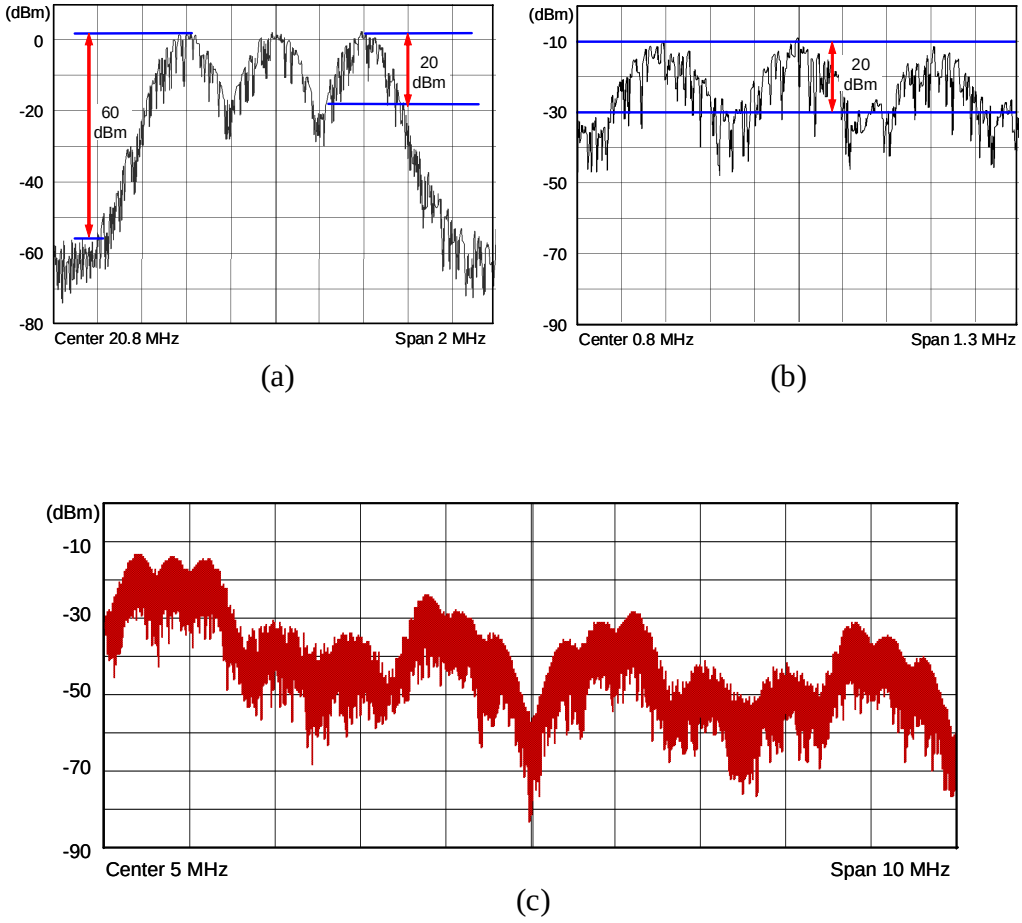

Fig.4.8 Measured RF power spectrum of (a) the original signal from the VSG, (b) the replica used to recover the data, (c) DAC output signal (RF carrier frequencies at 20.4 MHz, 20.8 MHz and 21.2 MHz)

Fig. 4.9 shows the measured EVM as a function of received optical power when the channel spacing is fixed at 0.4 MHz with a central frequency of 20.8 MHz. It shows that the multi-band DRoF transmission provides a satisfactory EVM performance for each of the three channels. From these results it is evident that the EVMs of all the channels remain constant at very low values (< 1%) for a received optical power below -27 dBm. The EVM

curves of the side channels (Channel 1 and Channel 3) are very similar with each other and are lower compared to the EVM curve of the central channel (Channel 2). This illustrates that the EVM performance in Channel 1 and Channel 3 are better than in Channel 2, and it is because the middle channel suffers most from the intermodulation distortion compared to the two adjacent channels on both sides.

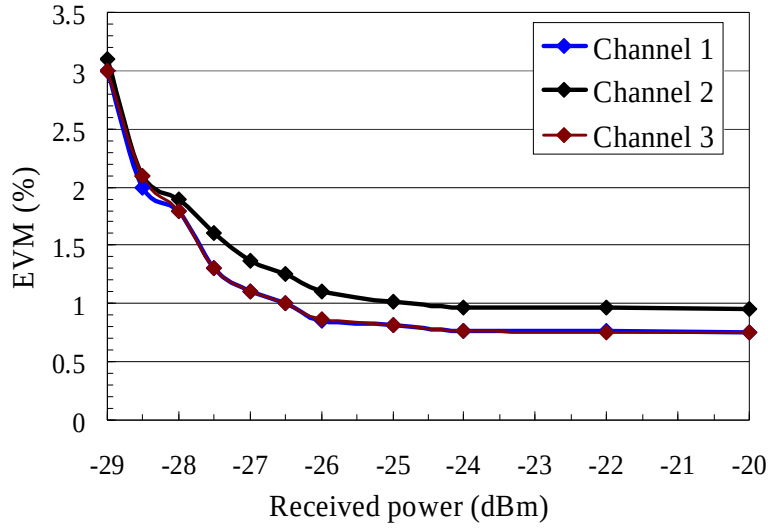

Fig.4.9 EVM curves of each channel in DRoF link

Table 4.3 Measured EVM with spacing at 0.4 MHz

System	Channel 1(20.4MHz)	Channel 2(20.8MHz)	Channel 3(21.2MHz)
B2B	0.6%	1.2%	0.6%
DRoF	0.75%	0.95%	0.75%
Analog	0.7%	1.4%	0.7%

Table 4.3 lists the EVM performances of the three channels in electrical back-to-back link, in the DRoF link, and in the analog RoF link, when the optical received power is fixed at -20 dBm. For Channel 1 and Channel 3, the EVM performances have deteriorated to a similar level in both DRoF link (from 0.6% to 0.75%) and analog link (from 0.6% to 0.7%). However, for Channel 2 the DRoF transmission link improved the EVM from 1.2% to 0.95% while the analog link has a worse EVM of 1.4%. The experimental results show that the DRoF transmission results in better SNRs for the central channel when the channel spacing is 0.4 MHz with severe inter-channel interference at the transmitter.

We have also investigated the performance of the multi-channel DRoF transmission when the RF carrier frequencies are located in different Nyquist regions to minimize inter-channel interference at the transmitter. Fig. 4.10 shows the RF power spectra of both the original signal and the recovered signal when the RF carrier frequencies are set at 15.4 MHz, 20.8 MHz and 26.2 MHz in the 4^{th}-order, 5^{th}-order and 6^{th}-order Nyquist region respectively. The noise level of the signal generated in the VSG is -52dBm. In the recovered signal, the noise levels of the side bands and the central band are -35 dBm and -20 dBm respectively. In the DRoF transmission link, the RF bands are downconverted to 0.4 MHz, 0.8 MHz and 1.2 MHz that fall within the same Nyquist region. Therefore, the channel spacing is reduced from 5.4 MHz to 0.4 MHz, which in turn increases the inter-channel interference of the middle channel at the receiver. From Table 4.4 it can be seen that in electrical back-to-back transmission the middle channel is not affected by inter-channel interference as compared to that when the channel spacing is 0.4 MHz. Table 4.4 also shows the measured EVMs of the three channels after the DRoF transmission. It is evident that the EVMs have increased due to the DRoF link noise and inter-channel interference; however the EVM is still less than 1% which guarantees a satisfactory link performance. Results obtained in Table 3 and 4 indicate that the level of inter-channel interference on the middle channel is not dependent on the initial channel spacing at the transmitter, but rather on the channel spacing after bandpass

sampling scheme at the receiver. Our investigation shows that for a channel spacing of 0.4 MHz after downconversion via bandpass sampling scheme the EVM of the middle channel remains constant at 0.95% regardless of the initial channel spacing at the transmitter.

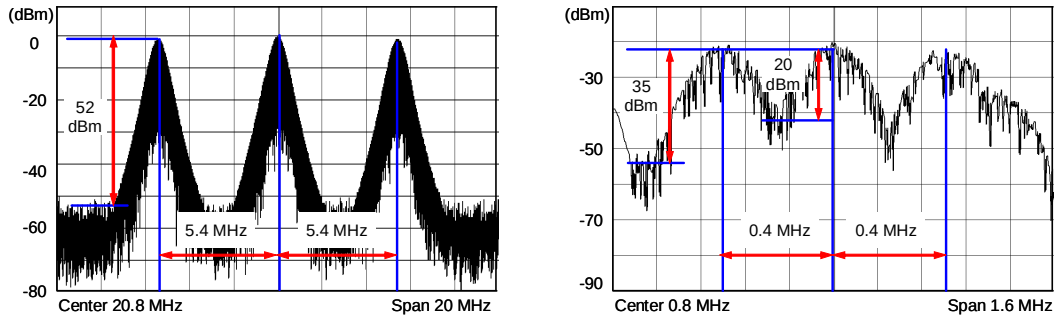

(a) (b)

Fig.4.10 Measured RF power spectrum of (a) the original signal from the VSG, (b) the replica used to recover the data (RF carrier frequencies at 15.4 MHz, 20.8 MHz and 26.2 MHz)

Table 4.4 Measured EVM with spacing at 5.4 MHz

System	Channel 1 (15.4MHz)	Channel 2 (20.8MHz)	Channel 3 (26.2MHz)
B2B	0.6%	0.6%	0.6%
DRoF	0.68%	0.95%	0.78%

4.5 Summary

In this chapter, we proposed multi-channel RF transmission using digitized RF-over-fiber technique, and realized frequency conversion using a single ADC and a single DAC. Bandpass sampling for multiple distinct bands is employed to sample and downconvert the

subcarrier multiplexed RF signals to IF signals ensuring no overlapping of the multiple frequency bands within each Nyquist window.

Secondly, the SNR and dynamic range of a multi-channel system are analysed in both analog and digitized RF-over-fiber links. The intermodulation distortion is the main reason of performance deterioration in analog links, while in digitized links the increased aliasing and quantization noises worsen the link performance. The degradations of SNR and dynamic range caused by the channel number increasing are quantized, and results show that the degradations in digitized links are less severe than in analog links.

Thirdly, we experimentally implemented a DRoF link for multi-channel RF systems by employing commercially available FPGA and ADC, and recovered the data with satisfactory EVM performance. We have experimentally shown that all of the RF bands can be downconverted to a same Nyquist region, and recovered from the first-order replica of the original signal in the frequency domain without the physical needs of a mixer and a local oscillator. Our experimental results show that the noise level in the DRoF link is -40 dBm, and the level of inter-channel interference on the middle channel after DRoF transport is not dependent on the initial channel spacing at the transmitter. It is dependent on the channel spacing after downconversion via bandpass sampling at the receiver. Our investigation shows that the EVM of the middle channel remained constant as long as the channel spacing of the received signals does not change, and it is regardless of the initial channel spacing before transmission. Both theoretical and experimental results show that the digitized RF-over-fiber technique provides a more efficient approach than the analog transmission in implementing multi-channel radio optical networks.

4.6 References

[4.1] W. Chen and W. Way, “Multi-channel signal-sideband SCM/DWDM transmission systems,” Journal of lightwave technology, vol. 22, no. 7, pp. 1679-1693, Jul. 2004.

[4.2] C. Lim, A. Nirmalathas, M. Attygalle, D. Novek, and R. Waterhouse, "On the merging of millimeter-wave fiber-radio backbone with 25 GHz WDM ring networks," Journal of lightwave technology, vol. 21, no. 10, pp. 2203-2210, Oct. 2003

[4.3] G. Smith, D. Novak, and Z. Ahmed, "Technique for optical SSB generation to overcome dispersion penalties in fiber-radio system," Electronic Letters, vol. 33, no. 1, pp. 74–75, Jan. 1997.

[4.4] A. Narasimha, X. Meng, M. Wu, and E. Yablonovitch, "Tandem singleside band modulation scheme for doubling spectral efficiency of analogue fiber links," Electronic Letters, vol. 36, no. 13, pp. 1135–1136, Jun. 2000.

[4.5] M. Bakaul, A. Nirmalathas, C. Lim, D, Novak, and R. Waterhouse, "Hybrid Multiplexing of Multiband Optical Access Technologies Towards an Integrated DWDM Network," IEEE Photonics Technology Letters, vol. 18, no. 21, pp. 2311-2313, Nov. 2006.

[4.6] C. Wu and X. Zhang, "Impact of Nonlinear Distortion in Radio Over Fiber Systems With Single-Sideband and Tandem Single-Sideband Subcarrier Modulations" Journal of lightwave technology, vol. 24, no. 5, pp. 2076-2090, MAY 2006

[4.7] D. Derickson, "Fiber Optic Test and Measurement", Upper Saddle River, New Jersey, 1998.

[4.8] S. Chandra, A. V. Vardhanan and R. Gangopadhyay, "Simultaneous dispersion and non-linearity compensation with mid-span optical phase conjugation and distributed Raman amplifier for a sub-carrier multiplexed optical transmission link", Optics Communications, vol. 279, pp. 177–182, 2007.

[4.9] D. M. Akos, M. Stockmaster, J. B. Y. Tsui, and J. Caschera, "Direct bandpass sampling of multiple distinct RF signals," IEEE Transaction on Communications, vol. 47, no. 7, pp. 983-988, July 1999.

[4.10] B. H. Wang, P. Chiang, M. Kao, and W. Way "Large-Signal Spurious-Free Dynamic Range Due to Static and Dynamic Clipping in Direct and External Modulation Systems", Journal of lightwave technology, vol. 16, no. 10, pp. 1773-1785, Oct. 1998.

[4.11] R. G. Vaughan, N. L. Scott, and D. R. White, "The theory of bandpass sampling," IEEE Transaction on Signal Processing, vol. 39, no. 9, pp. 1973-1984, Sep. 1991.

[4.12] Y. Sun, "Effects of noise and jitter on algorithms for bandpass sampling in radio receivers," ISCAS '04, vol. 1, pp. 761-764, May 2004.

[4.13] John G. Proakis, "Digital Signal Processing - Principles, Algorithms and Applications,"

[4.14] J. Lerdworatawee, and W. Namgoong, "Revisiting Spurious-Free Dynamic Range of Communication Receivers", IEEE Transactions on Circuits and Systems , vol. 53, pp. 937-943, Apr. 2006.

Chapter 5

Bidirectional Hybrid-Fiber Radio using Digitized RF-over-Fiber

5.1 Introduction

The proliferation of interactive multimedia applications such as online gaming coupled with the needs to be "connected-at-all-times" has fuelled the evolution of future broadband wireless networks. To improve the cost effectiveness of future wireless networks, simultaneous transmission of different signals for multiple radio services is an attractive option to enable the reuse of the existing wireless network infrastructure and the utilization of multi-band antennas in environments where antenna towers are sometimes rare and may already be overpopulated [5.1]. Hybrid Fiber-Radio (HFR) networks based on the integration of wireless and optical access network infrastructures via a common backhaul network is a promising solution for the future broadband wireless access which can lead to significant cost benefits for network operators in both operational and capital expenditures. Such network also offers the potential to support multiple wireless standards by employing distributed antenna systems in the base stations, and thus maximizing resource usage and infrastructure sharing [5.3].

As previously discussed Radio-over-Fiber (RoF) technique is an attractive scheme to provide transparent transmission of the radio signals via optical backhaul networks. This technology relies on simplifying the architecture of the base stations and centralizing most of the functionalities such as frequency up-conversion, carrier modulation, and multiplexing in

a centralized location, usually in the central office [5.2]. Though this approach has been well-suited for distribution of microwave and millimeter-wave wireless signals, it still demands highly linear optical links with sufficient link gain to accommodate for antennae emitting over a wide coverage area. This constraint is even more stringent when multiple radio services are simultaneously transmitted, due to the subcarriers multiplexing or wavelengths multiplexing techniques used for multiple-radio distributed Hybrid Fiber-Radio systems [5.3, 5.4].

In Chapter 3 and Chapter 4, we have demonstrated a digitized RF-over-fiber (DRoF) transport as a viable alternative to analog RoF links by merging digital optical links with electronic digitization [5.5, 5.6]. This scheme relies on bandpass sampling technique which results in relatively low overall data rates in comparison to the wireless carrier frequency [8]. An optical link employing DRoF technique can maintain its dynamic range independent of the fiber transmission distance until the signal level goes beyond the sensitivity of the link. The base stations of this link can be further simplified using bandpass sampling technique to establish frequency translation functionality via ADCs and DACs. Moreover, the digitized RF interfaces could be easily integrated with existing and future broadband optical and high speed networks. Therefore, the DRoF technique is potentially a promising solution for the future low-cost high-performance Hybrid Fiber-Radio implementation.

In this chapter, we propose and experimentally demonstrate an efficient full-duplex Hybrid Fiber-Radio transmission based on the digitized RF-over-fiber concept for multiple wireless signals transmission. For the first time we realize a downlink transmission link using digitized RF-over-fiber technique without the use of physical mixers and local oscillators. By using a single ADC and a single DAC, multiple wireless signals of different standards can be simultaneously supported resulting in a simple base station design without the needs for analog devices for frequency up- and down-conversion. Error-free detection of an HFR-DRoF link is achieved for the simultaneous transmission of three different wireless standards:

Global System for Mobile communications (GSM), the Universal Mobile Telecommunications System (UMTS), and the Worldwide Interoperability for Microwave Access (WiMAX). We also experimentally investigate the power requirement for the downlink transmission of multiple wireless services using digitized RF-over-fiber scheme to quantify the frequency up-conversion efficiency.

5.2 Proposed bidirectional HFR transmission using DRoF Technique

5.2.1 Frequency relocation principle

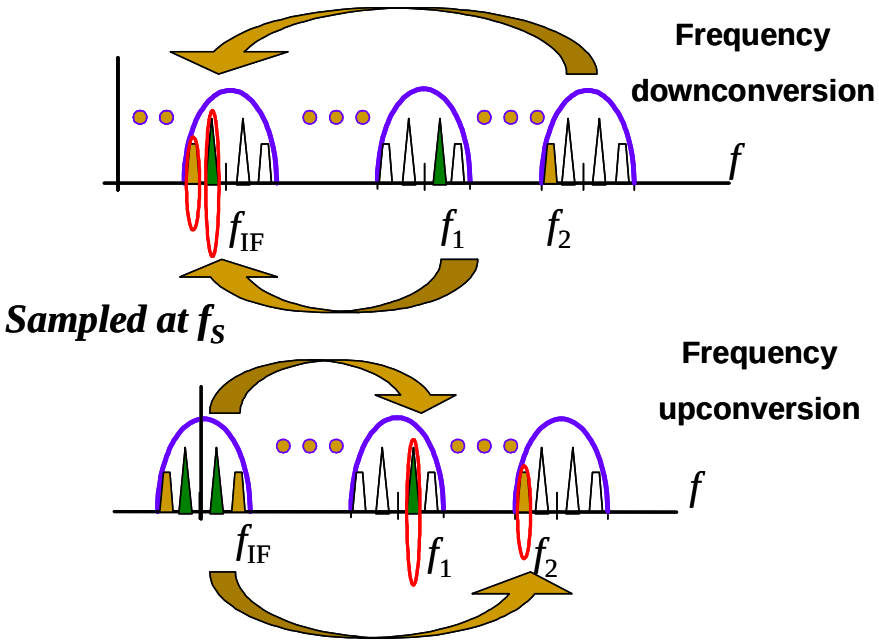

Fig.5.1 Frequency relocation scheme using bandpass sampling

As extensively discussed in Chapter 3 and Chapter 4, bandpass sampling is a sampling technique which undersamples a target signal with a much lower sampling frequency compared to direct sampling and it is applicable to single and multiple signals transmission. To ensure exact reconstruction of the original signals at lower frequencies and to prevent spectral aliasing, the sampling rate is strictly governed by the principles given in [5.8]. This

theory also enables a wireless signal to be frequency-translated to at a higher frequency. By sampling a low frequency signal and selecting the appropriate images in the higher frequency window, we are able to establish frequency up-conversion of the original signal. Fig. 5.1 demonstrates the synchronous frequency up- and down-conversion scheme of two separate radio frequency signals using bandpass sampling.

5.2.2 HFR-DRoF system

Based on the bandpass sampling theory, we propose a DRoF link that supports multi-channel full-duplex HFR transmission and the schematic is shown in Fig. 5.2. In the downlink path, wireless services at different IF frequencies are electrically combined within the central office before digitized using an ADC. The sampling rate of the digitization process is selected based on the bandpass sampling theory to avoid signal aliasing. Upon digitization, the samples are processed digitally via digital signal processing (DSP) modules including parallel-to-serial conversion and clock management. The digitized data stream is modulated onto an optical carrier before transported over the optical link and recovered using a photodetector. In the BSs, the analog signals including the image replicas are reconstructed using a DAC in conjunction with a DSP module. To extract the wireless signals in a multiple-wireless environment, the analog signal is further divided using a power splitter (PS) and the wireless signal at the desired wireless frequency is extracted separately using a bandpass filter (BPF) and amplified before the air-interface. In this instance, the wireless signals are essentially up-converted to the desired wireless frequencies (RF) without any physical mixers and local oscillators. The multiple wireless services are then radiated to the customers via the distributed antenna system (DAS). Similarly for the uplink transmission, the received wireless signals are combined before digitization in the base station and transported back to the CO for digital signal processing.

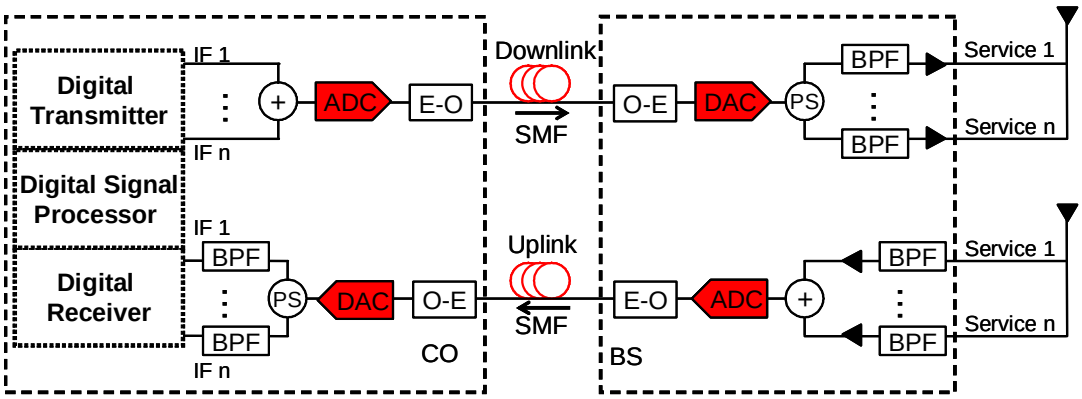

Fig.5.2 DRoF transmission scheme for HFR access

5.3 Experimental Setup and Results Analysis

We have experimental demonstrated a single channel DRoF uplink in Chapter 3 and our results indicated that 8-bit resolution for ADCs and DACs is sufficient to accurately reconstruct the wireless signals. In this work, we further extend our investigation and demonstrate both uplink and downlink paths incorporating the DRoF technique to distribute multiple wireless signals simultaneously. We will show that these wireless signals can be accurately reconstructed at the wireless carrier frequencies without any local oscillators and analog mixers. We will also quantify the amount of amplification required to establish the frequency up-conversion efficiency via bandpass sampling technique.

5.3.1 Experimental setup

The experimental setup of our proposed downlink HFR transmission of GSM, UMTS, and WiMAX wireless services at RF bands of 800 MHz, 1.8 GHz and 2.4 GHz using DRoF technique is shown in the dashed blue boxes of Fig. 5.3. The GSM, UMTS, and WiMAX signals used in our setup have the symbol rates of 1 MS/s (QPSK modulation), 5 MS/s (DQPSK modulation), and 5 MS/s (16QAM modulation), respectively. In our experiment, the three wireless signals were generated at IF frequencies (F_{IF}) using a VSG, then filtered

before combined into one multi-band signal. The power of the IF carriers for all the three signals were set to -5 dBm. The ADC sampling functionality was realized using a Tektronix TDS6154C Digital Sampling Oscilloscope (DSO) with a bit-resolution of 8 bits. The samples were quantized and serialized off-line using software implementation. In addition, preambles were also added for clock synchronization and bit identification purposes to simplify the signal reception at the BS. The digital data stream was then generated in an arbitrary waveform generator (AWG) with a resulting bit rate of 8 times the sampling rate. The digital data stream directly modulated a commercially available 2.5 Gbps VCSEL, which was biased at 5 mA. After transmission over 26.4 km of a single-mode fiber, the digital data stream was detected using a PIN receiver and captured using a DSO. The necessary digital signal processing functions such as clock recovery, the most significant bit identification, serial-to-parallel conversion and decoding of quantized data, were implemented using software to regenerate the samples offline. The AWG was then employed to reconstruct the signal from the discrete sampled format to the continuous analog format using the same sampling rate as in the transmitter to establish the DAC functionality. The reconstructed analog signal was equally split into three parts, and separately filtered using bandpass filters with centre frequencies corresponding to the GSM, UMTS and WiMAX wireless signals (F_{RF}). The recovered wireless signals were amplified to a common power level of -10 dBm using 40 dB, 45 dB and 50 dB amplifications for GSM, UMTS and WiMAX wireless signals respectively. The multiple radio services can then be radiated via the DAS antennae. In order to evaluate the performance of the transmission link, we used a VSA to measure the EVM for each wireless signal under investigation.

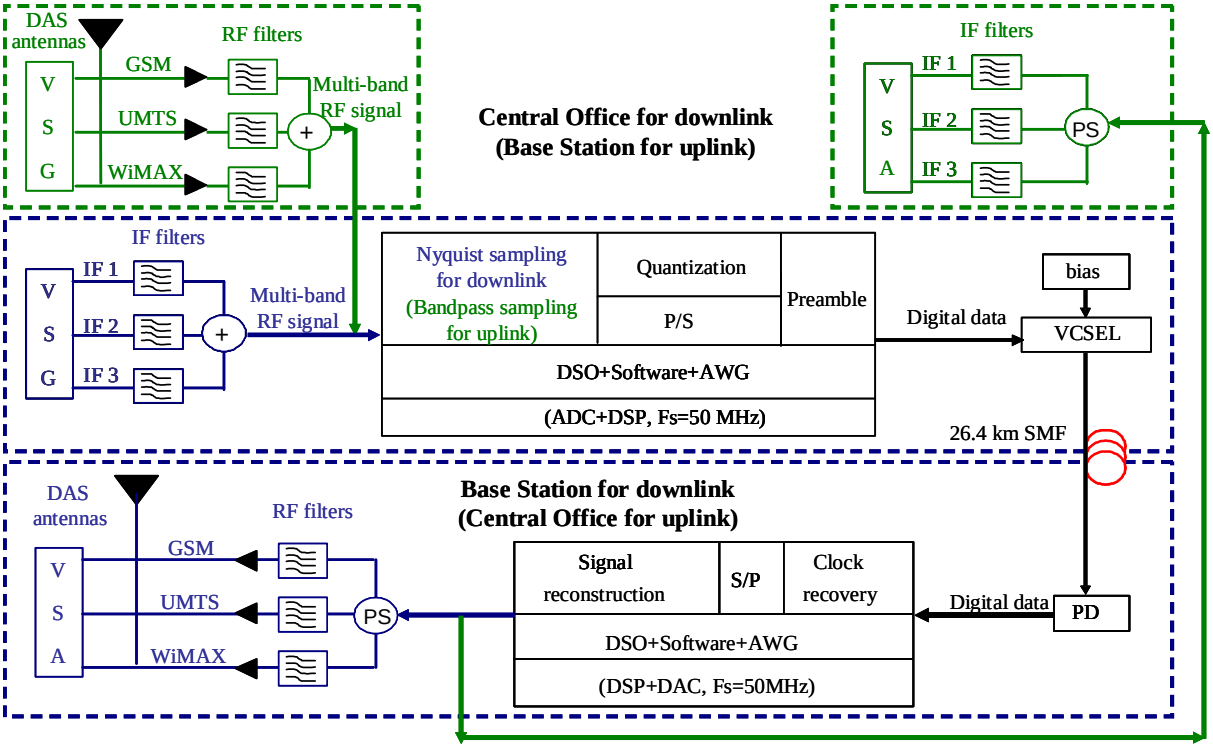

Fig.5.3 Experimental setup of the DRoF-HFR transmission

Uplink transmission was carried out in a similar manner with the three wireless channels electrically combined before digitization. The serial data stream was optically transmitted over the feeder fiber before the multiple wireless channels were recovered and processed at the CO as shown in Fig. 5.3. At the transmitter for the uplink transmission, three wireless services located at RF frequencies were generated and combined before the ADC functionality was accomplished. Uniform bandpass sampling for multiple bandpass signals was employed in order to reduce the sampling rate as well as to guarantee enough guard bands between adjacent channels [5.11]. At the receiver in the CO, the DAC functionality was to reconstruct the signals at IF frequencies and followed by bandpass filters to extract the signal band for each service. Since most power of the sampled signal falls within the first Nyquist region, no further power amplification was needed for the frequency down-conversion process in the uplink path.

5.3.2 Frequency allocation

Table 5.1 Frequency allocation for different sampling rates

Sampling rate (MHz)		25	50	100	125	250
F_{RF} (MHZ)	GSM	803.5	807	814	767.5	785
	UMTS	1807	1814	1828	1785	1820
	WiMAX	2410.5	2421	2442	2552.5	2605
F_{IF} (MHZ)	GSM	3.5	7	14	17.5	35
	UMTS	7	14	28	35	70
	WiMAX	10.5	21	42	52.5	105

To quantify the link performance as a function of sampling rate, the experiment was carried out using different sampling rates (F_S) of 25 MHz, 50 MHz, 100 MHz, 125 MHz and 250 MHz. In bandpass sampling theory, the frequency shift can only be an integral multiple of the sampling rate ($F_{IF}=F_{RF}-N*F_S$). In order to minimize the inter-channel interference of the sampled signal and to ensure that the signal bands are located at the same position with a maximum spacing in each Nyquist zone, we have chosen different IF (F_{IF}) and RF carrier frequencies (F_{RF}) for different sampling rates, which are tabulated in Table 5.1.

5.3.3 Link performance of the downlink

Fig. 5.4 shows the EVM values as a function of sampling rates for each wireless signal in the downlink transmission. It is clear that all of the three signals can be successfully

transmitted over the link when the sampling rate is >= 50 MHz. The link performance for each signal improves when increasing the sampling rate. The improvement levels off for sampling rate of > 125 MHz. When the sampling rate is 25 MHz, only the GSM signal can be detected; among the three wireless services, GSM always has the lowest EVM while UMTS has the highest. These are due to the smaller occupied bandwidth in GSM signal compared to that in UMTS and WiMAX signals in addition to the differences in modulation formats of the three services. The RF spectra of four Nyquist zones around 2.5 GHz of the reconstructed signals at the DAC output for different sampling rates are shown in Figs. 5.5a-e. It is evident that with increasing sampling rate, the RF spectrum becomes more pronounced with improved SNR that leads to the results shown in Fig. 5.4. In this downlink HFR-DRoF transmission, a sampling rate of 50 MHz is sufficient to recover all the three wireless signals error-free.

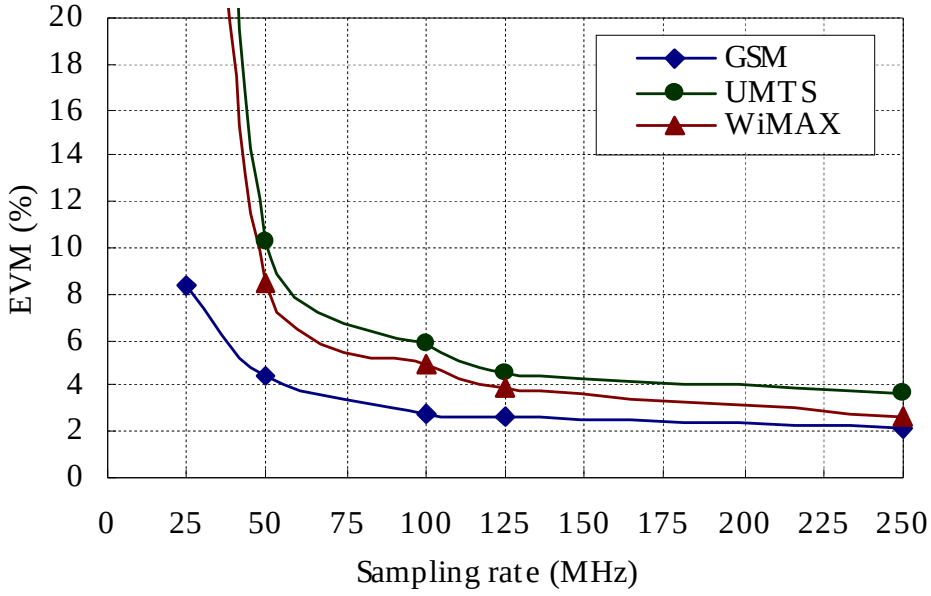

Fig.5.4 EVM performance in downlink

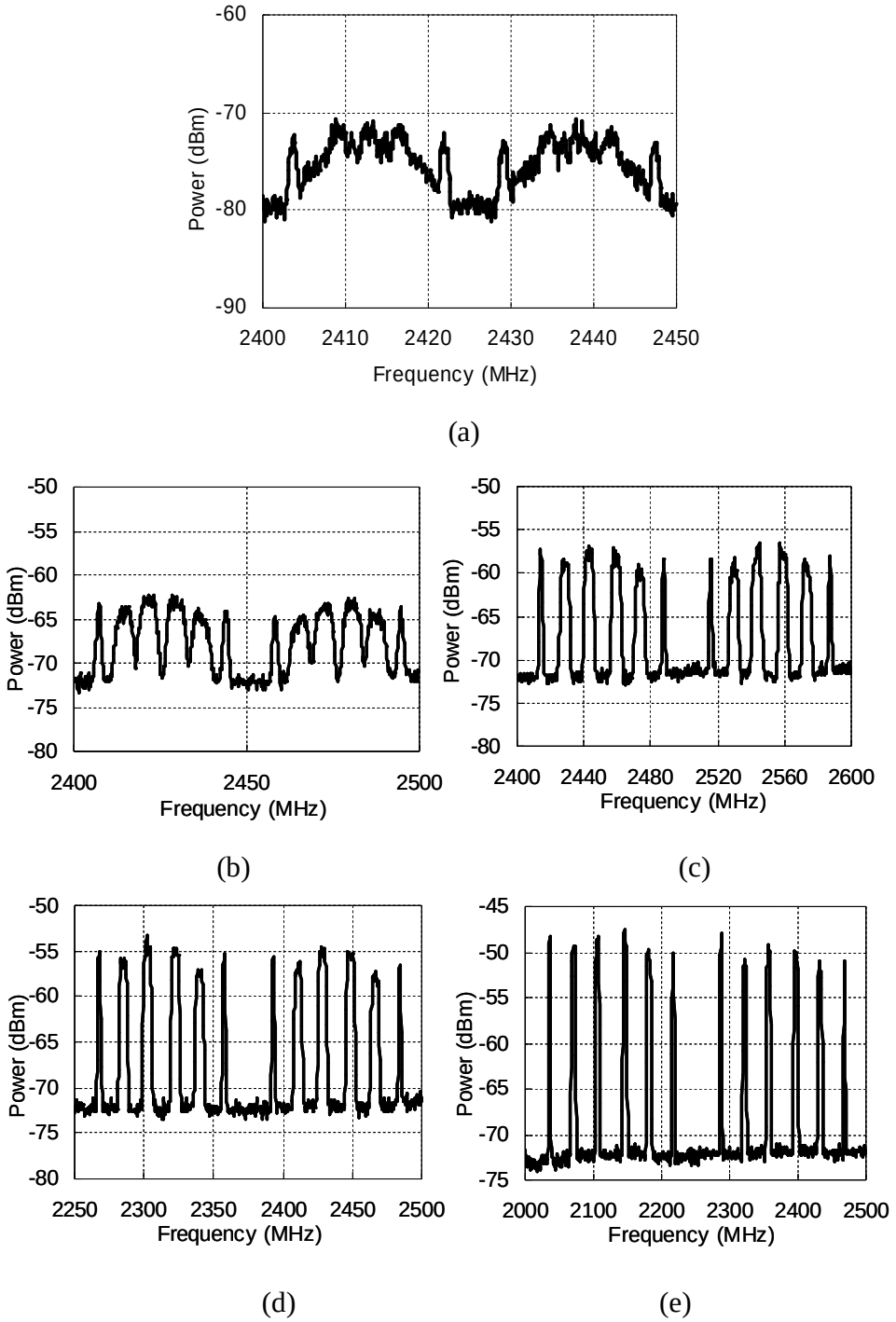

Fig.5.5 Frequency spectrum of the downlink up-converted RF signals with sampling rates at (a) 25 MHz, (b) 50 MHz, (c) 100 MHz, (d) 125 MHz, and (e) 250 MHz

It has been demonstrated that in a DRoF link, the aliasing noise is a key factor that limits the link performance [5.9]. In bandpass sampling, the aliasing noise is proportional to the frequency difference of the signals before and after the frequency relocation functionality, which in our case is the RF carrier frequency of the reconstructed radio signal at the BS. Therefore, the noise level will increase when the IF band signals are upconverted to higher RF frequencies. In this demonstration, we investigate and quantify the impact of noise contribution for the upconversion process using the bandpass sampling scheme. For instance, to quantify the upconversion efficiency for WiMAX transmission, we measure the EVM values of the upconverted WiMAX signal at different RF frequencies when it is digitized with a sampling rate of 50 MHz. Fig. 5.6 shows the measured EVM vs. the upconverted RF frequency. It illustrates that the EVM varies linearly with the RF frequency. Hence, in the downlink transmission, a higher sampling rate should be considered in order to maintain a good link performance when upconverting the wireless signals to high RF frequencies.

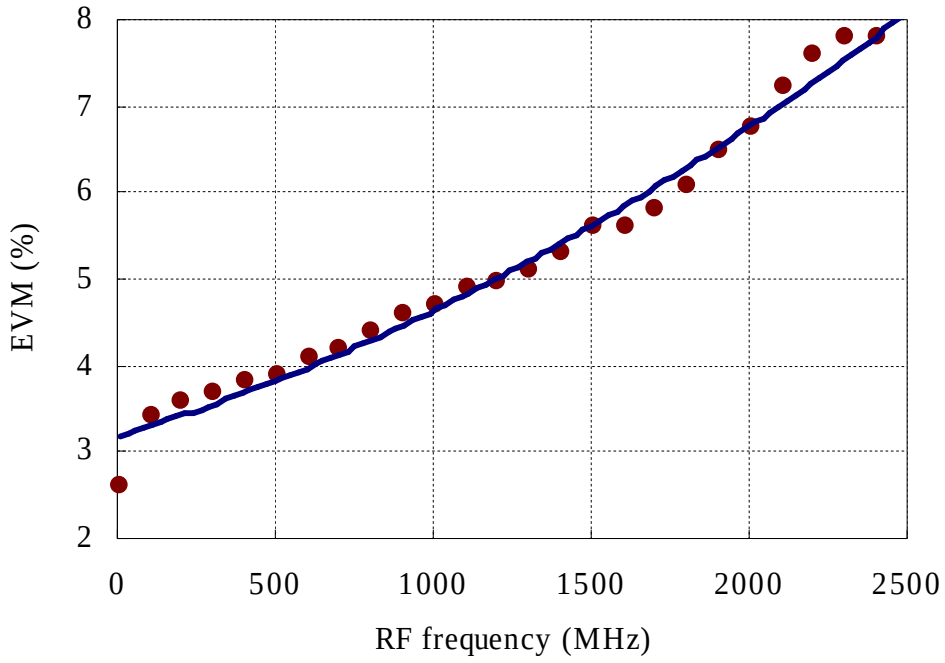

Fig.5.6 EVM Vs. up-converted RF frequency

5.3.4 Power amplification investigation

The sampling process essentially converts a continuous time signal to a discrete time signal in the time domain, while in the frequency domain; it redistributes the power in each Nyquist window following the square sinc function. Fig. 5.7 shows the power spectrum of the sampled IF band signal carrying all three wireless services when the sampling rate is 50 MHz and this spectrum covers over the range from 0 to 2.5 GHz. It is evidently shown that the power distribution of the sampled IF band signal follows a square sinc function where most power is concentrated at the lower frequencies. This implies that the power levels for images at higher frequency vary in accordance to the wireless carrier frequencies for different wireless signals. Since for the downlink path, the signal reconstruction originates from the high frequency image of the sampled signal, the amount of amplification in the receiver of this DRoF-HFR link is adjusted accordingly for each wireless signal.

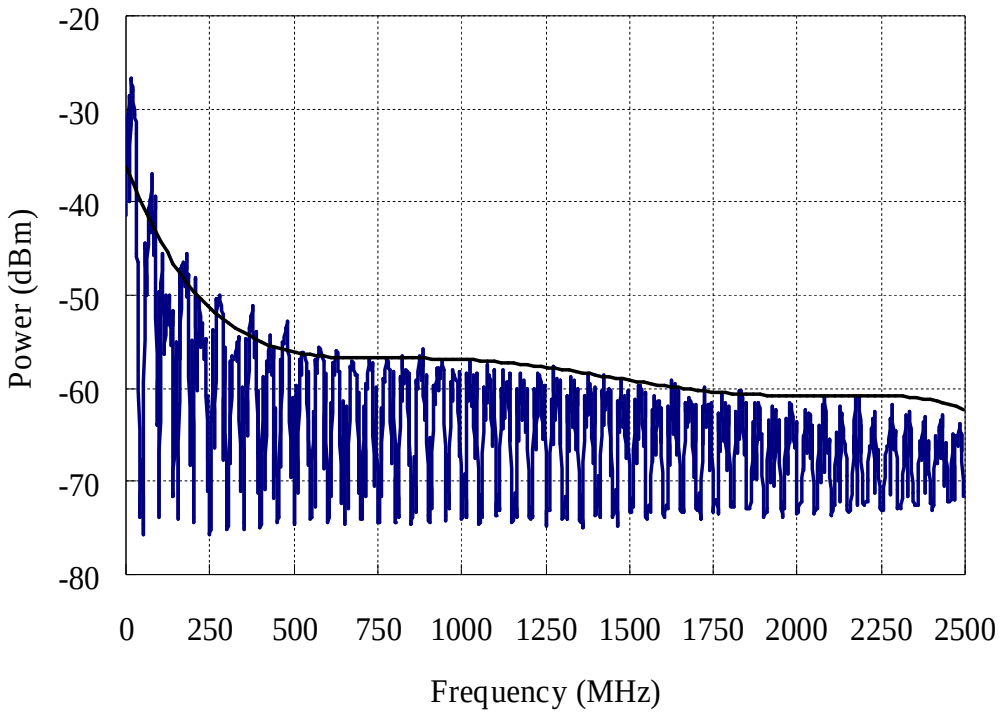

Fig.5.7 Frequency spectrum of the reconstructed signal on the receiver side

In the downlink DRoF-HFR link, the amount of amplification required is dependent on which Nyquist zones the wireless signals with the desired carrier frequencies reside. To quantify this, we experimentally investigate the amount of amplification needed to upconvert the IF band GSM signal to different wireless carrier frequencies. The results were measured using a sampling rate of 50 MHz and are depicted in Fig. 5.8. The amount of amplification increases rapidly with the up-converted RF carrier frequency when the wireless carrier frequency is < 500 MHz (where the spectrum image for signal recovery is located in the 20th Nyquist zone). When the upconverted wireless carrier frequency is > 500 MHz, the rate of increase in the amount of amplification decreases before it saturates at an amplification of 50 dB. Since the power allocation of a sampled signal in frequency domain is determined by the order number of Nyquist zone and regardless of the carried data, this result is also applicable in WiMAX and UMTS cases. Therefore, in the HFR-DRoF downlink transmission, under the condition of reconstructing the signal with an acceptable SNR, the RF amplification required will at most be 50 dB.

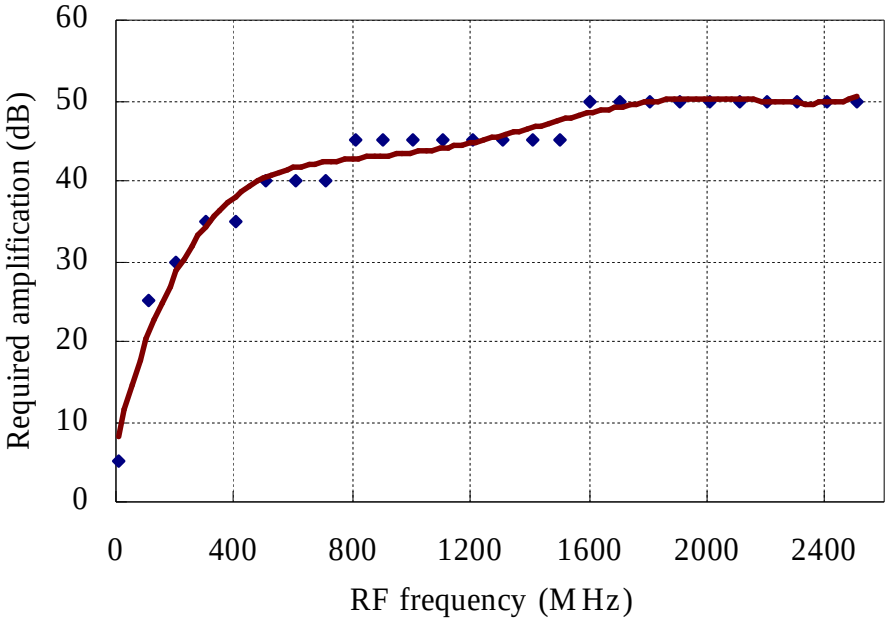

Fig.5.8 Amplification requirements for different RF frequencies

5.3.5 Link performance of the uplink

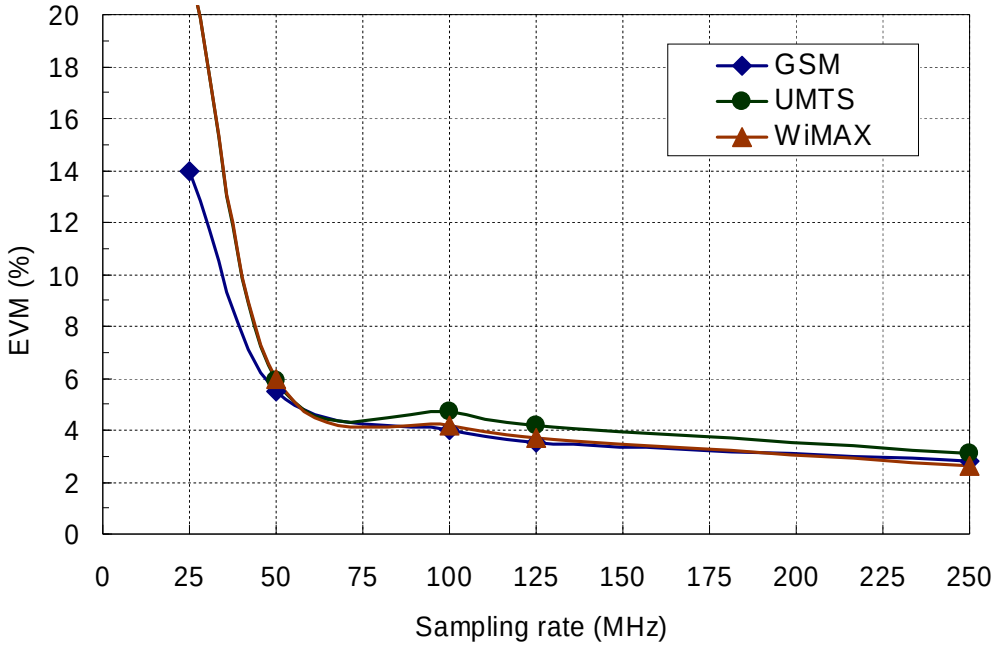

Fig.5.9 EVM performance in uplink

The uplink EVM performances are given in Fig. 5.9. The EVM varies in a similar trend as compared to the downlink case (Fig. 5.4) and a sampling rate of 50 MHz is sufficient to achieve error-free transmission in the uplink path. The spectra of the first four Nyquist windows for the reconstructed IF band signals are shown in Fig. 5.10a-e. Similarly, with increasing sampling rate, the SNR improves and the spectrum becomes more distinct for all three wireless services. Comparing with the RF power of the up-converted RF signal in the downlink path, the RF power of the down-converted IF signal in the uplink is much higher while the noise power is the same for both down and uplink. However, the interference power level is much higher comparing to the noise power for the uplink path, which makes it dominate the SNR. Therefore, despite the larger signal power for the uplink path, the EVM performance is similar to that of the downlink transmission which is attributed to the higher interference level.

We quantify the impact of inter-channel interference for the uplink transmission. Table 5.2 lists the EVM and SNR values of the three wireless services for the uplink transmission with a sampling frequency of 50 MHz (when transmitted separately and simultaneously). Fig. 5.11a-c show the spectra of the reconstructed IF signals of the wireless services within the first two Nyquist zones when transmitted separately. Fig. 5.11d shows the regenerated IF spectrum for simultaneous transmission. The results clearly illustrate that the inter-channel interference level for the simultaneous transmission is relatively higher which results in a higher EVM as evident in Table 5.2. In other words, simultaneous transmission improves the spectral efficiency and minimizes hardware usage but at the expense of increased inter-channel interference that may compromise the overall performance. Since the key factor determining the inter-channel interference level is the channel spacing, increasing the channel spacing is the most effective way to weaken the inter-channel interference and improve the link performance. After bandpass sampling, the channel spacing is proportional with the sampling rate and inversely proportional to the number of wireless services, which means we have to either increase the sampling rate or reduce the number of services. Therefore, to implement the uplink transmission of HFR signals based on DRoF technique, the balance among the hardware sharing, the spectral efficiency and the ADC sampling rate must be considered.

Table 5.2 Comparison of separate and simultaneous transmissions

Wireless Services	Separate Transmission			Simultaneous Transmission		
	GSM	UMTS	WiMAX	GSM	UMTS	WiMAX
EVM(%)	1.3	3.0	2.9	5.5	5.9	6.0
SNR(dB)	30	28	25	25	16	14

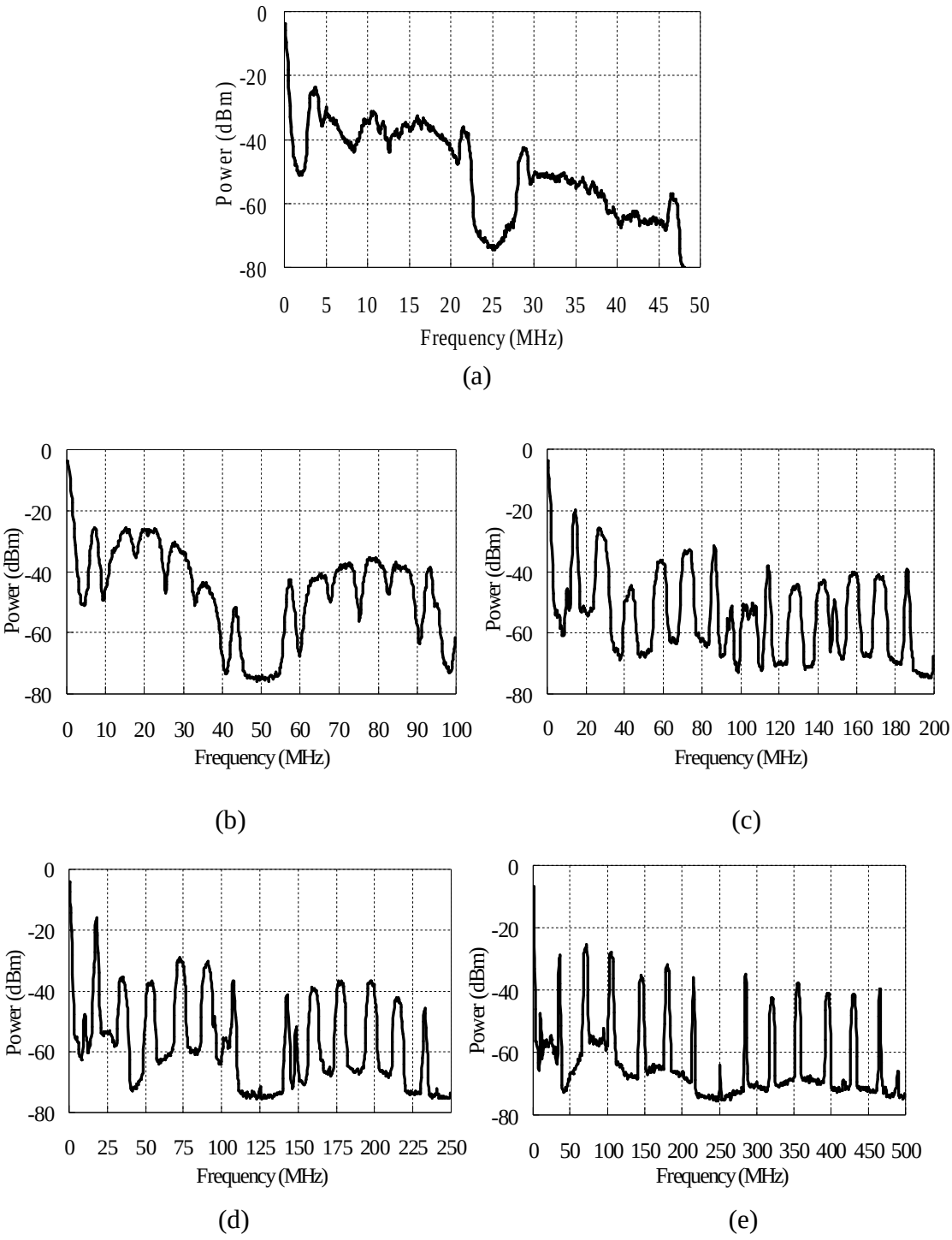

Fig.5.10 Frequency spectrum of the uplink down-converted IF signals with sampling rates at (a) 25 MHz, (b) 50 MHz, (c) 100 MHz, (d) 125 MHz, and (e) 250 MHz

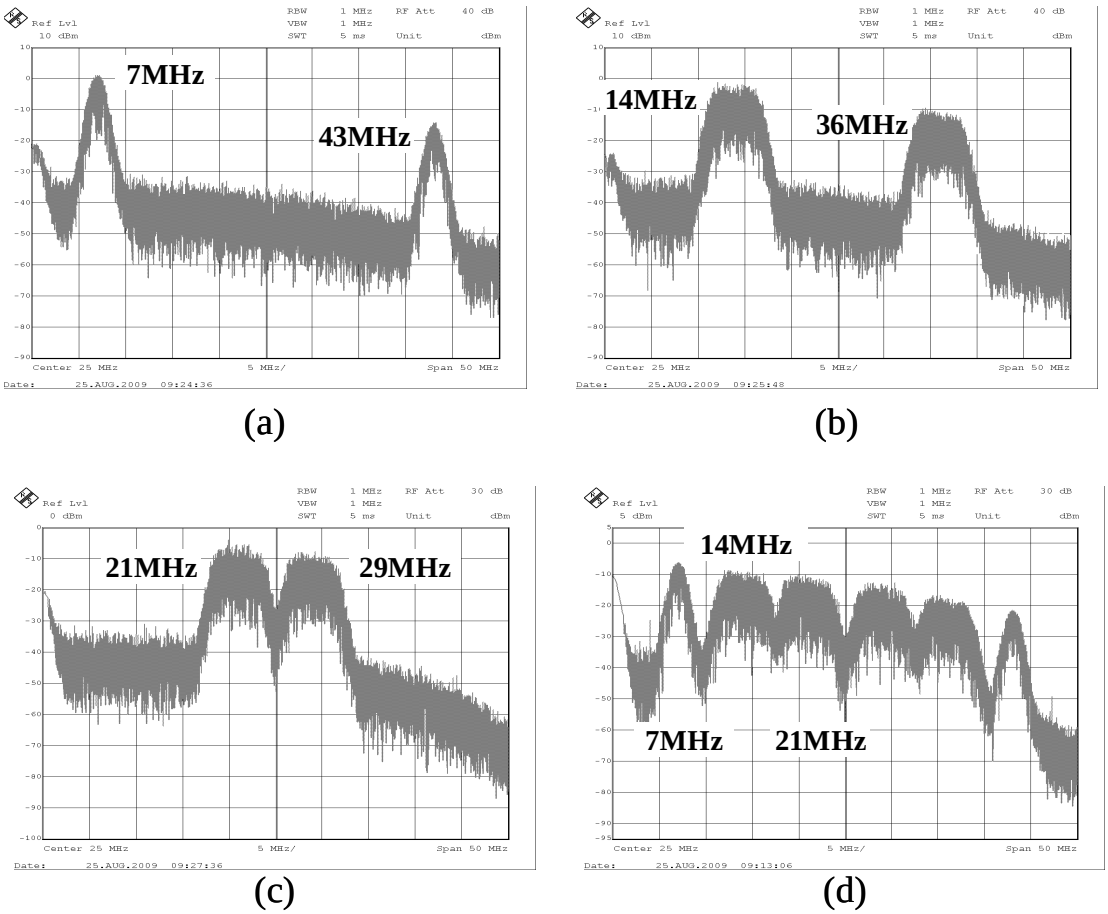

Fig.5.11 Regenerated IF signal of (a) GSM, (b) UMTS, and (c) WiMAX when transmitted separately; (d) Regenerated IF signal bands of three wireless services when transmitted simultaneously

5.4 Summary

In this chapter, we proposed an efficient bidirectional transmission scheme for Hybrid Fiber-Radio access using digitized RF-over-fiber technique that supports multiple wireless signals distribution for both uplink and downlink. The frequency allocation theory was presented to minimize the inter-channel interference of the sampled signal and to ensure that the signal bands are located at the same position with a maximum spacing in each Nyquist

zone. This scheme enables multiple wireless signals to be transported simultaneously and simplifies the BS design by performing the frequency translation processes without the needs of analog devices such as mixers and local oscillators.

We have experimentally demonstrated a proof-of-concept DRoF-HFR link for the simultaneous transmission of GSM, UMTS and WiMAX wireless services. Error-free transmission can be achieved for all three wireless signals in both the downstream and upstream directions when the sampling rate is >= 50 MHz and the total optical data rate after digitization is >= 400 Mb/s.

Experimental results show that in the downlink transmission the link EVM performance is linearly related to the up-converted wireless carrier frequency. Therefore, a higher sampling rate should be considered in order to maintain a good link performance when up-converting to high RF frequencies in the downlink path. The amount of amplification required for wireless services at different wireless carrier frequencies have been quantified, and the results indicate that a significant amount of amplification is required when the image with the desired wireless carrier frequency resides in the 20th or larger Nyquist zone. In the uplink transmission, although the noise power is relatively the same as in the downlink, the inter-channel interference level is much higher. The performance of the uplink is limited by inter-channel interference.

5.5 Reference

[5.1] A. Nirmalathas, P. A. Gamage, C. Lim, D. Novak, R. Waterhouse, “Digitized Radio-Over-Fiber Technologies for Converged Optical Wireless Access Network,” Journal of Lightwave Technology, vol: 28, Issue: 16, pp. 2366-2375, 2010.

[5.2] H. Chettat, L. M. Simohamed, Y. Bouslimani and H. Hamam, “RoF Networks: A comprehensive study,” in 3rd International Symposium on Wireless Pervasive Computing, pp. 495-498, May 2008.

[5.3] R. E. Schuh, D. Wake, B. Verri and M. Mateescu, “Hybrid Fibre Radio Access: A Network Operators Approach and Requirements,” Proc. 10th Microcoll Conference, pp. 211-214, Mar. 1999.

[5.4] A. Kaszubowska, P. Anandarajah and L. P. Barry, “Improved Performance of a Hybrid Radio/Fiber System Using a Directly Modulated Laser Transmitter With External Injection,” IEEE Photonics technology Letters, vol. 14, no. 2, Feb. 2002.

[5.5] A. Nirmalathas, P.A. Gamage, C. Lim, D. Novak, R.B. Waterhouse and Y. Yang, “Digitized RF over Fiber Transport,” Microwave Magazine, vol. 10, pp. 75-81, Jun. 2009.

[5.6] Y. Yang, C. Lim, and A. Nirmalathas, “Multi-Channel Digitized RF-over-Fiber Transmission based on Bandpass Sampling and FPGA,” accepted for publication by Journal of Lightwave Technology.

[5.7] R. G. Vaughan, N. L. Scott, and D. R. White, “The theory of bandpass sampling,” IEEE Trans. Signal Processing, vol. 39, no. 9, pp. 1973-1984, Sep. 1991.

[5.8] N. Wong, and Tung-Sang Ng, “An efficient algorithm for downconverting multiple bandpass signals using bandpass sampling,” IEEE ICC. vol. 3, pp. 910-914, June 2001.

[5.9] Ahmed I. Zayed, Advances in Shannon's sampling theory, CRC Press, 1993.

[5.10] Yi-Ran Sun, and Svante Signell, “Effects of noise and jitter on algorithms for bandpass sampling in radio receivers,” ISCAS '04, vol. 1, pp. 761-764, May 2004.

[5.11] Ching-Hsiang Tseng, and Sun-Chung Chou, “Direct Downconversion of Multiband RF Signals Using Bandpass Sampling,” IEEE Transaction on wWireless Communications, vol. 5, no. 1, 2006.

Chapter 6

High-frequency RF transport over Enhanced Digitized RF-over-fiber link

6.1 Introduction

The growing demand for multimedia services and broadband access has placed a huge bandwidth demand on the existing optical access network infrastructure. Radio-over-fiber technique is highly recognized as a promising solution to the last-mile access systems with high capacity and good mobility. However, the current wireless services operate at lower microwave frequencies (2-5 GHz), which put a burden on the signal bandwidth. This is the driving force that leads to new wireless technologies operating at higher frequencies with larger bandwidths, such as millimeter-wave. Nevertheless, the large propagation loss of high frequency radio signal leads to small transmission distance. For covering large areas by a broadband communication system, a huge number of microcell/picocell base stations are required. This large amount of base stations give rise to new system design criteria, whereas simplicity of base station design is the most important feature [6.1]. It becomes economically attractive to locate the radio generation and modulation at the central office, and keep the antenna base stations simplified only with the functionalities of optical-to-electrical conversion, wireless signal emitting and receiving [6.2]. Such analog RF-over-fiber link has stringent requirements on the bandwidth and the linearity of the optoelectronic devices, i.e. laser, external modulator and photodetector, which are still very costly according to the

current techniques. And also fiber dispersion compensation techniques will be essential at long fiber lengths.

In Section 6.2 of this chapter, we realize the transmission of high frequency RF signal up to 18 GHz via a digitized RF-over-fiber link, which takes advantage of the high performance and the straightforward implementation of digital optical links. This digitized RF-over-fiber link [6.3, 6.4] is based on intensity modulation-direct detection (IM-DD) optical link with low-cost digital optical transmitter and receiver, and realizes a highly linear optical link due to the lower optical data rates contributed by bandpass sampling [6.5]. The RF signal, which operates at 18 GHz with 50 Mbps of BPSK modulated data, is directly digitized using an ADC with 8 bit resolution and 500 MHz sampling rate. The bandpass sampling process generates image replicas of the wireless signals in lower frequency region as such the 18 GHz wireless signal can be downconverted without using any mixer and local oscillators. At the receiver, the wireless signal is reconstructed by using images at lower frequency region using a DAC. Experimental results show that there is a trade-off between the system performance and the hardware requirements for different optical data rates and ADC resolutions, and investigations are carried out by varying the ADC bit resolutions and the sampling rates.

Despite that the optical bandwidth of the digitized RF-over-fiber transmission is lower than in direct analog RF-over-fiber transmission, the overall bit rate in optical link could still be extremely high [6.6] since it equals to the sampling rate multiplied by the ADC bit resolution. This places a heavy bandwidth demand on the hardware requirements of optoelectronics devices in the optical link. Due to the interplay between the ADC sampling rate and bit resolution, the overall data rates after digitization do not vary significantly.. Therefore, we are not able to just reduce the ADC sampling rate or bit resolution to lower the hardware requirement of optoelectronics devices while maintaining the same link performance.

In Section 6.3, we propose a modified DRoF link utilizing oversampling and decimation to enhance the ADC bit resolution and reduce the overall bit rate in the optical link. Moreover, the energy consumption of the ADC and DAC will be greatly improved as power dissipation is exponentially related to the bit resolution; and the noise performance will also be improved for higher frequency operation using the oversampling and decimation scheme.

In Section 6.4, we introduce a multi-level optical link to the digitized RF-over-fiber technique, which reduce the overall optical data rate, moderate the requirements of O-E and E-O devices, and also maintain a simple base station configuration. The experimental setup to realize the digitized RF-over-fiber using multi-level optical transmission is proposed and the results show that four-level optical link using RZ signal is a promising solution to implement digitized RF-over-fiber transmission.

6.2 High-frequency RF transport using digitized RF-over-fiber technique

6.2.1 Experimental demonstration

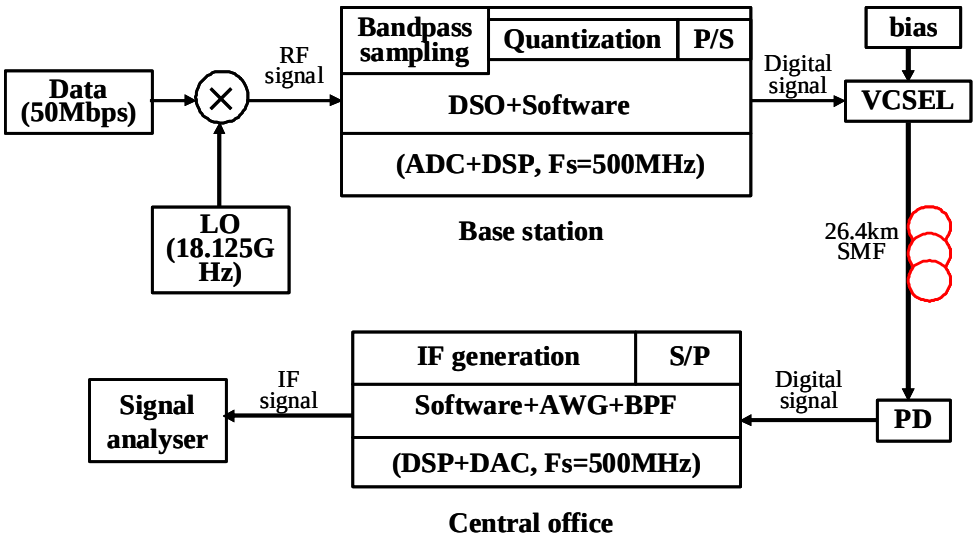

Fig.6.1 Experimental setup

To minimize the interference due to spectral aliasing as a result of bandpass sampling, we need to maximize the spacing between adjacent bands to be half of the sampling frequency. The RF carrier frequency is chosen to be 18GHz + Fs (sampling rate)/4.

The experimental setup of a digitized RF-over-fiber transmission link is shown in Fig. 6.1. The 18.125 GHz BPSK modulated RF signal is generated by mixing the baseband data and a local oscillator signal. In the BS, the Tektronix TDS6154C Digital Sampling Oscilloscope (DSO) with a sampling rate fixed at 500 MHz is employed as an ADC to perform the bandpass sampling function, and the quantization and the parallel-to-serial (P/S) conversion are done in software. The digital data stream is used to intensity-modulate the optical signal from a 1550 nm VCSEL biased at 5 mA, and converted to an optical signal which is sent to the CO over a 26.4 km SMF. In the CO, a PIN receiver with a received power at -23 dBm helps to achieve the direct detection. The detected digital data stream is converted from serial to parallel in software, and then imported into the Tektronix AWG7000 Arbitrary Waveform Generator (AWG) for the signal band regeneration at the corresponding IF frequency in every Nyquist zone, where the AWG acts as a DAC with the same sampling rate used for the A/D conversion in the BS. Finally a bandpass filter is used to extract the desired IF band in the first Nyquist zone. The performance evaluation of this digitized RF-over-fiber link is implemented by recovering the data from the IF signal in a vector signal analyzer.

Fig. 6.2a and Fig. 6.2b show the RF spectra of the original RF signals when the central frequency is at 18.125 GHz with a bit rate at 100 Mbps and when the central frequency is at 18.0625 GHz with a bit rate at 50 Mbps, respectively. The ADC sampling rates are set to be 500 MHz and 250 MHz for these two RF signals according to their bandwidths. After the bandpass sampling function, the RF bands are replicated in every Nyquist zone, and each of the bands carries the same data as the original RF bands.

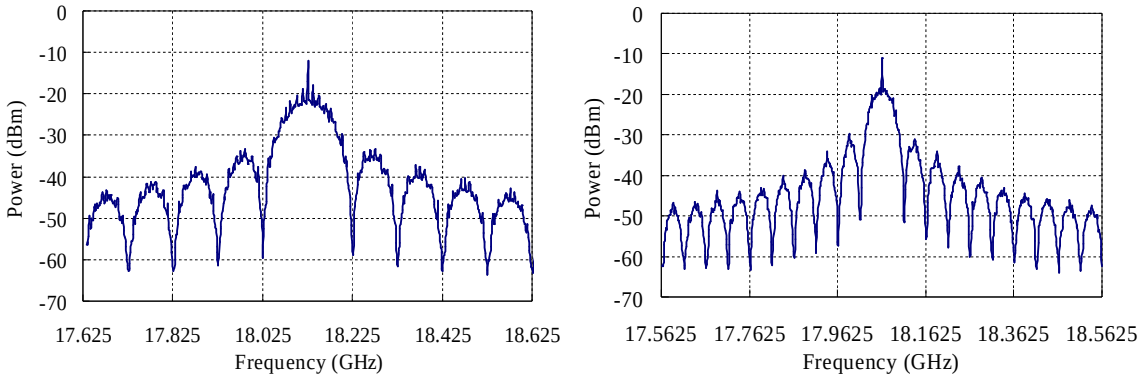

(a) (b)

Fig.6.2 RF spectrum of the original RF signal at (a) 18.125 GHz with a bit rate of 100 Mbps and (b) 18.0625 GHz with a bit rate of 50 Mbps

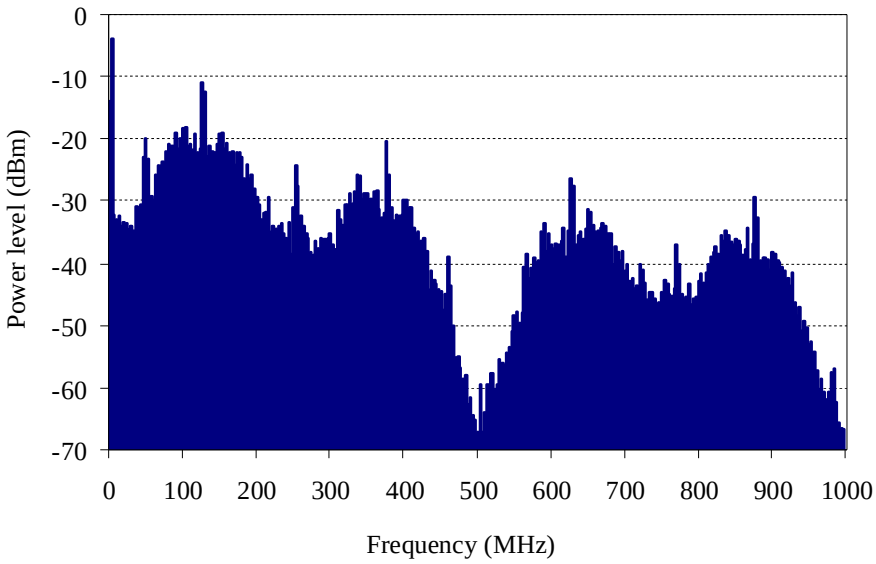

Fig.6.3 RF spectra of the regenerated IF signals with a bit rate at 100 Mbps

Fig. 6.3 and Fig. 6.4 show the RF spectra of the regenerated IF bands within 0-1000 MHz. It is clearly shown that the original RF band at 18.125 GHz has been down-converted to IF bands at 125 MHz, 375 MHz, 625 MHz and 875 MHz, and the original RF band at 18.0625 GHz has been down-converted to IF bands at 62.5 MHz, 187.5 MHz, 312.5 MHz, 437.5

MHz, 562.5 MHz, 687.5 MHz, 812.5 MHz, and 937.5 MHz. The reconstructed IF carrier frequencies strictly match the theoretical values at $F_{RF}+F_S/2*L$ (L is an integer). Moreover, the power of the regenerated IF signal concentrates in the band between 0 and Fs/2, which is the first Nyquist zone. Therefore, the IF band with the lowest carrier frequency is chosen to recover the wireless data.

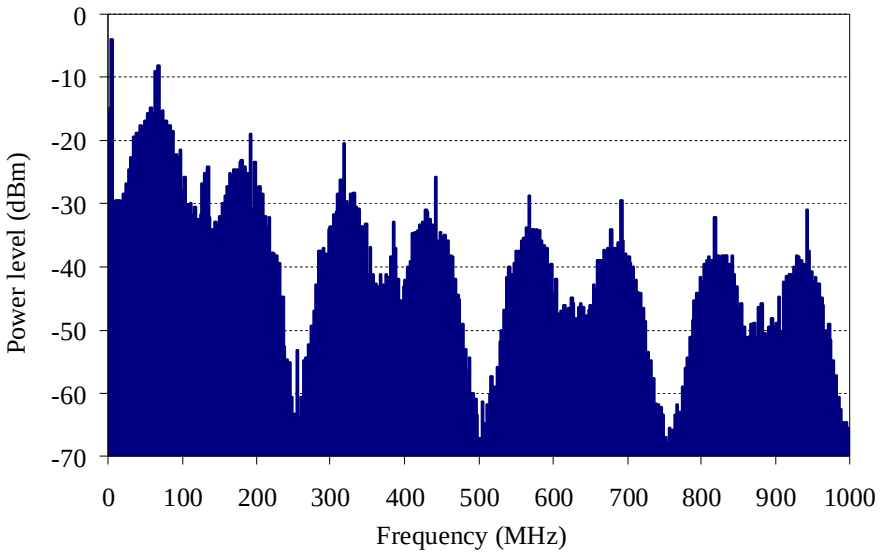

Fig.6.4 RF spectra of the regenerated IF signals with a bit rate at 50 Mbps

6.2.2 Performance evaluation

Fig. 6.5 shows the measured EVM values of the BPSK modulated signal with RF carrier frequency varyingfrom 10 GHz to 18 GHz. The blue curve is measured with the sampling rate fixed at 250 MHz and the bit rate (BR) fixed at 50 Mbps. It shows that the EVM value increases slowly with the increasing RF carrier frequency before increases rapidly for carrier frequency more than 16 GHz. The red curve is measured with the same bit rate as the blue one and the sampling rate is increased to 500 MHz. The EVM performance of the digitized RF link improves when we double the sampling rate; and the link can still achieve error free ($BER<10^{-12}$) when the RF frequency goes up to 18 GHz. The green curve shows the EVM vs.

RF frequency when the sampling rate stays 500MHz and the bit rate goes up to 100 Mbps. It is evident that: error free cannot be achieved after the RF frequency goes beyond 12 GHz. We are still able to achieve a BER<10^{-8} for RF carrier frequency < 15 GHz and beyond that the EVM increases dramatically and the wireless data recovery cannot be recovered.

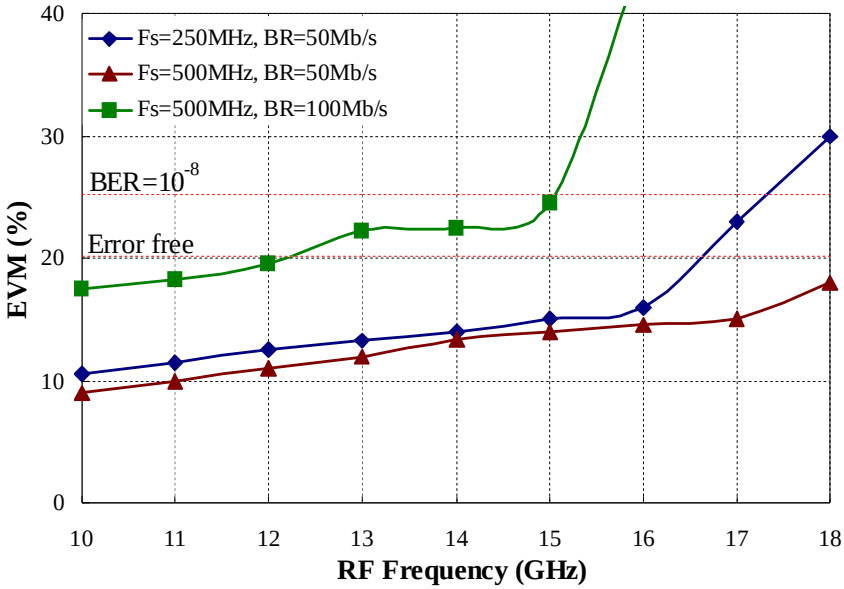

Fig.6.5 Measured EVM vs. RF carrier frequency

Fig. 6.6 illustrates the relationship between the link EVM and the bit rate. These results are measured with the sampling rate fixed at 500 MHz. All of the four curves show that increasing bit rate deteriorates the link performance. The solid red line and solid blue line, with the same ADC resolution of 8 bits, indicate that the digitized RF link can achieve a maximum bit rate at 50 Mbps and 80 Mbps with error free performance when the RF frequencies are 18 GHz and 15 GHz respectively.

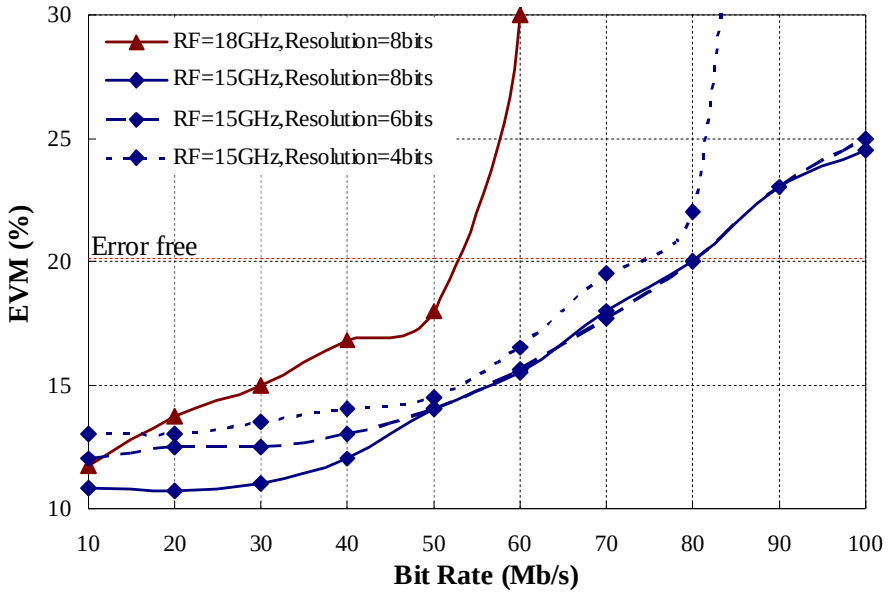

Fig.6.6 Measured EVM vs. bit rate at different ADC bit resolutions

6.2.3 Discussion on hardware requirement

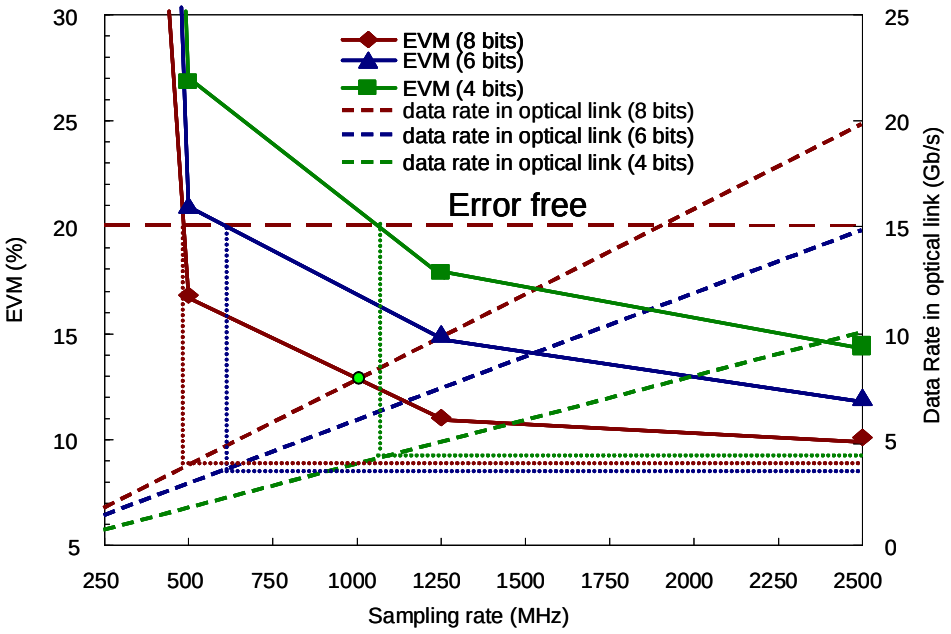

Fig.6.7 EVM vs. sampling rate vs. optical data rate (RF=18GHz, bit rate=50Mbps)

To implement the digitized RF-over-fiber link, the AD/DA (analog-digital and digital-to-analog) conversion and the O-E/E-O (optical-to-electrical and electrical-to-optical) conversion are the crucial elements. According to the high sampling rate ADC design technique, large bit resolution is very difficult to realize and also it is extremely costly and energy-consuming [6.7]. On the other hand, in digital optical transmission, the optical data rate is the limiting factor for O-E/E-O conversion with cost increases exponentially with speed. This section discusses how the ADC resolution and the overall optical data rate affect the digitized RF-over-fiber link.

In Fig. 6.6, the dashed blue line and the dotted blue line are for the same RF frequency as the solid blue line but with an ADC resolution reduced to 6 bits and 4 bits respectively. It is evident that before the bit rate reached 50 Mbps, 8 bits resolution achieves better link performances. However, for the bit rate from 50 Mbps to 100 Mbps, the EVMs are at the same level for the resolution at 8 bit and 6 bits. 4 bits resolution always gives the worst link performance, and the data cannot be recovered when the bit rate goes beyond 80 Mbps. Therefore, for the error-free transmission at 15 GHz, an ADC resolution at 6 bits is sufficent for the digitized RF-over-fiber link.

Fig. 6.7 shows the EVM performances and the total optical data rates after digitization plotted as a function of ADC sampling rates. It is obvious that by increasing the sampling rate, the digitized RF link can achieve a better link performance; however, the optical data rate also increases with the sampling rate, which will place a more stringent requirement on the optical link. Therefore, there is a trade-off between the link performance and the hardware requirements for the optical link. The red point shows that with an ADC resolution of 8 bits, the sampling rate at 1 GHz offers the best compromise in terms of link performance and optical data rate. The red, blue and green solid and dashed lines are for ADC resolution of 8 bits, 6 bits and 4 bits, respectively. To achieve the same EVM, different ADC resolutions will require very different sampling rates. In this case to achieve error-free EVM,

we require sampling rates of 500 MHz, 600 MHz, and 1050 MHz for ADC resolution of 8, 6 and 4 bits respectively. Despite the different sampling rates for different bit resolutions, the total optical data rate after sampling does not vary much for the three cases investigated (~4 - 4.5Gb/s). Therefore there is a tradeoff between sampling rate and bit resolution in ADC and the interplay between these two parameters have to be taken into account while designing such a link. In this investigation, the best choice of sampling rate and resolution bit to realize a digitized RF-over-fiber link for the transmission of an RF signal at 18 GHz with a bit rate at 50 Mbps would be an ADC with 6 bits resolution and 600 MHz sampling rate.

6.3 Bit resolution enhanced digitized RF-over-fiber link

As discussed above, the trade-off between the link performance and the hardware requirement due to the high optical data rate after digitization place a burden on the implementation of DRoF links. To moderate the hardware requirement due to the high optical data rate while maintaining a good link performance, we propose a modified DRoF link utilizing oversampling and decimation to enhance the ADC bit resolution and reduce the overall bit rate in the optical link. In this link, the noise power induced by the ADC is mitigated by oversampling and decimation and the power dissipations in both the ADC and the DAC are also moderated.

6.3.1 White noise approximation of ADC quantization noise

The power spectral density (PSD) is the Fourier transform of the autocorrelation function (Eq. 6.1). The autocorrelation function is given in Eq. 6.2; therefore the PSD can be rewritten as Eq. 6.3. Here, S is PSD; R is correlation; and F is Fourier transform; $x(t)$ is the input signal; $x'(t)$ is the quantized signal; $v(t)$ is the quantization noise. Since x and v are uncorrelated, the last term in Eq. 6.3 can be dropped [6.8].

(6.1) $$S(f) = F\left[R(\tau)\right]$$

(6.2) $$R_{x'x'}(\tau) = E\left[x'(t)x'(t+\tau)\right] = E\left[\left(x(t)+v(t)\right)\left(x(t+\tau)+v(t+\tau)\right)\right]$$
$$= R_{xx}(\tau) + R_{vv}(\tau) + \left[R_{xv}(\tau) + R_{vx}(\tau)\right]$$

(6.3) $$S_{x'x'}(\tau) = S_{xx}(\tau) + S_{vv}(\tau) + \left[S_{xv}(\tau) + S_{vx}(\tau)\right]$$

Q(x) is the quantization characteristic, *x'* = *Q(x)*; $Q_v(x)$ is the quantization noise characteristic, $v = Q_v(x)$. Quantizer characteristics of a rounding quantizer are shown in Fig. 6.8. The quantized value is given by Eq. 6.4, and the quantization noise is given by Eq. 6.5.

(6.4) $$Q_v = \sum_{k=1}^{\infty} (-1)^{k-1} (q \sin(2\pi kx/q))/\pi k$$

(6.5) $$v(t) = Q_v(x(t)) = \frac{q}{\pi} \sum_{k=1}^{\infty} (-1)^{k-1} \sin(2\pi kx/q)/k$$

The quantized signal can be expressed as a sum of phase-modulated signals by Eq. 6.6 (time domain) and Eq. 6.7 (frequency domain), and the spectrum of each term can be expressed with the probability density function (PDF) of the derivative of the signal *x(t)* (Eq. 6.8). Therefore, the noise spectrum can be approximated to be as described in Eq. 6.9.

(6.6) $$q_k(x(t)) = \frac{q}{\pi k} (-1)^{k-1} \sin(2\pi kx(t)/q)$$

(6.7) $$Q_v(x(t)) = \sum_{k=1}^{\infty} q_k(x(t))$$

(6.8) $$S_{qq}(f) = \frac{1}{2k^3\pi^2} P_{x'}\left(\frac{fq}{k}\right)$$

(6.9) $$S_{QQ}(f) = \sum_{k=1}^{\infty} \frac{1}{2k^3\pi^2} P_{x'}\left(\frac{fq}{k}\right)$$

The quantization noise spectrum for sine input signal ($x(t)=2\pi f_0 t+\varphi$) is investigated as following. The PDF of its derivative is given in Eq. 6.10.

(6.10)
$$P_{x'}(a)=\begin{cases}\dfrac{1}{2\pi^2 f_0 A}\dfrac{1}{\sqrt{1-\left(\dfrac{a}{2\pi f_0 A}\right)^2}} & \textbf{for } |a|<2\pi f_0 A \\ 0 & \textbf{for } |a|\geq 2\pi f_0 A\end{cases}$$

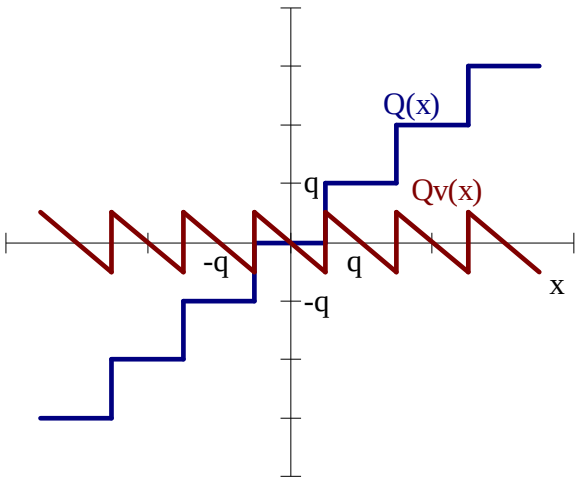

Fig.6.8 Characteristic of the input–output quantizer and the quantization noise

So, the quantization noise spectrum when the input signal is a sine wave is obtained in Eq. 11, where the condition means that for each value of f only those terms are summed for which the condition is satisfied. This spectrum is a sum of sine spectrums weighted inversely by k^3, as shown in Fig. 6.9. The irregularity occurs when $|f|=2\pi f_0 Ak/q$.

(6.11)
$$S_{QQ}(f)=\frac{q^3}{4\pi^4 f_0 A}\sum_{k=1}^{\infty}\frac{1}{k^3}\frac{1}{\sqrt{1-\left(\dfrac{fq}{2\pi f_0 Ak}\right)^2}} \quad \textbf{for } |f|<\frac{2\pi f_0 Ak}{q}$$

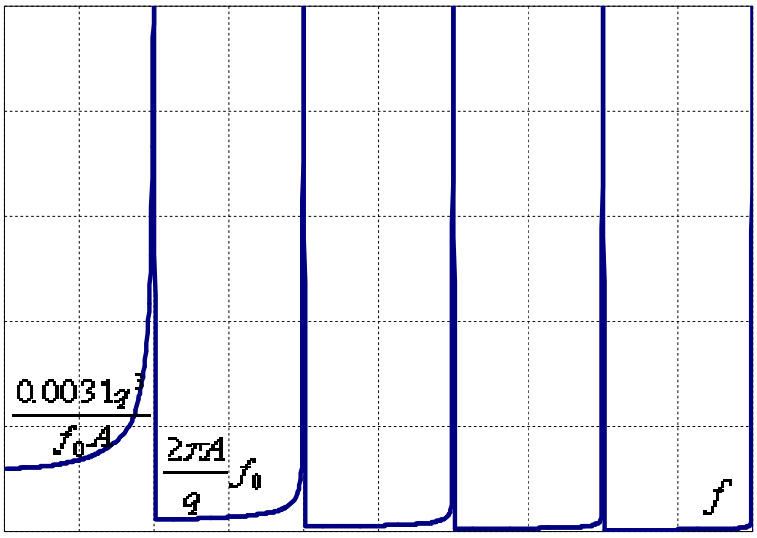

Fig.6.9 Quantization noise spectrum for sine input signal

Both quantization and sampling processes occur in analog-to-digital conversions. The spectrum of a sampled signal is associated with a folding of the corresponding spectrum around the sampling frequency, given by Poisson summation formula (Eq. 6.12). So, the quantization noise power spectrum of an ADC with a sampling rate at *fs* is obtained in Eq. 6.13.

(6.12) $$X_s(f) = \frac{1}{T}\sum_{m=-\infty}^{\infty} X(f - mf_s)$$

(6.13) $$S_{ADC\_Q}(f) = \frac{4\pi^2}{f_s^2}\sum_{m=-\infty}^{\infty} S_{QQ}(f - mf_s)$$

In the digitized RF-over-fiber case, we are using bandpass sampling, and the ADC bit resolution is at least 4 bits. So, the sampling rate is far smaller than the frequency where the

irregularity occurs in the quantization noise spectrum. According to Eq. 6.13, the ADC quantization noise spectrum in DRoF link can be considered as white noise.

6.3.2 White noise approximation of aperture jitter noise

ADC signals sampled at nT without and with jitter noise are expressed using Fourier series expansion in Eq. 6.14 and Eq. 6.15. The jitter error is given by Eq. 6.16 and error autocorrelation function is described by Eq. 6.17 [6.9].

$$x(n) = \sum_{k=-\infty}^{\infty} c_k e^{j2\pi f_k nT} \tag{6.14}$$

$$x'(n) = \sum_{k=-\infty}^{\infty} c_k e^{j2\pi f_k (nT+J_n)} \tag{6.15}$$

$$e(n) = x(n) - x'(n) = \sum_{k=-\infty}^{\infty} c_k e^{j2\pi f_k nT}(1 - e^{j2\pi f_k J_n}) \tag{6.16}$$

$$\begin{aligned} R_{ee}(n,m) &= E\left(e(n)e^*(m)\right) \\ &= E\left(\sum_{k=-\infty}^{\infty} c_k e^{j2\pi f_k nT}(1 - e^{j2\pi f_k J_n}) \sum_{k=-\infty}^{\infty} c_k e^{-j2\pi f_k mT}(1 - e^{-j2\pi f_k J_m})\right) \\ &= \sum_{k=-\infty}^{\infty} c_k^2 e^{j2\pi f_k (n-m)T}\left(1 - E\left(e^{j2\pi f_k J_n}\right) - E\left(e^{-j2\pi f_k J_m}\right) + E\left(e^{j2\pi f_k (J_n - J_m)}\right)\right) \end{aligned} \tag{6.17}$$

Aperture jitter stands for the random sampling time variation in ADCs, which is commonly modelled as a stationary white Gaussian process. The corresponding sampling time variations $J^{ap}{}_n = t_n - nT$ are assumed to be independent identical distributed Gaussian random variables with zero mean and the variance σ^2_{ap}. Hence, the characteristic functions of $J^{ap}{}_n$ and $J^{ap}{}_n - J^{ap}{}_m$ are given in Eq. 6.18 and Eq. 6.19. Substituting them into Eq. 6.17 yields the error auto-correlation function for aperture jitter (Eq. 6.20), which is composed of two terms: the first

is accounted for a periodic part and the second is for an aperiodic part. We are able to obtain the PSD function (Eq. 6.21) after transforming to the frequency domain.

(6.18) $$E(e^{\pm j2\pi f J_n^{ap}}) = E(e^{\pm j2\pi f J_m^{ap}}) = e^{-2\pi^2 f^2 \sigma_{ap}^2}$$

(6.19) $$E(e^{j2\pi f (J_n^{ap} - J_m^{ap})}) = \begin{cases} 1 & \textbf{if } \mathbf{n = m} \\ e^{-4\pi^2 f^2 \sigma_{ap}^2} & \textbf{if } \mathbf{n \neq m} \end{cases}$$

(6.20)
$$\begin{aligned} R_{ee}(n,m) &= E\left(e(n)e^*(m)\right) \\ &= \sum_{k=-\infty}^{\infty} c_k^2 e^{j2\pi f_k (n-m)T} \left(1 - E\left(e^{j2\pi f_k J_n}\right) - E\left(e^{-j2\pi f_k J_m}\right) + E\left(e^{j2\pi f_k (J_n - J_m)}\right)\right) \end{aligned}$$

(6.21)
$$\begin{aligned} S_{ee}(f) &= F\left(R_{ee}(n,m)\right) \\ &= \frac{1}{T}\sum_{l=-\infty}^{\infty}\sum_{i=-\infty}^{\infty} c_i^2 \delta(f - f_i - \frac{l}{T}) g_i^2 + \sum_{i=-\infty}^{\infty} c_i^2 \left[2g_i - g_i^2\right] \\ &\textbf{Here, } g_i = 1 - e^{-2\pi^2 f_i^2 \sigma_{ap}^2} \end{aligned}$$

The transformation of the periodic part yields a periodic line spectrum comprising the spectral components of the input PSD weighted with the squares of the spectral gain. The transformation of the aperiodic error auto-correlation term yields a constant component in the error power spectrum, which is the white part of the error power spectrum. For majority applications the spectral gain is relatively small so that the aperture jitter noise spectrum can be approximated as a constant and the aperture jitter noise can be treated as white noise.

6.3.3 Oversampling effect on white input noise

Under the assumption that ADC noise is white noise, the noise power is uniformly distributed between DC and half the sampling frequency. With a constant noise power, the noise PSD is linearly related to the sampling rate. If the sampling rate of the ADC is multiplied by L times

(F'_s=L.F_s), the same amount of noise power spreads over a bandwidth which is L times the previous bandwidth as shown in Fig. 6.10. Only a relatively small fraction of the total noise power falls in the signal band (0-Fs/2), and the noise power outside the signal band can be greatly attenuated by a decimation filter with a decimation factor (DF) of L and passband from 0 to Fs/2. As a result, the total noise power is spreaded over a wider band and the SNR increases by L-fold (PSD'=PSD/L, SNR'=L*SNR). Therefore, oversampling and decimation can successfully enhance the bit resolution [6.10].

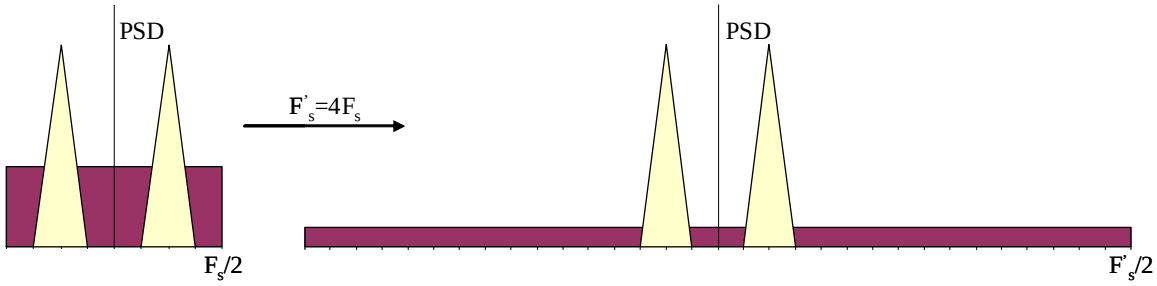

Fig.6.10 Sampling rates effect on the PSD of white ADC input noise

In high-frequency wide-bandwidth radio transport, the implementation of digitized RF-over-fiber technique is limited by the transmission of high bit-rate digital data over optical fiber and the increased noise level when working at high frequencies. Fig. 6.11 illustrates the signal-to-quantization-noise ratio (SNR_Q) and signal-to-jitter-noise ratio (SNR_J) in the DRoF link. SNR is limited by low ADC bit resolution and high RF carrier frequency. In practical networks, RF carrier frequency is fixed for certain wireless service. To maintain an acceptable SNR performance in such DRoF system, sufficient bit resolution is necessary. However, high bit resolution is against the requirements of a relatively low optical data rate which is proportional to ADC resolution and sampling rate.

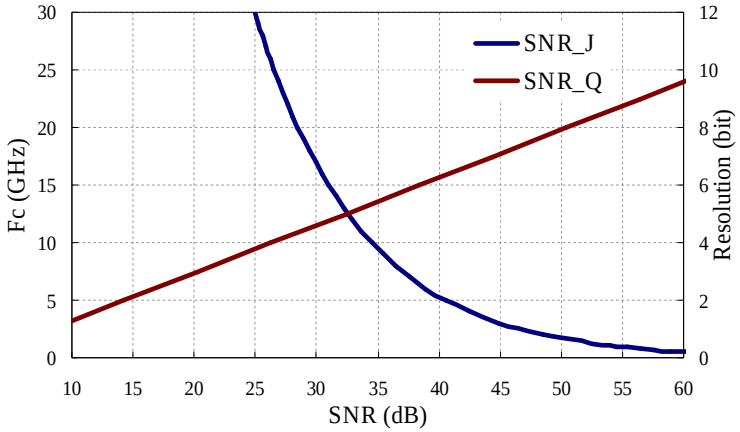

Fig.6.11 SNR_Q vs. resolution, and SNR_J vs. RF carrier frequency

As we have discussed before, in the DRoF link, the ADC quantization noise and the aperiodic term of jitter noise can be considered as white noise, which can be reduced by oversampling and digital filtering; and only the non-white part of jitter noise determines the upper limit for the achievable SNR. According to the previous discussion, the signal-to-white-noise-ratio increases linearly with the sampling rate. On the contrary, the optical data rate also increases linearly with the sampling rate. Therefore, to maintain a low data rate, downsampling should be employed to reduce the sampling rate in conjunction with digital signal processing functions in the DRoF link. In this case, the DAC in the receiver also uses the low sampling rate.

6.3.4 Proposed scheme and experimental setup

We introduce oversampling and decimation in DRoF link to enhance the bit resolution while maintaining the same effective sampling rate, such that the noise due to ADC is moderated and the overall bit rate over optical link is reduced.

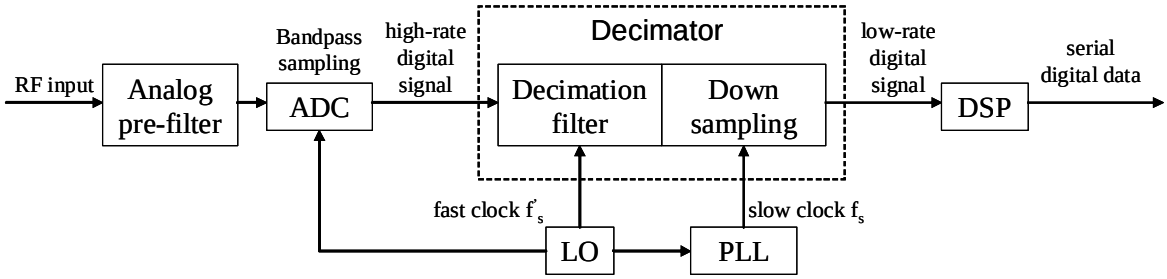

Fig.6.12 Scheme of oversampling and decimation for DRoF link

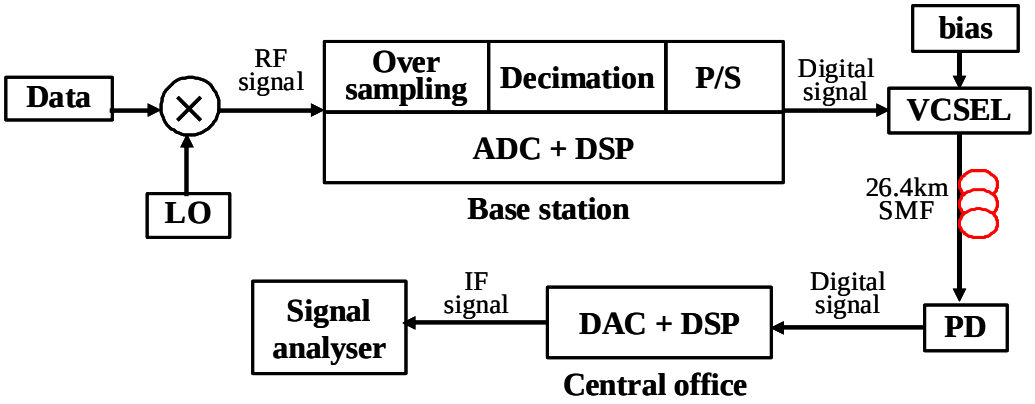

Fig.6.13 Experimental setup of bit resolution enhanced DRoF link

The scheme to realize bit resolution enhancement for DRoF link is illustrated in Fig. 6.12. The RF signal is pre-filtered and then sampled by an ADC with a sampling rate at L times the sampling rate determined by the bandpass theory and with a lower bit resolution. The resulting high bit rate digital signal is processed in a decimator, which contains a digital filter to mitigate the band white noise and a downsampler to obtain a lower data rate. The bandwidth of the digital filter is half of the sampling frequency given by bandpass sampling theory, and the passband is centred at the signal carrier frequency. The decimation factor

(DF) is set to L in order to convert the sampling rate back to the one determined by the bandpass sampling theory. Therefore the effective sampling rate after oversampling and decimation processes will be the same as that in regular DRoF links while the bit resolution and the digital optical data rate are lower. The low data rate digital signal output from the decimator can then be operated following the same procedures as in normal DRoF links. To demonstrate the merits of the bit resolution enhancement in DRoF link, we experimentally realize our proposed scheme with the setup as shown in Fig. 6.13 and compare it with our previous demonstration [6.6].

6.3.5 Experimental results and analysis

To demonstrate the advantages of oversampling and decimation in DRoF links, we implement the bit resolution enhanced scheme using the same physical parameters as in our previous experiment setup, and compare the results when with and without the oversampling procedure.

Table 6.1 EVM and eye opening comparison

Resolution at 4 bits	Fs=500 MHz	Fs=2.5 GHz	Fs=2.5G with decimation
EVM	27%	14.5%	16%
Eye Opening	1.3875	1.6125	1.5675
Optical bit rate	2Gb/s	10Gb/s	2Gb/s
SNR(dB)	5.14	7.13	6.65

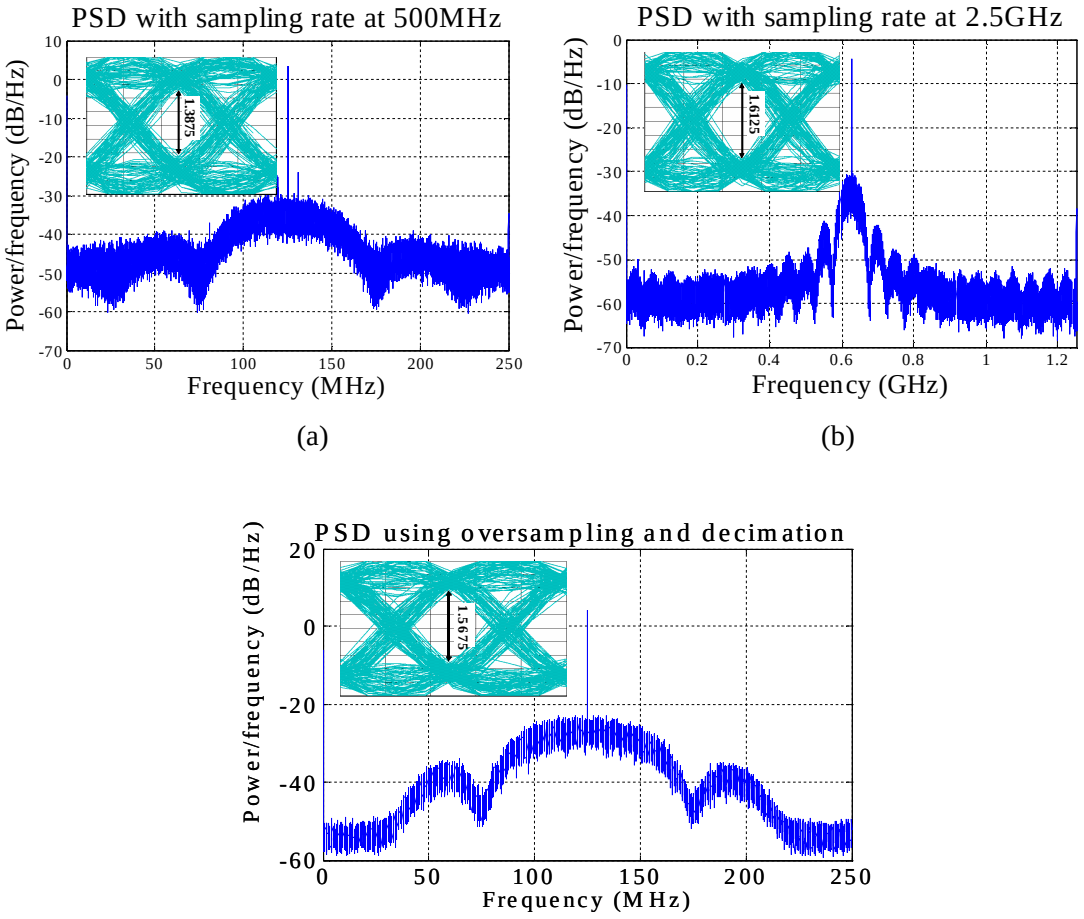

Fig.6.14 PSDs and eye diagrams of (a) reconstructed IF signal over conventional DRoF link with a sampling rate at 500 MHz, (b) reconstructed IF signal after electrcal B2B transmission with a sampling rate at 2.5 GHz, (c) reconstructed IF signal over bit resolution enhanced DRoF link with a sampling rate at 2.5 GHz.

In our demonstration, the RF carrier frequency is set to 18.125 GHz, the data rate is 50 Mbps, and the ADC bit resolution is 4 bits. Fig. 6.14a shows the RF spectrum and the eye diagram of the reconstructed IF signal when the sampling rate is 500 MHz, which results in an overall bit rate for the optical link of 2 Gbps. When the sampling rate is increased to 2.5 GHz, the corresponding overall bit rate for the optical link becomes 10 Gbps and the RF spectrum of the reconstructed IF signal and the eye diagram are shown in Fig. 6.14b. Fig.

6.14c shows the power spectrum and the eye diagram of the reconstructed IF signal using our proposed bit resolution enhanced DRoF technique, with the sampling rate for oversampling of 2.5 GHz and a DF of 5. This gives an effective sampling rate of 500 MHz and an overall bit rate of 2 Gbps for the optical link. The comparison between Fig. 6.14a and Fig. 6.14c illustrates that the bit resolution enhanced DRoF link achieves a cleaner spectrum with an improved SNR while maintaining the same optical bit rate of 2 Gbps. Table 6.1 lists the EVM, eye opening, overall bit rate, and SNR for the above three cases under investigation. It is evident that a sampling rate at 2.5 GHz provides a much better link performance comparing with a sampling rate at 500 MHz; however, without decimation the overall bit rate will be 10 Gbps which places a stringent constraint on the optical interface. Through the implementation of decimation (with a DF of 5) for a sampling rate of 2.5 GHz, the overall bit rate is reduced from 10 Gbps to 2 Gbps, comparable to the case where a sampling rate at 500 MHz without decimation but with much improved link performance (EVM of 16% comparing to EVM of 27%)).

Table 6.2 Overall bit rate and EVM comparison

	Fs=500 MHz			Fs=2.5G With Decimation
Resolution	8 bits	6 bits	4 bits	4 bits
EVM	17%	21%	27%	16%
Bit rate	4Gb/s	3Gb/s	2Gb/s	2Gb/s

We vary the bit resolution from 4 to 8 bits whilst maintaining the sampling rate at 500 MHz and then compare the results to that incorporating decimation (DF of 5) with a sampling rate of 2.5 GHz and a bit resolution of 4 bits. The results are tabulated in Table 6.2.

The results indicate that: an increase of the bit resolution in a conventional DRoF link improves the link performance; when the bit resolution is 8 bits, the link performance of the conventional DRoF link with a sampling rate at 500 MHz matches the performance of the bit resolution enhanced DRoF link with a bit resolution at 4 bits; however, the overall bit rate in the conventional DRoF link is twice that of the bit resolution enhanced DRoF link.

We also investigate the bit resolution enhanced DRoF link when utilizing different sampling rates and bit resolutions. In this case the decimation factors are determined by the sampling rates to ensure that the same overall bit rate is achieved for the same bit resolution. The following results are obtained when the RF carrier frequency is fixed at 15.125 GHz with data rate of 100 Mbps, and bit resolution of 4 bits. Fig. 6.15 illustrates the EVM performances after electrical back-to-back transmission of the digitized RF signals with different sampling rates. It is obvious that: the link performance is better when sampling rate is increased; however further increment in the sampling rate after 5 GHz does not warrant further improvement in the EVM. The increase in bit resolution also improves the link performance, however the impact of bit resolution becomes less pronounce with increasing sampling rate.

Fig. 6.16 shows the EVM performance versus bit resolution in the bit resolution enhanced DRoF links. It is seen that the overall data rate is reduced from 4 Gbps (when sampling rate at 500 MHz, and bit resolution at 8 bits) to 1.5 Gbps (when sampling rate at 1.25 GHz, DF of 2.5, and bit resolution at 3 bits) with a similar EVM performance at around 17%. Alternatively, the total bit rate can also be reduced from 4 Gbps to 2 Gbps (using a sampling rate of 1.25 GHz, DF of 2.5, and bit resolution at 4 bits) and achieves a better EVM of 14 %. From Fig. 6.16 it can be seen that the performance of our proposed bit resolution enhanced DRoF links degrades with increasing sampling rate despite the noise reduction characteristics of the digital decimation filter. This is due to the same decimation filter used for all the sampling rates investigated in our analysis which is optimized for lower sampling rates. We

require a digital filter with a narrower passband for higher sampling rates which necessitates the use of higher order digital filter which demands for more complicated signal processing.

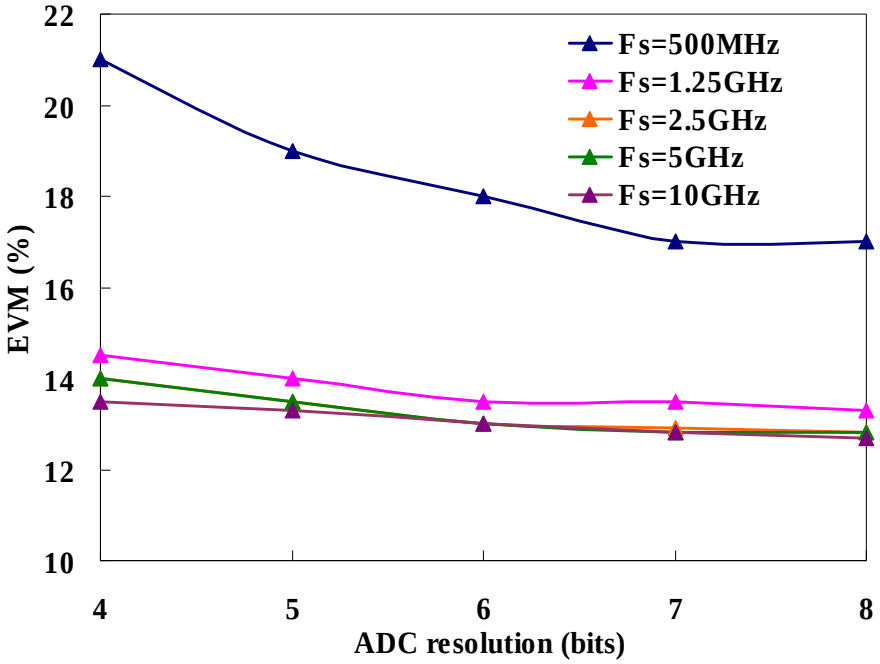

Fig.6.15 EVM perfomance after electrical B2B transmission

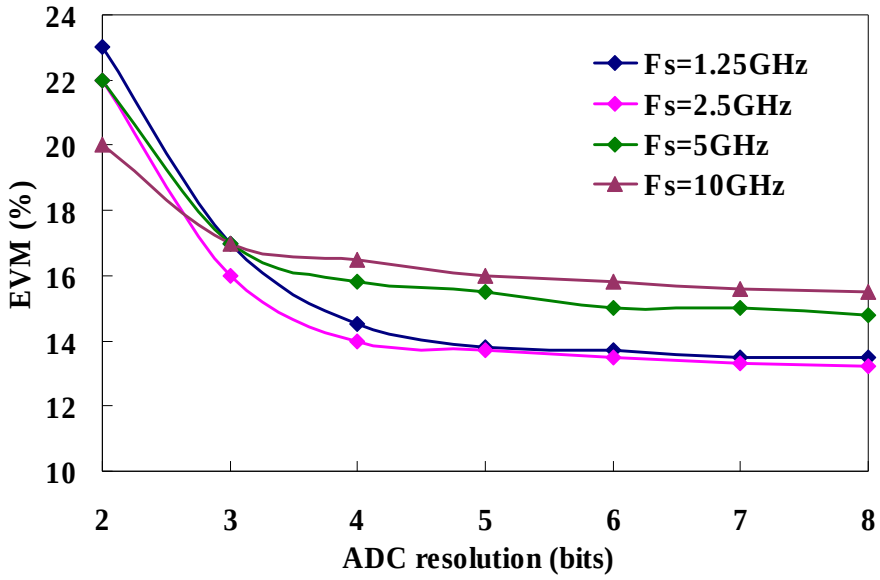

Fig.6.16 EVM performance in bit resolution enhanced DRoF link

6.4 Multi-level optical link for digitized RF-over-fiber technique

As we have discussed in Section 6.2, the ultra high overall optical data rate places a heavy burden on the implementation of digitized RF-over-fiber links for high frequency RF signal transmission. In order to reduce the overall optical data rate and also maintain a simple base station configuration, we introduce another technique based on a multi-level intensity-modulated optical link [6.11] to the digitized RF-over-fiber technique. Here, we use a four-level optical link instead of normal binary optical link to transmit the digitized RF signal over fiber. Therefore, we can easily reduce the optical data rate to half of the original one, and the required bandwidths of the transmitter and receiver are also reduced by a factor of two.

6.4.1 Proposed multi-level optical link

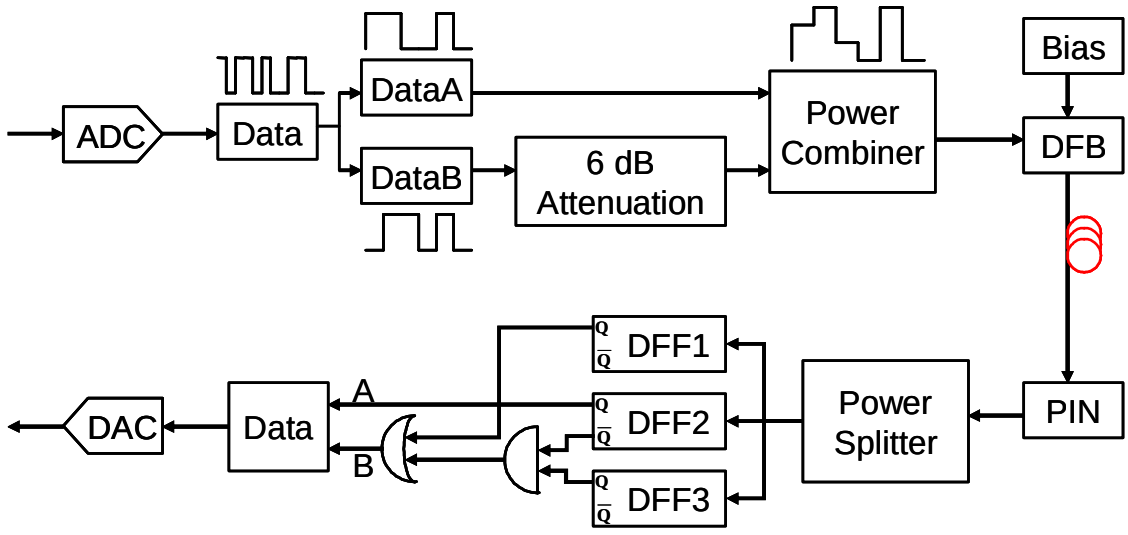

Fig.6.17 Four-level optical link for DRoF transmission

Fig. 6.17 demonstrates the experimental setup of the digitized RF-over-fiber using multi-level optical transmission. In this schematic, the serial digital data stream generated after the ADC in the regular digitized RF-over-fiber link is converted to two digital data streams. The

second stream goes through a 6-dB attenuator and reduces its power by half. After that, the two digital data streams are combined to generate the four-level electrical signal before intensity-modulating the distributed feedback laser (DFB). At the receiver side, the received signal is split into two halves, and sent to the decoder circuit [6.12] which uses three Data flip-flops (DFF) connected as shown in Fig. 6.17.

6.4.2 Experimental results analysis

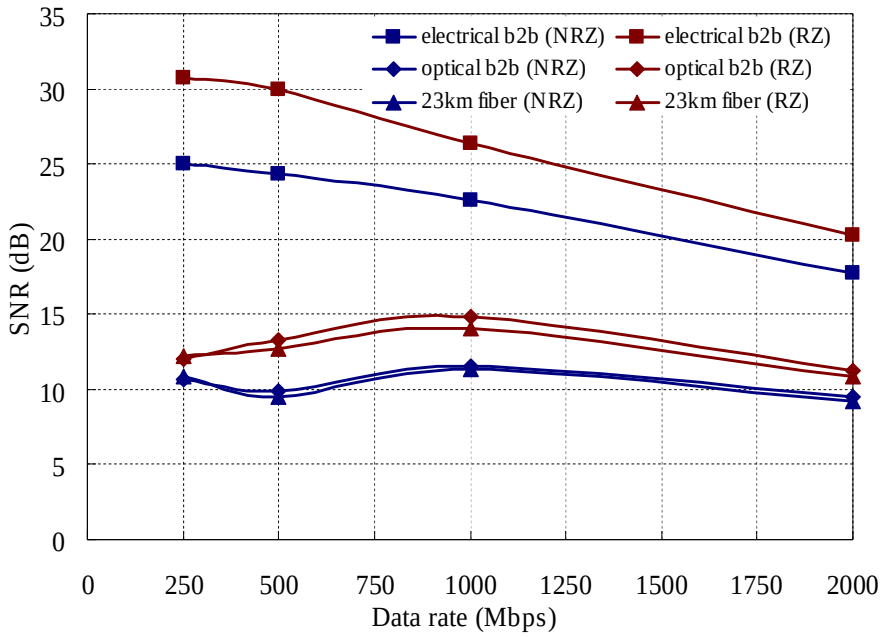

Fig.6.18 SNR performance of the four-level optical links

Since we are using a 2.5 GHz DFB laser, we vary the overall optical data rate from 250 Mbps to 2 Gbps, which means the actual digital data rate ranges from 500 Mbps to 4 Gbps. Fig. 6.18 illustrates the SNR of the four-level optical link when applying return-to-zero (RZ) and non-return-to-zero (NRZ) signals in cases of transmitting over electrical back-to-back (B2B), optical back-to-back and 23 km optical fiber links. Comparing the optical B2B results with electrical B2B results, we can see that after adding the E-O/O-E conversion functions

SNR deteriorates by more than 5 dB for the entire data rate investigated. ; However the SNR does not degrade by much with the inclusion of 23 km of transmission fiber. Another important observation from Figure 6.18 is that RZ signals have better SNR performance compared to NRZ. Fig. 6.19a and Fig. 6.19b show the eye diagrams of 1-Gbps 4-level NRZ signal and RZ signal after transmission over 23 km optical link respectively. Clearly, we can see that the eye diagram of the NRZ signal is noisier, and the eye opening is smaller than in the case of RZ signal. This can be attributed to the higher average power of NRZ signal and the response characteristic of semiconductor lasers.

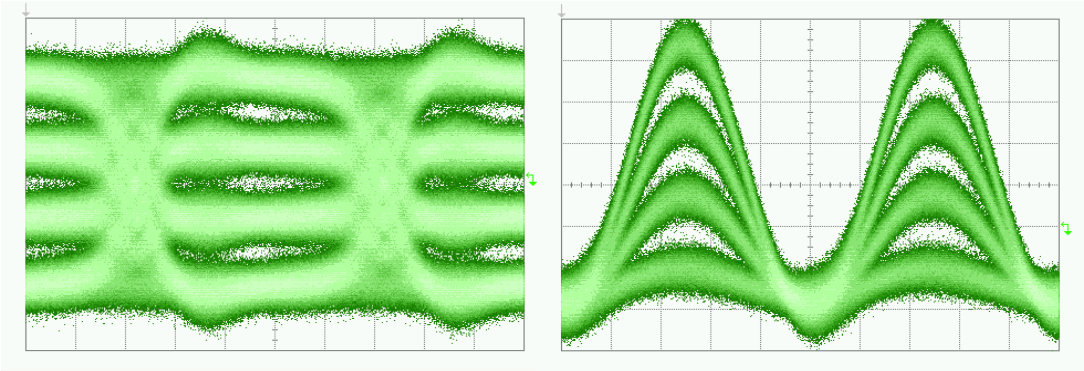

Fig.6.19 Eye diagrams of 1Gbps 4-level NRZ signal (a) and RZ signal (b) after transmission over 23 km optical link

We also investigate the SNR of the RF signal for the cases investigated in Fig. 6.18. Since one sample of the RF signal is converted to several bits of digital data according to the bit resolution of the ADC used, the SNR of the RF signal has to be higher than the SNR of the digital data. The SNR relationship between the digital data and the RF signal is given in Fig. 6.20. According to Fig. 6.20, a digital link with a SNR more than 11.5 dB can secure the SNR of the whole RF transmission link to be above 20 dB. With a minimum detectable SNR of 20 dB, by applying the four-level optical link in digitized RF-over-fiber technique, we

only need to make sure that the SNR of the optical link is above 11.5 dB, which is easy to achieve in practice.

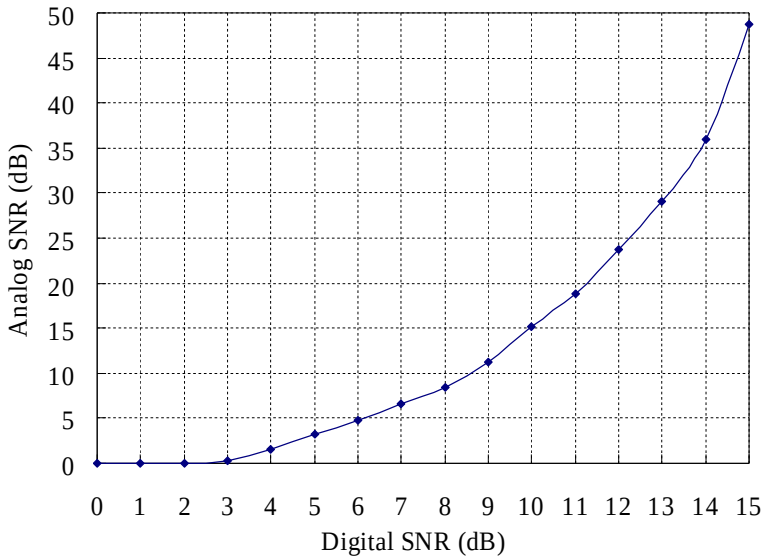

Fig.6.20 Digital SNR vs. analog SNR

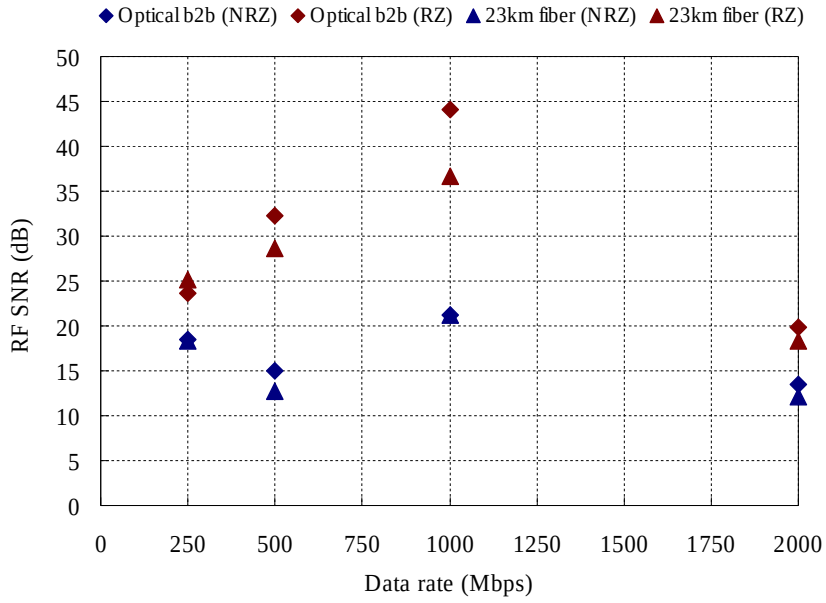

Fig.6.21 Overall SNR of RF signal after digitized RF over 4-level optical link

Based on this relationship, we can measure the SNR of the RF signal after transmission over a digitized RF-over-fiber link employing the four-level optical link and the results are shown in Fig. 6.21. It can be seen that the RZ signal performs better than NRZ for a 4-level digitized RF transportoptical link. Therefore, the four-level optical link using RZ signal offers a promising approach to reduce the overall optical data rate and moderate the hardware requirement of digitized RF-over-fiber link.

6.5 Summary

In this chapter, firstly we demonstrated a digitized radio-over-fiber link for 18 GHz RF signal transmission, and implemented error-free transmission with an optical data rate of 4 Gbit/s. We also investigated the impact on the system performance from the link parameters, such as carrier frequency, bit rate, ADC resolution and sampling rate. For RF frequency at 18 GHz and 15 GHz, a digitized RF link with 8-bit resolution and 500 MHz sampling rate reaches bit rate at 50 Mbps and 80 Mbps separately with error free. There is a trade-off between the link performance and the optical hardware requirements in this technique. An ADC with 6 bits resolution and 600 MHz sampling rate implements the best digitized RF-over-fiber link for the transmission of an 18 GHz RF signal with the bit rate at 50 Mbps.

Secondly, we have further improved our previous DRoF technique by taking advantage of oversampling and decimation to enhance the bit resolution that reduces the overall bit rate for the optical link as well as the hardware requirements on optoelectronics devices in the DRoF link. Furthermore, the noise power induced by the ADC is mitigated by oversampling and decimation and the power dissipations in both ADC and DAC are moderated. The mathematical AWGN approximation of the link noise in digitized RF over-fiber technique is given in terms of ADC quantization noise and jitter noise, and the oversampling effect is analyzed based on the AWGN assumption. Experimental demonstration of the bit resolution enhanced DRoF link is realized. By using the bit resolution enhanced DRoF technique

instead of the previous DRoF technique, the overall data rate is reduced from 4 Gbps to 1.5 Gbps with a similar EVM performance at around 17%, or to 2 Gbps with a better EVM at 14%.

We proposed another approach to reduce the overall optical data rate, which is to apply a multi-level optical link to the digitized RF-over-fiber technique. By doing so, we not only reduce the overall optical data rate, but also moderate the requirements of O-E and E-O devices while maintaining a simple base station configuration. The experimental setup to realize the digitized RF-over-fiber using multi-level optical transmission is proposed by employing simple electrical devices like attenuator, power combiner/splitter and DFF. The experimental results show that four-level optical link using RZ signal is a promising solution to implement the digitized RF-over-fiber transmission.

6.6 Reference

[6.1] H. Chettat, L. M. Simohamed, Y. Bouslimani, H. H. Hamam, “RoF Networks: A comprehensive study,” 3rd International Symposium on Wireless Pervasive Computing, 2008.

[6.2] A.M.J. Koonen, M. García Larrodé, A. Ng’oma, K. Wang, H. Yang, Y. Zheng, and E. Tangdiongga, “Perspectives of Radio over Fiber Technologies,” Conference on Optical Fiber communication/National Fiber Optic Engineers Conference OFC/NFOEC, 2008.

[6.3] A. Nirmalathas, P.A. Gamage, C. Lim, D. Novak, R.B. Waterhouse and Y. Yang, “Digitized RF over Fiber Transport,” Microwave Magazine, vol. 10, pp. 75-81, June 2009.

[6.4] Y. Yang, P.A. Gamage, C. Lim, and A. Nirmalathas, “Demonstration and Performance Analysis of an Uplink based on Digitized RF-over-fiber Signal Transport”, Asia-Pacific Microwave Photonics Conference, 2009.

[6.5] R. G. Vaughan, N. L. Scott, and D. R. White, “The theory of bandpass sampling,” IEEE Trans. Signal Processing, vol. 39, no. 9, pp. 1973-1984, Sep. 1991.

[6.6] Y. Yang, C. Lim, and A. Nirmalathas, “18 GHz RF Transport based on Digitized Radio-over-Fiber technique,” Asia-Pacific Microwave Photonics Conference (APMP), 2010.

[6.7] B. Razavi, Principle of data conversion system design, IEEE Press.

[6.8] Bernard Widrow, and István Kollár, “Quantization Noise: Roundoff Error in Digital Computation, Signal Processing, Control, and Communications,” Cambridge University Press, 2008.

[6.9] Michael Lohning, and Gerhard Fettweis, “The effects of aperture jitter and clock jitter in wideband ADCs,” Computer Standards & Interfaces, vol. 29 Issue 1, pp 11-18, 2007.

[6.10] http://www.actel.com/documents/Improve_ADC_WP.pdf.

[6.11] Sheldon Walklin, and Jan Conradi, “Multilevel Signaling for Increasing the Reach of 10 Gb/s Lightwave Systems,” Journal of Lightwave Technology, vol. 17, Issue: 11, 1999.

Chapter 7

Energy consumption of Integrated Optical-Wireless Access Networks

7.1 Introduction

In the last decade, global warming has become an increasingly important item on the global political agenda. In December 2008, the European Commission (EC) decided to cut greenhouse gas emissions by 20%, to establish a 20% share for renewable energy, and to improve energy efficiency by 20% [7.1]. Information and communication technology (ICT) has a profound impact on the environment, and the energy consumption of ICT is currently becoming a social and political issue [7.2]. Telecommunication network that forms the heart of Internet remains a major contributor to the overall energy consumption of ICT and thus has attracted specific focus on a global scale towards the development of energy efficient ("green") networking solutions [7.1-7.4].

The modern telecommunication network can be generally divided into three parts, namely the access network, the core network and the transmission network. The energy consumptions of these three parts are extremely different. Among them, the access network remains a major contributor since it encompasses a large number of active elements. The proportion of access network in the modern telecommunication network may vary from 50% to 70% as a result of different operating environments [7.3], and it is foreseen to continue to

be the major internet energy consumer for the next decade with its ever-increasing demand for bandwidth [7.4].

The wireless base station, which accounts for up to 70% of the total power consumption in a number of mobile operators, is found to have the most feasible energy-saving potential [7.3]. Furthermore, wide spread deployment of broadband wireless access networks would be required to meet the rising demand for mobile broadband, scale and bandwidth of future wireless systems would rise and their energy consumption would need to be a big factor in design and deployment of next generation wireless access networks.

In recent years, there are many research dedicated in greening the wireless base station and can be catalogued into three groups according to different approaches used in reducing energy waste. The first approach is to simplify the base station architecture, eliminate the active elements, and improve energy efficiency of base station components, especially the power amplifier [7.5-7.6]; the second one is to reduce power consumption during leisure time and build up an energy aware network [7.2]; the third one is focusing on the energy saving of base station cooling system [7.7]. Our research is dedicated to the first category.

Radio-over-fiber (RoF) technique has been long considered as an energy efficient way of simplifying the architecture of remote antenna base stations and realizing high-performance backhaul networks that connect the base stations to the central offices. In this chapter we will investigate the power consumptions and energy-saving potentials of the radio-over-fiber techniques. It is organized as follows. In Section 7.2, we study the power consumptions of the fiber optical backhaul and the conventional microwave backhaul. The fiber optical backhaul shows its energy-saving advantage in terms of both link propagation loss and hardware power consumption. In Section 7.3, we first demonstrate an estimating model of the base station power consumption, and apply to various base station architectures in accordance with different transport schemes of wireless signals; secondly we investigate and

compare the base station power consumptions for baseband-over-fiber, RF-over-fiber, IF-over-fiber, DIF(digitized IF)-over-fiber, and DRF(digitized RF)-over-fiber transmission schemes. In section 7.4, we focus on the digitized RF-over-fiber link and investigate the power consumption of ADCs for bandpass sampling. The sampling rate and the bit resolution are found to be the deciding parameters of the ADC power consumption. In the digitized RF technique, the sampling rate is reduced by bandpass sampling and the bit resolution requirement can be loosened using enhanced DRoF technique. Therefore, the power consumption of the ADC employed in the proposed digitized RoF link is much less than that in the direct-digitized RF link.

7.2 Energy issues in backhaul networks

Two common backbone networks are utilized in delivering wireless signals from central offices to base stations. One is the conventional point-to-point microwave link, and the other is the growing fiber-optical link. In telecommunication market, they both have a standardized interface, and the main difference is the transmission medium, which is also the key factor determining the propagation loss and consequently the link power consumption.

In a microwave link, the path loss is the largest and most variable quantity in the link budget. It depends on frequency, antenna height, receiver terminal location relative to obstacles and reflectors, and link distance, among many other factors. Usually a statistical path loss model or prediction program is used to estimate the median propagation loss in dB. The estimate takes into account the situation -- line of sight (LOS) or non-LOS -- and general terrain and environment using more or less detail, depending on the particular model. Here, the Free Space Path Loss model [7.8] is used to estimate the optimistic situation, since it only takes into consideration distance and frequency. Eq. 7.1 gives the path loss using the Free Space Pass Loss model, where F is the RF frequency of the transmitting signal and L is the transmitting distance.

$$\textbf{Path Loss} = 36.6 + 20\log(F) + 20\log(L) \tag{7.1}$$

On the other hand, the propagation loss of a fiber-optical link is linearly related with the transmission distance, and nearly immune to the environmental changes. The fiber loss is around 0.2 dB/km for single mode fibers, and about 2 dB/km for multi-mode fibers. Based on the above analysis, we calculate the propagation losses in both microwave and optical links as given in Fig. 7.1, where we assume that the RF frequency is 6 GHz and the fiber loss is 0.25 dB/km. It is clearly shown that the propagation loss in microwave link is remarkably larger than in optical link. When the transmission distance between the base station and the central office is 10 km, path loss in microwave link is around 130 dB whilst it is only 2.5 dB in optical link. Large amount of power is wasted in the channel of microwave link. In order to achieve a desired link budget, power consumption of the microwave transmitter/receiver will be much larger than it in optical link. Alcatel-lucent 9500 microwave cross-connect [7.9] and FIBERER-OLT/ONU [7.10] are used to demonstrate the power consumptions of both links in practical uses. As a result, the microwave backhaul consumes 129 W of energy, and the fiber optical backhaul shows its energy-saving advantage with a less power consumption of 5.5 W.

Point to point microwave backhaul:

Transmitter: Alcatel-lucent 9500 microwave cross-connect terminal
Outdoor unit and indoor unit power consumption 50+10=60 W
Output power: 28.5 dBm (QPSK, F=6 GHz)
Receiver: Alcatel-lucent 9500 microwave cross-connect node
Outdoor unit and intelligent node unit power consumption 50+6+3+4+4+2=69 W
Receiver sensitivity: -92 dBm (QPSK, 7MHz channel spacing, F=6 GHz)
Free space loss=36.6+20log (F) +20log (L) =28.5-(-92)
Transmission distance L=13 km
Link power consumption: 129 W

Fiber optical backhaul:

OLT: FIBERER-OLT supporting 32 EPON long-distance ON equipments

Power consumption: 15 W

ONU: FIBERER-ONU

Power consumption: 5 W

Transmission distance up to 20 km

Link power consumption: 15/32+5=5.5 W

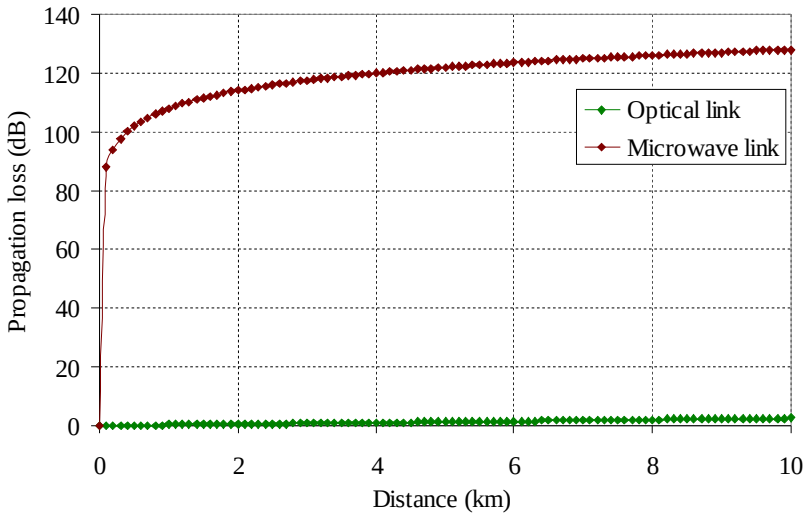

Fig.7.1 Propagation loss vs. distance

7.3 Base station power consumption

7.3.1 Power consumption modeling

Previously a power consumption model of a macro base station was introduced, which focused on each component within the base station [7.11]. In this section, we present a generic power consumption model for RoF wireless base stations, which supports various wireless transport schemes. It is well-established that the power consumption of a base station varies with traffic load. The higher the traffic, the higher the power consumed by the

base station. To simplify the model, we only consider the network when the traffic is at its peak and is heavily loaded.

The architecture of a conventional base station utilizing baseband-over-fiber transmission scheme is shown in Fig. 7.2. It includes the following units.

Baseband Unit (BBU) is mainly comprised by digital signal processor (DSP) to realize MAC layer functionality, modulation and demodulation, etc.

Data converter unit contains digital up/down converter (DUC/DDC), digital pre-distortion (DPD), and AD and DA converter (ADC/DAC) including auto gain control.

RF unit puts the signal on the desired radio frequency, and includes local oscillator, and mixer.

Power amplifier is for the wireless signal amplification. The power consumption of power amplifier (PA) is determined by the transmitting power and amplifier efficiency. Class-A and B amplifier efficiency can be increased from 15% to 25% by digital pre-distortion. The power consumption of the low noise amplifier (LNA) in the uplink is negligible comparing to the power amplifier.

Feeder connects the base station and the antenna which may be located in a location different from the base station, using a copper coaxial cable with a loss of 3 dB.

Clock management provides synchronized clock for each unit.

Power supply and battery backup The loss within these two components is typically 10%-15% of the functional power consumption, and mainly depends on the employed technology.

Cooling depends on the environmental conditions, and the cooling loss is typically between 0 and 40% of the functional power consumption.

Sector number A cell is subdivided to a fixed number of fields, every one of which is illuminated from an antenna that concentrates the flow of power within a particular area of the cell, known as sector. Every field can therefore be considered like one new cell. A typical structure is the trisector, in which there are three sectors.

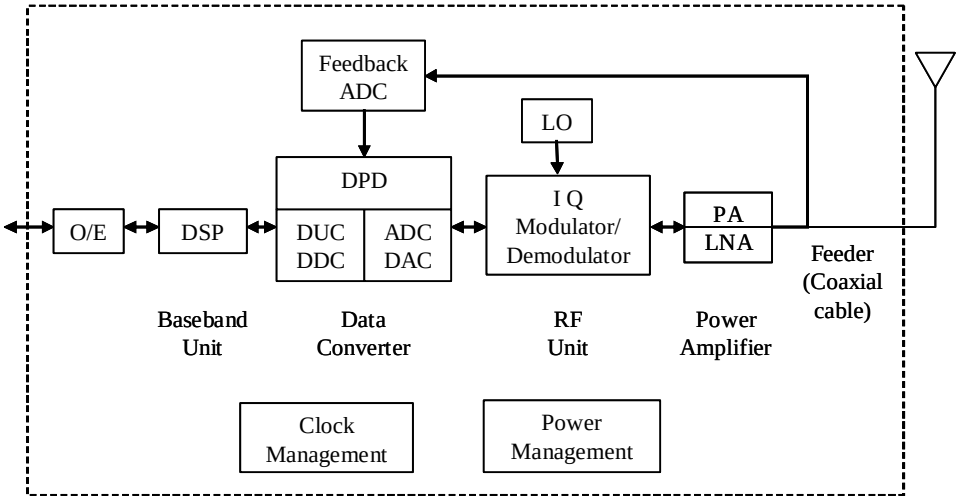

Fig.7.2 Base station architecture for baseband-over-fiber transmission scheme

The power consumptions and the factors regarding power consumptions of the elements within each unit are approximated using the commercial-available devices [7.11] and listed in Table. 7.1. The power consumption of a base station using baseband-over-fiber transmission scheme can be estimated by the Eq. 7.2 using parameters given in Table. 7.1. The result is 1619 W, which matches the power consumption of the currently used base station in the telecommunication market [7.12].

(7.2)
$$P_{BBoF} = N_{sector} \times (P_{Tx} / \mu_{PA} / L_{feeder} + P_{BBU} + P_{DDC/DUC} + P_{ADC/DAC} + P_{DPD} + P_{RFU} + P_C) \times (1 + L_{PS}) \times (1 + \mu_C)$$

Table 7.1 Power related parameters in Base Station

Parameter	Estimated value	Parameter	Estimated value
Power consumption of baseband unit (P_{BBU})	58 W	PA efficiency (μ_{PA})	25%
Power consumption of DUC/DDC ($P_{DUC/DDC}$)	3 W	Transmitting power (P_{TX})	40 W
Power consumption of ADC/DAC ($P_{ADC/DAC}$)	2 W	Feeder loss (L_{feeder})	0.5
Power consumption of digital pre-distortion (P_{DPD})	5 W	Power supply loss (L_{PS})	0.15
Power consumption of RF unit (P_{RFU})	2 W	Cooling efficiency (μ_C)	0.2
Power consumption of clock management (P_C)	1 W	Number of sectors (N_{sector})	3

Assuming when using different transmission schemes the power regarding factors of each element remain the same, we can apply the model to other transmission schemes. The base station configurations for analog RF-over-fiber, analog IF-over-fiber, digitized IF-over-fiber, and digitized RF-over-fiber transmission schemes are illustrated in Fig. 7.3a-d. Table 7.2 lists the elements required in different transmission schemes, and the corresponding power consumptions estimated using this model.

Table 7.2 Elements and power consumption in each link

Transmission scheme	BBoF	DIFoF	DRFoF
Power related elements	Baseband unit DUC/DDC ADC/DAC DPD Clock management RF unit Power amplifier Feeder Power supply Cooling	ADC/DAC DPD Clock management RF unit Power amplifier Feeder Power supply Cooling	ADC/DAC DPD Clock Management Small signal amplifier Power amplifier Feeder Power supply Cooling
Total power consumption	1619 W	704 W	696 W
Transmission scheme	IFoF	RFoF	
Power related elements	Clock management RF unit Power amplifier Power supply Cooling	Power amplifier Power supply Cooling	
Total power consumption	1116.5 W	1104 W	

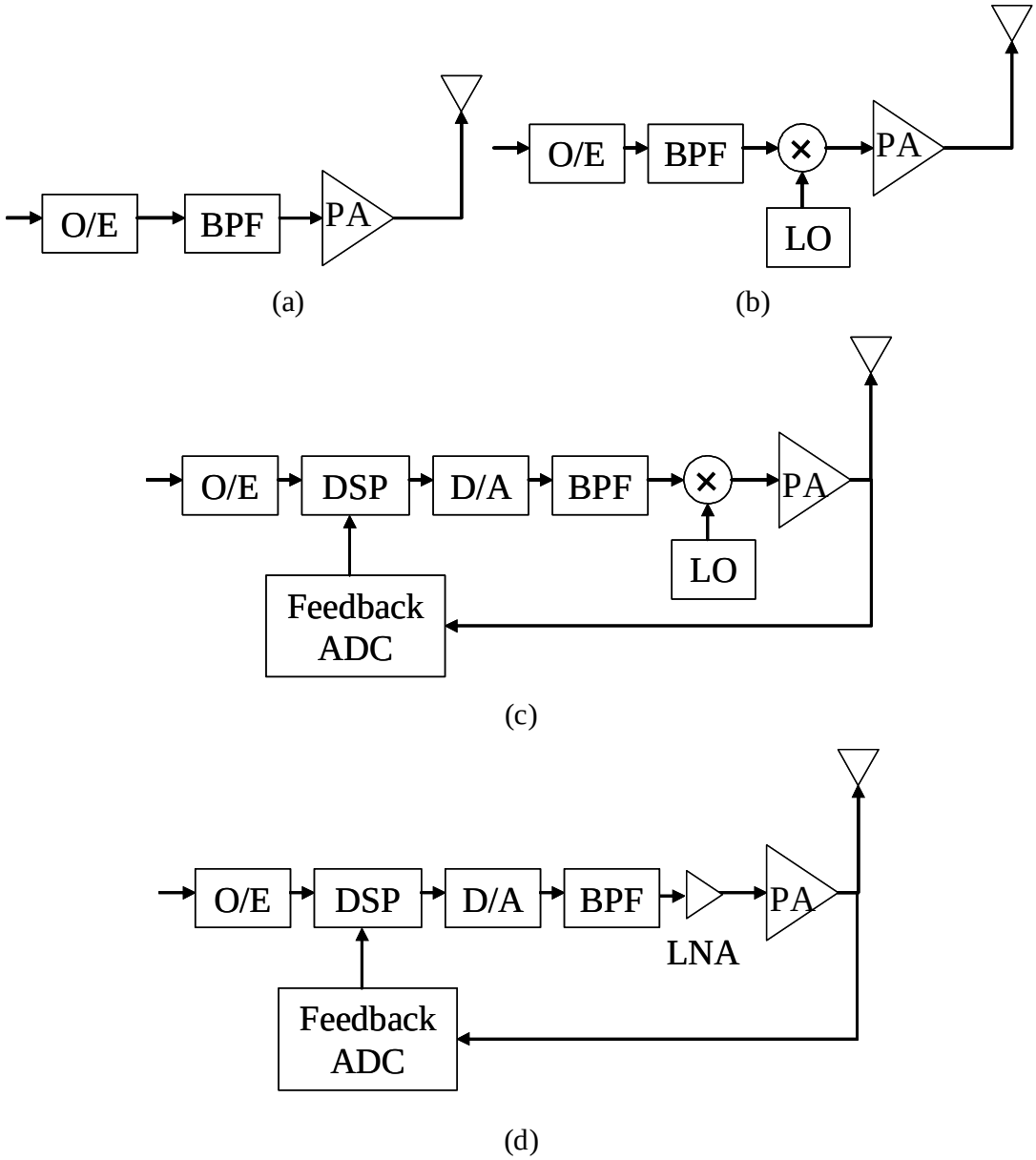

Fig.7.3 Base station architectures of analog RF-over-fiber (a), analog IF-over-fiber (b), Digitized IF-over-fiber (c), and Digitized RF-over-fiber (d)

In analog RF-over-fiber (RFoF) case (Fig. 7.3a), only the power amplifier in the base station architecture is needed. The base station can be located near the antenna, so no feeder loss should be considered. However no digital pre-distortion function can be performed in the

analog domain, the PA efficiency will only be about 15%. Eq. 7.3 is the formula to calculate the power consumption in analog RFoF links.

$$P_{RFoF} = N_{sector} \times (P_{Tx} / \mu_{PA}) \times (1 + L_{PS}) \times (1 + \mu_C) = 1104W \quad (7.3)$$

In analog IF-over-fiber (IFoF) case (Fig. 7.3b), the situation is similar as in analog RF-over-fiber except that the RF unit and the clock block are required. Eq. 7.4 is the formula to calculate the power consumption in analog IFoF links.

$$P_{IFoF} = N_{sector} \times (P_{Tx} / \mu_{PA} + P_{RFU} + P_C) \times (1 + L_{PS}) \times (1 + \mu_C) = 1116.5W \quad (7.4)$$

In digitized IF-over-fiber case (Fig. 7.3c), the baseband unit and the digital up/down converter are located in the central office comparing with baseband-over-fiber scheme. The digital pre-distortion can still be used to increase the PA efficiency to 25%. Since the BBU is mitigated, the base station can be smaller enough to be located near the antenna and make the feeder loss ignorable. Eq. 7.5 is the formula to calculate the power consumption in digitized IFoF links.

$$P_{DIFoF} = N_{sector} \times (P_{Tx} / \mu_{PA} + P_{ADC/DAC} + P_{DPD} + P_{RFU} + P_C) \times (1 + L_{PS}) \times (1 + \mu_C) = 704W \quad (7.5)$$

In digitized RF-over-fiber case (Fig. 7.3d), comparing with digital IF-over-fiber link, the RF unit is no longer needed. Since in digitized RF-over-fiber link the power of the RF signal generated by bandpass sampling is very low (about -50 dBm) [7.13], a small signal amplifier will be required before the power amplifier, and the power consumption of this amplifier is

approximately 0.1 W. Eq. 7.6 is the formula to calculate the power consumption in digitized RFoF links.

$$(7.6)\quad P_{DRFoF} = N_{sector} \times (P_{Tx} / \mu_{PA} + P_{ADC/DAC} + P_{DPD} + P_C + P_A) \times (1 + L_{PS}) \times (1 + \mu_C) = 696\ W$$

7.3.2 Analysis and comparison

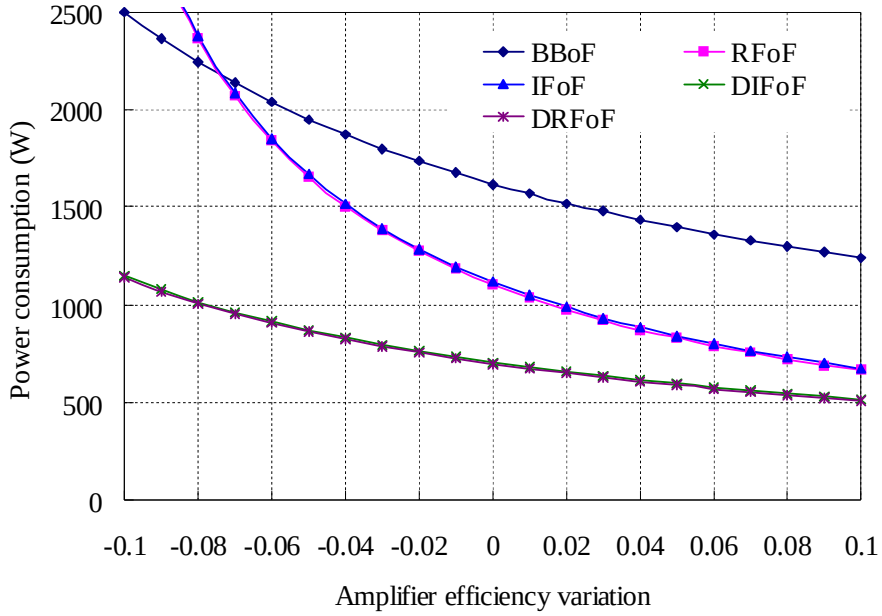

Fig.7.4 Amplifier efficiency effect on power consumption

In Section 7.3.1, we have estimated the base station power consumptions of five radio-over-fiber transmission schemes. The digitized RF/IF-over-fiber techniques show an evident advantage in energy-saving, whilst the currently used baseband-over-fiber technique consumes the most power. This large power consumption can be attributed to the high active element and component count within the baseband unit of the base station. Although analog RF/IF-over-fiber techniques need fewer elements compared to the digitized RF/IF-over-fiber techniques,

the power consumptions are ~400W larger. From the model, we can see that the amplifier efficiency parameter plays a very important role in the total power consumption. In the digitized RF/IF-over-fiber techniques, digital pre-distortion is employed to improve the amplifier efficiency, and it consequently leads to lower power consumptions relative to the analog techniques. Fig. 7.4 illustrates the impact of the amplifier efficiency on the base station power consumption for the investigated transport schemes. The power consumption changes with the amplifier efficiency with the analog techniques being more sensitive compared to the digital schemes (BBoF, DRFoF, and DIFoF). Amplifier efficiency is a sensitive parameter for base station power consumption as well as an essential factor in the overall energy-saving.

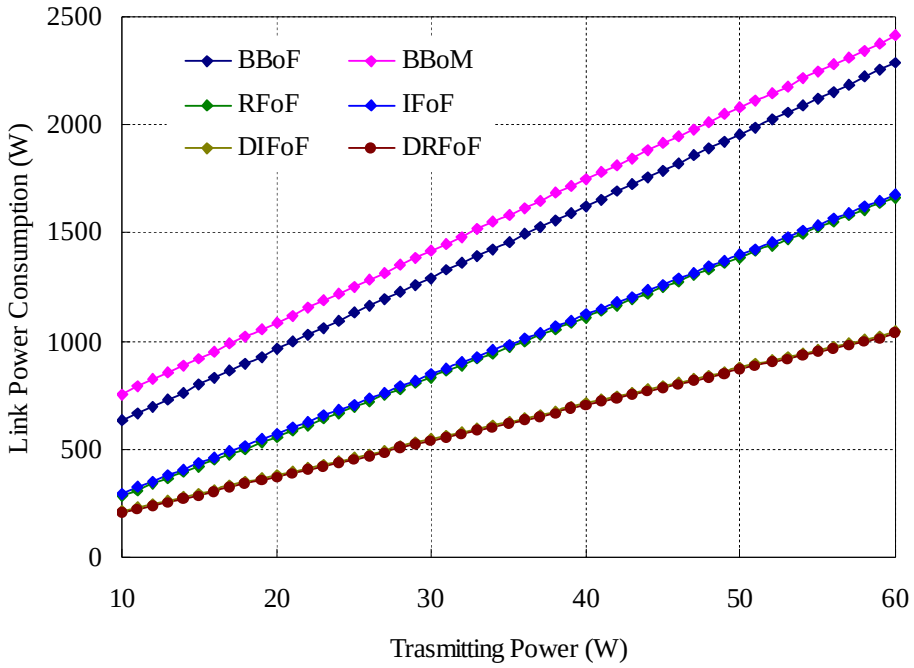

Fig.7.5 Transmitting power Vs. Power consumption

Another parameter with high energy-saving potential is the transmitting power, which is also the key parameter determining the cell size of mobile networks. Fig. 7.5 shows the curves of transmitting power vs. link power consumption in cases of baseband-over-

microwave, baseband-over-fiber, analog RF-over-fiber, analog IF-over-fiber, digitized IF-over-fiber, and digitized RF-over-fiber. The power consumption is linearly increasing with the transmitting power in each case, with baseband links having the largest increment rate and digitized links having the lowest. This result indicates that the digitized techniques have bigger energy-saving ability with larger transmitting power. Fig. 7.6 shows the energy saving in percentage, and illustrates the energy savings of the advanced base station architectures become more significant when the transmitting power is small. As the mobile cell is getting smaller and smaller, the implementation of radio-over-fiber techniques will not only realize a simplified architecture, but also make a great contribution on greening the mobile access networks.

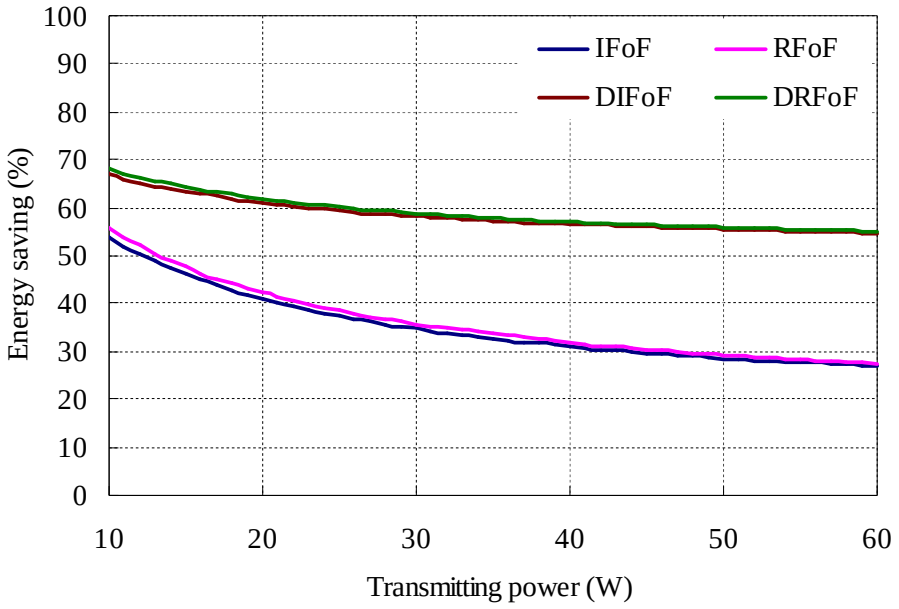

Fig.7.6 Energy saving in percentage

7.4 ADC power consumption in digitized RF-over-fiber

Besides the power amplifiers, the ADC power consumption plays a significant role in the total energy consumption of the base station transceiver. As we discussed before, the ADCs in the digitized RF-over-fiber technique is used to perform the bandpass sampling function, which have different characteristics compared to the normal ADCs used in direct-digitized RF transceivers. The received analog bandwidths of these ADCs should match the carrier frequencies of the RF signals, while the required sampling frequencies are much lower comparing to the analog bandwidths due to bandpass sampling theory. In this section, we will investigate the power consumption of this type of ADCs used in digitized RF-over-fiber links, and discuss the practicability of digitized RF-over-fiber technique with regards to energy efficiency.

7.4.1 ADC power consumption modeling

During the past two decades, the rapid evolution of digital integrated circuit technologies has led to ever more sophisticated signal processing systems. One of the keys to the success of these systems has been the advancement in ADC technology which convert the continuous-time signals to discrete-time, binary-coded form [7.14]. In the telecommunications arena, advances in software radio development and AD conversion technologies have provided impetus for the digital RF distribution in fiber-wireless access networks. Consequently, the power consumptions of ADCs are one of the key issues in implementing digitized fiber-wireless access networks. A generic form of ADC is shown in Fig. 7.7 and consists of an anti-alias filter, a sample-and-hold circuit, a method of converting the (now constant level) analog voltage into a digital word (the “quantizer”), and finally a digital buffer. The quantizer element may be implemented in a wide variety of ways, including flash, successive approximation, sigma-delta, bandpass sigma-delta, and

subranging. The analysis presented below is independent of the implementation technology and is based on the requirements of the sample-and-hold element [7.15].

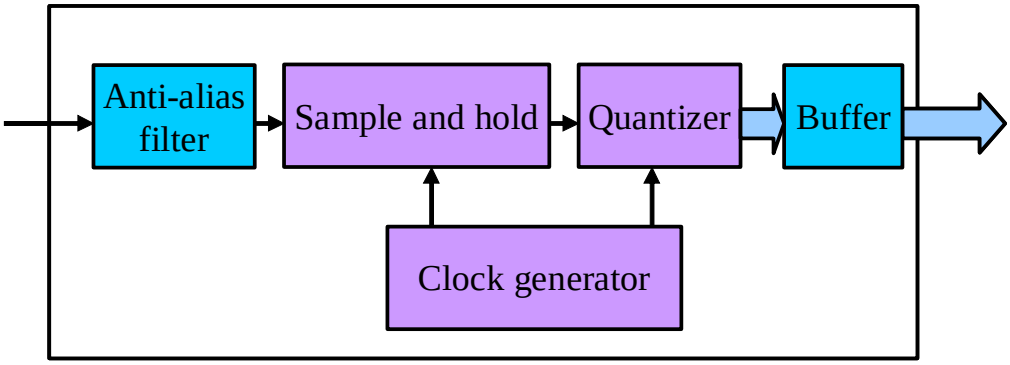

Fig.7.7 Generic form of an A/D converter

One of the basic operations performed by an ADC is the data sampling, which can be performed either in a separate circuit or inherently inside the ADC. The power needed to perform sampling is therefore the lower bound to the power dissipation. The noise of the sampling circuit is given in Eq. 7.7, where C_S is the sampling capacitor. In a Nyquist ADC, is typically chosen large enough such that the sampling noise is comparable to or at least not significantly larger than the converter's quantization noise, which is given by Eq. 7.8. Here, n and V_{FS} are the ideal bit resolution and full-scale range of the ADC, respectively. We assume that the sampling noise is assigned to be equal to the quantization noise as in commercial ADCs, so the sampling capacitor is given by Eq. 7.9 [7.16].

(7.7) $$\overline{v_{ns}^2} = kT/C_S$$

(7.8) $$\overline{v_{qn}^2} = V_{FS}^2 \times 2^{-2n}/12$$

(7.9) $$C_S = 12kT \times 2^{2n}/V_{FS}^2$$

To charge this capacitor to V_{FS} within the sampling aperture α_t which is inversely proportional to the RF carrier frequency, we need a current of $I=C_S V_{FS}/\alpha_t$. The power consumption of the sample and hold element is expressed as Eq. 7.10.

(7.10) $$P_S = IV_{FS} = 12kT \times 2^{2n} / \alpha_t$$

In the quantizer element, comparators are the major energy-consuming components. In comparators, a fundamental limitation on the available resolution stems from thermal noise, and the input-referred noise of the widely used regenerative-latch comparator is given by Eq. 7.11, where γ is the so-called thermal-noise factor (for a long-channel device), C_{LC} is the load capacitance at the bandwidth-limiting node of the comparator, and κ is a constant that depends on the comparator architecture. Equalizing this noise voltage to the quantization noise of an n-bit converter gives a minimum load capacitance that satisfies the constraint in Eq. 7.12 [7.17, 7.18].

(7.11) $$\overline{v_{nC}^2} = \kappa \frac{kT\gamma}{C_{LC}}$$

(7.12) $$C_{LC} = 12kT\gamma\kappa \frac{2^{2n}}{V_{FS}^2}$$

The speed of the comparator is controlled by its time constant $t=C_{LC}/g_m$. Since the comparator must be able to resolve a voltage of $V_{FS}2^{-n}$ within a certain decision time $T_d=1/2f_S$, we find the minimum g_m can be expressed as Eq. 7.13.

(7.13) $$g_m = 2n \ln 2 \times f_S C_{LC}$$

In order to achieve this minimum g_m, we need a minimum supply current I_D to the transistor. Defining a parameter V_{eff}, the minimum supply current can be written as Eq. 7.14. For a classical MOS transistor in strong inversion $V_{eff}=(V_{GS}-V_T)/2$, where V_{GS} and V_T are the gate-to-source and threshold voltages, respectively. In modern technologies (e.g., 90-nm CMOS) $V_{eff}=80\text{-}100mV$ are typical values for high-speed design. Assuming that the comparator runs continuously with a supply voltage of V_{FS}, the power dissipation per comparator can be expressed by Eq. 7.15. For a comparator that is constrained by noise, we can substitute Eq. 7.12 into Eq. 7.15 to obtain Eq. 7.16.

(7.14) $$I = g_m V_{eff}$$

(7.15) $$P_C = 2n\ln 2 \times f_S C_{LC} V_{FS} V_{eff}$$

(7.16) $$P_C = 24kT\gamma\kappa n \ln 2 \times 2^{2n} f_S \frac{V_{eff}}{V_{FS}}$$

In an n-bit flash ADC, (2^n-1) comparators are used in the quantizer, so the quantizer power consumption is given in Eq. 7.17. Using a cross-coupled inverter-type comparator, the input capacitance is equal to the load capacitance, and Eq. 7.17 can be rewritten as Eq. 7.18. Consequently, the total power consumption of an ideal ADC can be expressed as Eq. 7.19.

(7.17) $$P_Q = \left(2^{2n}-1\right)2n\ln 2 \times f_S C_{LC} V_{FS} V_{eff} = \left(2^{2n}-1\right)24kT\gamma\kappa n \ln 2 \times 2^{2n} f_S \frac{V_{eff}}{V_{FS}}$$

(7.18) $$P_Q = 2n\ln 2 \times f_S C_S V_{FS} V_{eff} = 24nkT \ln 2 \times 2^{2n} f_S V_{eff} / V_{FS}$$

(7.19) $$P_{ADC} = 12kT \times 2^{2n} / \alpha_t + 24nkT \ln 2 \times 2^{2n} f_S V_{eff} / V_{FS}$$

Current ADCs are very far from meeting the theoretical limit discussed above. However, the power consumption performance of an ADC can be quantified by the energy per conversion and per unit of resolution. For a non-ideal converter, the conversion energy E_{CR} exceeds the ideal value of kT (Eq. 7.20), where ENOB is effective number of bits.

(7.20) $$E_{CR} = \frac{P}{f_S (S/N)^2} = \frac{P}{f_S 2^{2ENOB}}$$

The ratio E_{CR}/kT represents an excess power consumption factor, and is defined as ADC factor of merit (Eq. 7.21), which is around 10^5 in current AD conversion technology [7.16]. An ideal converter would have a factor of merit of unity. Therefore, the power consumption of a practical ADC is given by Eq. 7.22.

(7.21) $$M = E_{CR}/kT$$

(7.22) $$P_{ADC} = M \times P_{ideal} = M \times \left(12kT \times 2^{2n}/\alpha_t + 24nkT \ln 2 \times 2^{2n} f_S V_{eff}/V_{FS}\right)$$

7.4.2 Power consumption comparison of direct and bandpass sampling

According to Eq. 7.22, the sample-and-hold device should dominate the ADC power consumption. However, in practical ADCs, the sample-and-hold device consumes a fraction of the power of the complete chip (10-15%), and it indicates that the other technology areas have a long way to go before the sample-and-hold circuit dominates the total power consumption. As we can see, no matter what kind of ADC design techniques is used, the total power consumption of an ADC grows exponentially with bit resolution. Moreover, the power consumption of the sample-and-hold element is proportional to the RF carrier frequency and

the power consumption of the quantizer element is proportional to the sampling frequency. Since the quantizer dominates the total power consumption, apart from designing techniques, the sampling rate and the bit resolution are the deciding parameters of the ADC power consumption.

Based on the above results, we compare the power consumptions of ADCs for direct sampling and bandpass sampling. For an RF signal at 2.4 GHz with a bandwidth of 100 MHz, the sampling frequencies for direct Nyquist and bandpass sampling are 5 GHz and 250 MHz respectively. We assume that the sample-and-hold element consumes 10% power. By reducing the sampling rate to 1/20, the quantizer power consumption is reduced to 1/20, and the total power consumption is reduced to 15%, where the sample-and-hold element becomes dominant in the total power consumption. Furthermore, as we discussed in Chapter 6, in the digitized RF link, a decimation filter can be employed to reduce the bit resolution. Consequently the power consumptions in both the sample-and-hold element and the quantizer can reduce exponentially with minimal additional power consumption for signal processing functionality.

7.5 Summary

In this chapter we investigated the power consumptions and energy-saving potentials of the fiber-wireless integration techniques.

In Section 7.2, we have studied the power consumptions of the fiber optical backhaul and the conventional microwave backhaul. The propagation losses in both links were modelled and compared. To achieve a same link budget, power consumption of the microwave transmitter/receiver will be much larger than it in optical links. The power consumptions of both links in practical uses are demonstrated. As a result, the microwave backhaul consumes

129 W of energy, and the fiber optical backhaul shows its energy-saving advantage with a less power consumption of 5.5 W.

In Section 7.3, we first proposed an estimating model of the base station power consumption by evaluating each component within the base station, and applied to various base station architectures in accordance with different transport schemes of wireless signals; secondly we investigated and compared the base station power consumptions for baseband-over-fiber, RF-over-fiber, IF-over-fiber, digitized IF-over-fiber, and digitized RF-over-fiber transmission schemes. The digitized RF/IF-over-fiber techniques consume the least power, whilst the currently used baseband-over-fiber technique consumes the most power. In the model, the amplifier efficiency parameter and the transmitting power are the key parameters with high energy-saving potential.

In section 7.4, we investigated the power consumption of ADCs in digital RF distribution techniques, which inceases exponentially with bit resolution. Reducing the bit resolution using enhanced DRoF technique can lead to a big reduction in power consumption. Moreover, the quantizer power consumption dominates in direct-digitized ADCs and is proportional to the sampling rate. Therefore, the power consumption of the ADC for bandpass sampling operating at a low sampling frequency in the proposed digitized RF technique is much less than that in the direct-digitized RF link.

7.6 Reference

[7.1] “Climate change: Commission welcomes final adoption of Europe’s climate and energy package,” EC press release Dec. 2008.

[7.2] P. Chowdhury, M. Tornatore, S. Sarkar, and B. Mukherjee, “Building a Green Wireless-Optical Broadband Access Network (WOBAN),” Journal of Lightwave Technology, vol. 28, pp. 2219-2229, 2010.

[7.3] “Improving energy efficiency, Lower CO2 emission and TCO,” Whitepaper, Huawei energy efficiency solution, Oct. 2009.

[7.4] C. Lange, and A. Gladisch, “On the energy consumption of FTTH access networks,” OFC/NFOEC’09, March, 2009.

[7.5] V. Bassoo, K. Tom, A.K. Mustafal, E. Cijvat, H. Sjoland, and M. Faulkner, “Potential Architecture for Future Generation `Green' Wireless Base Station,” 4th International Symposium on Wireless Pervasive Computing (ISWPC 2009), pp. 1–5, 2009.

[7.6] “The power play: Reducing the build and power consumption costs of WiMAX base stations,” Whitepaper, Motorola new design for WiMAX base stations, Nov. 2009.

[7.7] Y. Maeda, Y. Seshimo, and T. Okazaki, “Study of a cooling system for the telecommunication base site. Discussion,” ASHRAE transactions, vol. 111, pp. 746-755, 2005.

[7.8] W. Debus, “RF Path Loss & Transmission Distance Calculations,” Axonn Global Data Solutions, August 4, 2006.

[7.9] Alcatel-Lucent, “Alcatel-Lucent 9500 Microwave Cross-Connect Datasheet”.

[7.10] www.fiberer.com

[7.11] O. Arnold, F. Richter, G. Fettweis, and O. Blume “Power Consumption Modeling of Different base station types in heterogeneous cellular networks,” Future Network and MobileSummit Conference Proceedings,2010

[7.12] Texas Instrument, “Communication Infrastructure Guide”.

[7.13] Y. Yang, C. Lim, P.A. Gamage, and A. Nirmalathas, “Experimental Demonstration of a Downlink Multi-Channel Hybrid Fiber-Radio using Digitized RF-over-Fiber Technique,” IEEE MTT 2010 International Microwave Symposium, 2010.

[7.14] Robert H. Walden, “Analog-to-Digital Converter Survey and Analysis,” IEEE Journal of selected areas in communications, vol. 17, no. 4, 1999.

[7.15] Timmy Sundström, Boris Murmann, and Christer Svensson, “Power Dissipation Bounds for High-Speed Nyquist Analog-to-Digital Converters,” IEEE Transactions on Circuits and Systems, vol. 56, no. 3, 2009.

[7.16] Peter B. Kenington, and Luc Astier, “Power Consumption of A/D Converters for Software Radio Applications,” IEEE Transactions on Vehicular Technology, vol. 49, no. 2, 2000.

[7.17] P. Nuzzo, F. De Bernardinis, P. Terreni, and G. Van der Plas, “Noise analysis of regenerative comparators for reconfigurable ADC architectures,” IEEE Transactions on Circuits and Systems, vol. 55, no. 6, pp. 1441-1454, 2008.

[7.18] I. E. Opris, “Noise estimation in strobed comparators,” Electronic Letters, vol. 33, no. 15, pp. 1273-1274, 1997.

Chapter 8

Conclusions

8.1 Thesis overview

The integration of wireless broadband access and the optical access network infrastructure via a common backhaul network can lead to significant benefits to network operators through savings in operational and capital expenditure associated with the broadband deployment. This thesis is focused on the investigation and development of novel technologies for the implementation of fiber-wireless integration networks in order to realize ultra-high-speed, high-quality, and multi-service links that connect large numbers of radio base stations with the central office, simplify the architecture of remote base stations, and achieve both cost and energy efficiency.

In Chapter 2, a comprehensive literature review on the investigation of the radio-over-fiber technology has been presented. The radio-over-fiber systems and their benefits were introduced. Three conventional analog radio-over-fiber schemes (BBoF, IFoF and RFoF) and two novel digital radio-over-fiber schemes (Digitized IFoF, Direct-Digitized RFoF) were presented and discussed. Some implementation issues and previous research were reviewed in terms of RF signal generation, linearization techniques, chromatic compensation, base station simplification techniques, and multiplexing techniques. The last section of this chapter introduced the power consumption issues and energy-efficient solutions in the current research of access networks.

Chapter 8 Conclusions

In Chapter 3, we first introduced the digitized RF-over-fiber technique based on bandpass sampling theory and commercial-available ADCs/DACs. It takes advantage of the higher performance of digital optical links, the benefits of direct RF distribution to realize simpler base stations, and the use of existing optical access and metro network infrastructures. Secondly, we theoretically analyzed the digitized RF-over-fiber link in terms of different noise sources, such as ADC jitter noise, ADC quantization noise, bandpass sampling aliasing noise, DAC jitter noise, and photo-receiver noise. We have also carried out a comparison of SNR and dynamic range between digitized and analog RF-over-fiber links. The results indicated that for digitized link, the increase of the laser launched power has no impact on the SNR but it increases the fiber transmission distance. However, in the analog link, the transmission distance does not increase with laser launched power due to system nonlinearity. The dynamic range in the analog link decreases steadily with fiber length; while in the digital link, it remains constant until the transmission distance reaches a specific length where the power goes beyond the sensitive of the link. The high dynamic range of digitized RF transport offers a distinct advantage over an analog link. Finally, we experimentally demonstrated a low-cost digitized RF-over-fiber uplink transmission using commercially available FPGA boards. Our studies have confirmed that digitized RF-over-fiber links can support extended reach well in excess over 60 km and can easily be integrated with any digital optical transmission technologies. We also have experimentally investigated the link performance of digitized RF-over-fiber transport for different ADC resolutions, different carrier frequencies, different symbol rates and different sampling rates. The results indicated that: (1) 8 bits resolution was sufficient to construct a high-performance cost-effective digitized RF over fiber link; (2) link EVM performance improved almost linearly with carrier frequency and symbol rate; (3) link performance was independent of sampling rate, as long as the sampling rate satisfies the bandpass sampling theory.

In Chapter 4, we proposed a multi-channel RF transmission scheme using digitized RF-over-fiber technique, and realized frequency conversion processes using a single ADC and a single DAC. Bandpass sampling for multiple distinct bands is employed to sample and downconvert the subcarrier multiplexed RF signals to IF bands ensuring no overlapping of the multiple frequency bands within each Nyquist window. The SNR and dynamic range of a multi-channel system are analyzed in both analog and digitized RF-over-fiber links. Intermodulation distortion is the main reason for performance deterioration in analog links, while in digitized links the increased aliasing noise and quantization noise worsen the link performance. The degradations of SNR and dynamic range due to increasing channel number are quantized, and the results show that the degradations in digitized links are less severe than in analog links. Moreover, we experimentally implemented a DRoF link for multi-channel RF systems by employing commercially available FPGA and ADC, and recovered the data with satisfactory EVM performance. We have experimentally shown that all the RF bands can be downconverted to the same Nyquist region, and recovered without the physical needs of a mixer and a local oscillator. Our experimental results show that the noise level in the DRoF link is -40 dBm, and the level of inter-channel interference on the middle channel after DRoF transport is not dependent on the initial channel spacing at the transmitter. It is dependent on the channel spacing after downconversion via bandpass sampling at the receiver. Our investigation shows that the EVM of the middle channel remained constant regardless of the initial channel spacing before transmission. Both theoretical and experimental results indicate that the digitized RF-over-fiber technique provides a more efficient approach than analog transmission to implement multi-channel radio optical networks.

In Chapter 5, we proposed an efficient bidirectional transmission scheme for Hybrid Fiber-Radio access using digitized RF-over-fiber technique that supports multiple wireless signals distribution for both uplink and downlink. The frequency allocation theory was presented to

minimize the inter-channel interference of the sampled signal and to ensure that the signal bands were located at the same position with a maximum spacing in each Nyquist zone. This scheme enables multiple wireless signals to be transported simultaneously and simplifies the BS design by performing the frequency translation processes without the needs of analog devices such as mixers and local oscillators. We have experimentally demonstrated a proof-of-concept DRoF-HFR link for the simultaneous transmission of GSM, UMTS and WiMAX wireless services. Error-free transmission can be achieved for all three wireless signals in both the downstream and upstream directions when the sampling rate was >= 50 MHz and the optical data rate was >= 400 Mb/s. Experimental results showed that in the downlink transmission the link EVM performance was linearly related to the up-converted wireless carrier frequency. Therefore, a higher sampling rate should be considered in order to maintain a good link performance when up-converting to high RF frequencies in the downlink path. The amount of amplification required for wireless services at different wireless carrier frequencies has also been quantified, and the results indicated that significant amount of amplification was required when the image with the desired wireless carrier frequency was located in the 20th or larger Nyquist zone. In the uplink transmission, although the noise power was similar to that in the downlink path, the inter-channel interference level was much higher. The performance of the uplink was limited by inter-channel interference.

In Chapter 6, firstly we have demonstrated a digitized radio-over-fiber link for 18 GHz RF signal transmission, and implemented error-free transmission with an optical data rate at only 4 Gbit/s. We also investigated the impact of carrier frequency, bit rate, ADC resolution and sampling rate on the system performance. For RF carrier frequencies at 18 GHz and 15 GHz, a digitized RF link with 8-bit resolution and 500 MHz sampling rate is able to transport a wireless data rate of 50 Mbps and 80 Mbps with error-free reception respectively. There is a trade-off between the link performance and the optical hardware requirements. An ADC with

6 bits resolution and 600 MHz sampling rate implements the best digitized RF-over-fiber link for the transmission of an 18 GHz RF signal with a bit rate at 50 Mbps. Secondly, we have further improved our previous DRoF technique by taking advantage of oversampling and decimation to enhance the bit resolution that reduces the overall bit rate for the optical link as well as the hardware requirements on optoelectronics devices in the DRoF link. Furthermore, the noise power induced by the ADC was mitigated by oversampling and decimation and the power dissipations in both the ADC and the DAC were moderated. The mathematical AWGN approximation of the link noise in digitized RF over-fiber technique was given in terms of ADC quantization noise and jitter noise, and the oversampling effect was analyzed based on the AWGN assumption. We have demonstrated this scheme in a proof-of-concept experiment. By using the bit resolution enhanced DRoF technique instead of the previous DRoF technique, the overall data rate was reduced from 4 Gbps to 1.5 Gbps with a similar EVM performance at around 17%, or to 2 Gbps with a better EVM at 14 %. Thirdly, we proposed another approach to reduce the overall optical data rate, which was based on multi-level optical link in conjunction with thedigitized RF-over-fiber technique. By doing so, we not only reduce the overall optical data rate, but also moderate the requirements of O-E and E-O devices while maintaining a simple base station configuration. The experimental setup to realize the digitized RF-over-fiber using multi-level optical transmission was carried out using simple electrical devices like attenuator, power combiner/splitter and DFF. The experimental results showed that four-level optical link using RZ signal was a promising solution to implement digitized RF-over-fiber transmission.

In Chapter 7, we investigated the power consumptions and energy-saving potentials of the fiber-wireless integration techniques. We have studied the power consumptions of the fiber optical backhaul and the conventional microwave backhaul. The propagation losses in both links were modelled and compared. To achieve a same link budget, power consumption of the microwave transmitter/receiver will be much larger than it in optical links. The power

consumptions of both links in practical uses were demonstrated. We have proposed model for estimating the base station power consumption by evaluating power consumption of each component within the base station and applied to various base station architectures in accordance with different transport schemes of the wireless signals. Using this model, we compared the base station power consumptions for baseband-over-fiber, RF-over-fiber, IF-over-fiber, digitized IF-over-fiber, and digitized RF-over-fiber transmission schemes. The digitized RF/IF-over-fiber techniques consume the least power, whilst the currently used baseband-over-fiber technique consumes the most power. In the model, the amplifier efficiency parameter and the transmitting power are the key parameters with high energy-saving potential. We also investigated the power consumption of ADCs in digital RF distribution techniques, which was exponentially increasing with the bit resolution. Reducing the bit resolution using enhanced DRoF technique can induce a big reduction in power consumption. The quantizer power consumption dominates in direct-digitized ADCs and is proportional to the sampling rate. Therefore, the power consumption of the ADC for bandpass sampling operating at a low sampling frequency in the proposed digitized RF technique is much less than in the direct-digitized RF link.

8.2 Future Work

The experimental studies and theoretical analysis that are presented in this thesis consists of detailed investigations of high-performance low-cost fiber-wireless integration networks, novel radio-over-fiber techniques using digitized RF distribution, energy consumptions in radio-over-fiber access networks. In carrying out this work, a number of related topics were identified but could not be pursued as part of this thesis, which would be interesting for further investigations.

- In the digitized radio-over-fiber transmission scheme that we proposed in Chapter 3, we use a DAC at the receiver side to convert the digital data stream back to

analog signal and recover the information. Since the received signal is in digital domain, further work should be done to recover the data in digital domain and avoid using any analog devices at the receiver side.

- According to the analytical and experiment results of this work, there are tradeoffs between the link performance and the hardware requirement in the digitized RF-over-fiber links. Works should be done to balance the ADC sampling rate, the signal bandwidth, and the RF carrier frequency. We have proposed two methods to improve the digitized RF-over-fiber technique. However, additional processes are required in both. More detailed analysis should be carried out to evaluate the benefits comparing to the original digitized RF-over-fiber technique.

- New wireless technologies that can exploit the large unused bandwidths of sub-millimeter or millimeter-wave (mm-wave) frequency regions have been recognized by researchers for the provision of future broadband wireless services. One particular band of interest is the unlicensed 60 GHz frequency band (57–64 GHz) which is targeted towards short range in-building high-speed applications, and has gained significant popularity in the last few years. The investigation of 60 GHz RF over fiber transmission using the DRoF technique will dramatically reduce the sampling rate of 60 GHz transceivers and make it possible to distribute multiple MMW signals via a simple fiber-optical link.

- The fiber-wireless integration networks based on digitized RF-over-fiber technique transmit digital data instead of analog signal over fiber, which will enable the radio-over-fiber access networks to coexist with the optical access networks. The investigation on such converged optical access networks need to be carried out in order to maximise the hardware sharing and cost effectiveness.

- As we discussed, the ADCs for bandpass sampling purpose have different characteristic requirements, such as sampling rate and analog bandwidth. Nowadays the commercial ADCs are designed for Nyquist sampling. The design of ADCs with the sample-and-hold device having quick response as commercial ADCs and quantizer having sampling rates much lower will be necessary to practically implement digitized RF-over-fiber technique in optical access networks.

- In Chapter 7, we evaluate energy consumption in fiber-wreless integration networks. The transmitting power and amplifier efficiency are the key parameters determining the total power consumption of a wireless base station. Therefore, the investigations on reducing the transmitting power requirement and improving the amplifier efficiency will be interesting topics to achieve energy efficiency.

Appendix: Acronyms

ADC	analog-to-digital converter
ADSL	asymmetric digital subscriber line
AWG	arrayed waveguide gratings
AWG	arbitrary waveform generator
AWGN	additive white Gaussian noise
BB	baseband
BPF	bandpass filter
CO	central office
DAC	digital-to-analog converter
DAS	distributed antenna system
DFB	distributed feedback laser
DFF	data flip-flops
DRoF	digitized RF-over-fiber
DSB	double-sideband
DSL	digital subscriber line
DSLAM	DSL access multiplexer
DSO	digital sampling oscilloscope
DSP	digital signal processing
DSSC	double-sideband suppressed-carrier
EAM	electro-absorption modulators

EVM	error vector magnitude
FBG	fiber bragg grating
FDM	frequency division multiplexing
Fi-Wi	fiber-wireless
FPGA	field-programmable gate array
FTTH	fiber to the home
FTTN	fiber to the node
FWM	four-wave mixing
GSM	global system for mobile communications
HD	harmonic distortion
HDSL	high data rate digital subscriber line
HFC	hybrid fiber coax
HFR	hybrid fiber-radio
ICT	information and communication technology
IF	intermediate frequency
IMD	third-order intermodulation
IM-DD	intensity-modulation and direct-detection
IP3	3rd-order input intercept point
LAN	local area network
LO	local oscillator
LPF	low pass filter
LSB	least significant bit

MMF	multimode fiber
mm-wave	millimeter wave
MZI	Mach Zehnder Interferometer
MZM	Mach-Zehnder modulator
NF	noise figure
OLT	optical line terminal
ONU	optical network unit
OSSB+C	optical single sideband with carrier
PMD	polarization mode dispersion
PS	power splitter
PSD	power spectral density
RF	radio frequency
RN	remote node
RoF	radio-over-fiber
SCM	subcarrier multiplexing
SDSL	symmetric digital subscriber line
SFDR	spurious free dynamic range
SIR	signal-to-interference ratio
SMF	single mode fiber
SNR	signal-to-noise ratio
SNR_J	signal-to-jitter-noise ratio
SNR_Q	signal-to-quantization-noise ratio

TSSB	tandem single-sideband
VCSEL	vertical cavity surface emitting lasers
VSA	vector signal analyzer
VSG	vector signal generator
WDM	wavelength division multiplexing
WiMAX	worldwide interoperability for microwave access
XPM	cross-phase modulation